UNIVERSIDAD DE CHILE

FACULTAD DE CIENCIAS FISICAS Y MATEMATICAS

DEPARTAMENTO DE GEOLOGIA

METALOGÉNESIS, PETROGÉNESIS Y TECTÓNICA DEL DISTRITO MINERO DE MANTOS BLANCOS, CORDILLERA DE LA COSTA, NORTE DE CHILE.

Tesis para optar al grado de Doctor en Ciencias

Mención Geología

Luis Ernesto Ramírez Ovalle

PROFESOR GUIA:

Miguel Angel Parada Reyes

MIEMBROS DE LA COMISION:

Carlos Palacios Monasterio

Luis Aguirre Le-Bert

Gabriel A. González López

Shoji Kojima

SANTIAGO DE CHILE

Diciembre 2007

RESUMEN

El yacimiento de cobre Mantos Blancos (500 Mt @ 1.0 % Cu), se ubica en la Cordillera de la Costa del Norte de Chile, en la región de Antofagasta. La mineralización se hospeda en rocas ígneas, las cuales fueron agrupadas y denominadas informalmente como Complejo Igneo de Mantos Blancos. Este consiste en rocas riolíticas hipabisales emplazadas como domo y brechas ígneas-hidrotermales monomícticas de composición riolítica, intruidas por pórfidos dioríticos y granodioríticos, en forma de stocks y sills. Los pórfidos dioríticos-granodioríticos localmente gradan hacia superficie a brechas ígneas-hidrotermales polimícticas. Todas estas rocas se encuentran mineralizadas en grados variables. Diques máficos (dioríticos principalmente) cortan todas las rocas mencionadas previamente y son esencialmente tardi-mineral y estériles. El objetivo central de este trabajo de Tesis es desarrollar un modelo conceptual integrado sobre el origen y evolución del yacimiento Mantos Blancos, determinando las características de los procesos de evolución magmática y establecer el rol genético con la mineralización hidrotermal. El yacimiento Mantos Blancos se habría formado por dos eventos hidrotermales de edad Jurásico superior-Cretácico inferior. El evento más antiguo ocurrió en el Jurásico superior (~155 Ma), coetáneo con brechización magmático-hidrotermal de composición riolítica y alteración fílica asociada. El evento más joven representa la etapa principal de mineralización ocurrida durante el Cretácico inferior (~141-142 Ma) y está genéticamente relacionado al emplazamiento de sills-stocks granodioríticos y dioríticos de textura porfídica, y la formación coetánea de las brechas polimícticas, a una paleo-profundidad aproximada de entre 3.5 y 2.0 km. Este evento principal, está caracterizado por tres tipos de alteración-mineralización: una etapa temprana de alteración potásica, propilítica y una tardía de alteración sódica desarrollada centralmente en las brechas ígneas-hidrotermales polimícticas y sus cercanías. La alteración sódica está asociada a un intenso fracturamiento y brechización y la depositación principal de mineralización. La distribución de leyes, alteración, y la zonación de sulfuros de cobre indican que los cuerpos de brechas ígneas-hidrotermales polimícticas representan los conductos alimentadores del sistema hidrotermal.

En base a observaciones petrográficas y datos geoquímicos, se identificaron dos tipos de pórfidos granodioríticos: pórfido granodiorítico I (GP I) y pórfido granodiorítico II (GP II), los cuales se generaron a partir de dos *trends* diferentes de evolución magmática: i) los diques máficos, pórfidos dioríticos y pórfidos granodioríticos I (GP I), siguen una evolución dominada por fraccionamiento de hornblenda, a partir de un magma parental diorítico de afinidad mantélica y ii) los pórfidos granodioríticos II (GP II), muestran indicios de fraccionamiento dominado por plagioclasa, sin embargo, su génesis se explica de mejor manera por mezcla magmática y la generación de las brechas ígneas-hidrotermales polimícticas por *mingling*, entre fundidos dioríticos y siliceos. La signatura isotópica de Sr-Nd enriquecida del domo riolítico sugiere una fuente cortical dominante para estas rocas félsicas.

Observaciones petrográficas y de campo, además de datos geoquímicos, apuntan a que la interacción de magmas dioríticos de afinidad mantélica y fundidos silicios de origen cortical, pudo inducir la liberación de fluidos hidrotermales para formar la mineralización del Cu.

Un estudio paleomagnético fue realizado en el depósito y sus alrededores para definir los eventos de deformación y sus relaciones temporales con la mineralización. Se perforaron 37 sitios en granodioritas del Jurásico superior, domo riolítico tobas riolíticas y diques basálticos del Cretácico inferior, indican rotaciones horarias de 30º a 50º, a excepción de una localidad cercana al Sistema de Fallas de Atacama. En el distrito de Manos Blancos, se reconocieron cuatro eventos de deformación: i) basculamiento de las rocas del distrito hacia el sur-oeste, previo a la alteración hidrotermal relacionada a la mineralización de cobre, ii) transcurrencia sinestral en una zona de deformación principal actualmente orientada NE durante el Cretácico inferior, iii) rotaciones en sentido horario con eje vertical, durante el Eoceno-Oligoceno y iv) una última etapa de deformación asociada a extensión EW, contemporánea y posterior a la mineralización supergena, de probable edad Miocena. Para conocer la geometría original del cuerpo mineralizado, se restauraron los desplazamientos de las fallas principales en el yacimiento y las rotaciones tectónicas en una vista en planta 2D. El cuerpo mineralizado tuvo una geometría elongada en dirección EW, sugiriendo que esta dirección favoreció el emplazamiento de la mineralización.

AGRADECIMIENTOS

En estas lineas deseo expresar mis mas sinceros agradeciemientos a toda la gente e instituciones que han sido fundamentales en la elaboración de este trabajo de Tesis.
En primer lugar quisiera agradecer a la Empresa Minera de Mantos Blancos que permitió acceder a mucha información y que sin su permiso no podría haber accedido a las rocas del yacimiento. A los colegas que trabajan en la mina Mantos Blancos, que colaboraron, discutieron y ayudaron a enfocar y materializar este trabajo. De manera especial quiero agradecer a Regina Toloza, Cesar Ulloa y todo el grupo de Geologia de la empresa.
Gran parte de los estudios que comprenden esta tesis fueron iniciados en el marco del Proyecto FONDEF 1012 “Fundamentos metalogénicos, mineralógicos y geoquímicos para una exploración innovativa de depósitos de cobre: aplicaciones en la Cordillera de la Costa del Norte de Chile”, del que estoy muy agradecido y feliz de haber formado parte. El director de este proyecto, Carlos Palacios M. fue quien me incentivó a participar de éste. Le agradezco toda su ayuda, colaboración y amistad entregada incondicionalmente hacia mi persona y mi familia, durante estos años.
Deseo agradecer al Departamento de Geología de la Universidad de Chile, por haberme acogido en su programa de Post-grado y al proyecto MECESUP 010, el cual fue un gran apoyo economico, a través de la beca de Doctorado. Agradezco, muy especialmente, a mi profesor guia Miguel Angel Parada por su apoyo y supervisar mi trabajo de Tesis. Del mismo modo, agradezco las observaciones a este trabajo realizadas por la comisión examinadora, conformada por los académicos del Departamento de Geología Dr. Carlos Palacios y Dr. Luis Aguirre y por los integrantes invitados Dr. Gabriel González (Universidad Catolica del Norte) y Dr. Shoji Kojima (Universidad Catolica del Norte). También agradezco la cooperación, asistencia y tiempo de otras personas del Departamento de Geología, con quienes he tenido la fortuna de trabajar o discutir algunos aspectos de este trabajo: Cesar Arriagada, Brian Townley, Francisco Munizaga, Katia Dekart, Andres Tassara y Jaime Martínez. De modo especial queiro agradecer a Pierrick Roperch (IRD), por su colaboración y apoyo.
Agradezco su generosa colaboración y amistad a los colegas españoles J.L. Fernandez-Turiel, D. Gimeno y M. Garcia-Valles. De manera especial agradezco a A. Sial (Universidad de Pernambuco, Brasil), de quien guardo un especial recuerdo de nuestro trabajo en terreno y por su generosa colaboración con esta investigación.
Agradezco su acogida, colaboracion y discusión de los datos obtenidos al proferosor Dr. Bernd Lehmann, durante mi estadia en el Institut für Mineralogie und Mineralische Rohstoffe, Technische Universität Clausthal, en Alemania, y a mi amigo Dr. Jens Wittenbrink, de quienes guardo grandes recuerdos.
En el trabajo de campo, agradezco a toda la gente que me acompaño en las diversas etapas de este trabajo, en especial quisiera agradecer a Pedro Sepúlveda, por su amistad y buena disposición frente al trabajo. Y a Edi, muchas gracias por la buena onda y el apoyo durante el muestreo de Paleomag.

A Cristina, María Rosa, Verónica, Carlos Gomez, el Kilo y Carlitos Alvarado. Gracias por todo. Y como no estar agradecido de todos mis compañeros, amigos y colegas. A todos los chic@s del postgrado...muchisimas gracias. De manera especial a mis coleguitas: Luciano, Watong, Chuncho y Pelao, muchas gracias por su amistad.

Todas las personas e instituciones mencionadas anteriormente han contribuido directa o indirectamente a enriquecer mis conocimientos y formación profesional. Espero que no me falte ninguno. También ha sido vital en la culminación de este trabajo el apoyo incondicional de mis seres queridos, mis padres, hermanos y amigotes, pero sobretodo, de mi chica y compañera de viaje Francisca José y nuestro hijo Martín.

Mis más grandes agradecimientos para todo el mundo…

INDICE

I. INTRODUCCIÓN

En base a estudios geológicos, geoquímicos y geofísicos, el presente trabajo de Tesis propone un modelo genético del yacimiento Mantos Blancos (Cu-Ag). El yacimiento se ubica a ~ 45 km al NE de la ciudad de Antofagasta, en la Cordillera de la Costa de la II Región.

Gran parte de los estudios que comprenden esta tesis fueron iniciados en el marco del Proyecto FONDEF 1012 "Fundamentos metalogénicos, mineralógicos y geoquímicos para una exploración innovativa de depósitos de cobre: aplicaciones en la Cordillera de la Costa del Norte de Chile".

I.1 Exposición del problema estudiado

El yacimiento Mantos Blancos (Cu-Ag) ha sido considerado el representante más grande de los depositos estratoligados del Norte de Chile (Espinoza et al., 1996; Maksaev y Zentilli, 2002). Sin embrago, en este yacimiento no se han realiado estudios de detalle desde hace mas de 20 años (e.g. Chavez, 1985). Durante esos años la extracción de mineral se realizaba de manera subterránea, en cambio, actualmente existe un rajo abierto de 3 km de largo, 1 km de ancho y 500 m de profundidad, por lo que es posible acceder a niveles más profundos y no estudiados del yacimiento.

Clásicamente se ha considerado que el yacimiento está emplazado en rocas de la secuencia volcánica de Mantos Blancos (SVMB; Chávez, 1985), nombre informal aplicado a un conjunto de rocas estratiformes de tipo intermedio a

ácido, aparentemente restringido a las inmediaciones del Distrito minero de Mantos Blancos. Este mismo autor obtuvo edades K-Ar (en hornblenda) de 147±13 Ma 149±13 Ma en diques que cortan la secuencia volcánica, permitiendo asignar a estas una edad mínima, correspondiente al Jurásico superior. Sin embargo, otros autores han asignado estas rocas al Triásico (Espinoza et al., 1996). Debido a la intensa alteración hidrotermal que afecta estas rocas, no se ha podido establecer con claridad su edad por metodos radiométricos y no han sido llevados a cabo estudios petrogenéticos, que permitan comprender su génesis y su potencial relacion con la mineralización.

La edad de la mineralizacion – alteración hidrotermal es tambien motivo de debate. Tassinari et al. (1993) propone una edad torno a los ~150 Ma, mediante una errorcrona Rb-Sr en rocas alteradas. Por otra parte, edades radiométricas previas, realizadas por Munizaga et al. (1991) indican que la alteración hidrotermal sódica en el yacimiento ocurrió entre los 145-147 Ma ($^{40}Ar/^{39}Ar$ en albita).

La mayoría de los depósitos de Cu en la Cordillera de la Costa del norte de Chile, se localizan alrededor de cuerpos intrusivos subvolcánicos porfídicos que incluyen gabros, dioritas, monzodioritas y granodioritas que constituyen diques, filones-mantos y stocks. Generalmente estos intrusivos son estériles y en algunos de los depósitos cortan cuerpos mineralizados (Buena Esperanza, Lince-Estefanía, Santo Domingo). Sin embargo, también existen filones-mantos mineralizados en Mantos Blancos, Santo Domingo y Rencoret (Boric et al., 1990).

En el caso particular de Mantos Blancos existen distintos cuerpos intrusivos que se encuentran ocasionalmente mineralizados, la edad de estos es incierta, al igual que su relación con la mineralización. No existe conocimiento de cuales son las zonas alimentadoras de la mineralización. Por lo tanto, aún no es claro el origen y a que tipo de depósito corresponde Mantos Blancos.

En este contexto se espera contribuir con este trabajo de tesis al conocieminto de la geología, petrogénesis y metalogénesis del yacimiento Mantos Blancos.

I.2 Objetivos

El objetivo central de este trabajo de Tesis es desarrollar un modelo conceptual integrado sobre el origen y evolución del yacimiento Mantos Blancos, determinando las características de los procesos de evolución magmática y establecer el rol genético con la mineralización hidrotermal.

Para esto se han planteado diversos objetivos específicos:

- Carcterizar la geología, mineralización y alteración de yacimiento, en base a los nuevos antecedentes disponibles.
- Determinar la evolución química de los fluidos causantes de la alteración hidrotermal en Mantos Blancos
- Determinar la edad de las rocas intrusivas y de la alteración-mineralización en el distrito Mantos Blancos.
- Determinar la evolución magmática desde la fuente hasta el nivel de emplazamiento de los intrusivos en el distrito Mantos Blancos.
- Estudiar el rol de los cuerpos intrusivos del distrito en la génesis de la mineralización, centrado en la transición magma-fluido hidrotermal.
- Caracterizar el control estructural del depósito y los distintos eventos de deformación ocurridos.

I.3 Metodología general

La metodología empleada para alcanzar los objetivos mencionados anteriormente, consistió en aproximadamente 100 dias de trabajo en terreno donde se efectuó la descripción y caracterización de las unidades geológicas presentes en el área de estudio, la alteración hidrotermal y la mineralización. Se usó el análisis de inclusiones fluidas para caracterizar la evolución de los fluidos hidrotermales, además de datos de isótopos estables (C – O en calcita y S en sulfuros). Además se realizó un estudio de geocronología (U-Pb en

circones) para determinar la edad de las rocas de caja de la mineralización y de $^{39}Ar/^{40}Ar$ (en colaboracion con V. Oliveros, datos presentados en su tesis de doctorado; Oliveros, 2005) para establecer la edad de la alteración-mineralización y cuerpos intrusivos cercanos al yacimiento. Por otra parte, se realizó un análisis de inclusiones fundidas (*melt inclusions*), isótopos de Sr-Nd y geoquímica de roca total para establecer la evolución magmática de las rocas presentes en el yacimiento y la potencial relación de los cuerpos intrusivos con la mineralización. Por último, se efectuó un estudio paleomagnético para caracterizar los distintos eventos de deformación ocurridos en el yacimiento.

I.4 Hipótesis de trabajo

La mayoría de los depósitos estratoligados, en la Cordillera de la Costa de la región de Antofagasta, están asociados a brechas hidrotermales alimentadoras de la mineralización (Ej.: Buena Esperanza, Lince-Estefanía, Inán-Zar, Gimena, Santo Domingo), en los cuales dichas brechas contienen al menos el 50 % de la mineralización comercial y las mas altas leyes de Cu (Palacios, 1990).

Una hipótesis investigada en esta Tesis es que el yacimiento Mantos Blancos tendría un origen epigenético, relacionado al emplazamiento de intrusivos de tamaños discretos y a la formación de brechas ígneas-hidrotermales, de edad Jurásico superior - Cretácico inferior. Los fundamentos que sustentan esta hipótesis son la gran cantidad de cuerpos intrusivos (con y sin mineralización) que se observan en Mantos Blancos, las edades radiométricas disponibles y al hecho de que la mayoría de los depósitos estratoligados, en la Cordillera de la Costa de la región de Antofagasta, están asociados a brechas ígneas-hidrotermales alimentadoras de la mineralización.

En el Capítulo II de la presente tesis se sugiere un origen magmático para el yacimiento Mantos Blancos, probablemente debido a procesos de despresurización y brechización magmático-hidrotermal inducida por la interacción de magmas composicionalmente contrastantes. En el capitulo III se intenta probar esta hipótesis mediante el estudio de inclusiones fundidas,

geoquímica y análisis isotópicos de Sr-Nd. Los fundamentos que sustentan esta hipótesis son las observaciones petrográficas y de campo que sugieren mezcla o interacción de dos tipos de magmas en Mantos Blancos. Además, datos isotópicos disponibles en estas rocas y de rocas alteradas en el depósito, indican que los fluidos hidrotermales en el yacimiento serían más radiogénicos que los magmas del arco Jurásico en la región.

Otra hipótesis investigada en esta Tesis es que el yacimiento presenta una larga y compleja historia de deformación, la cual enmascara la geometría original de los cuerpos mineralizados. Los fundamentos que sustentan esta hipótesis son las claras evidencias de desplazamiento que muestran cuerpos mineralizados, importantes rotaciones horarias registradas en el yacimiento (tanto en rocas mineralizadas como en estériles) (Tassara et al., 2000) y a nivel regional (Arraigada et al., 2003), las claras evidencias de deformación en la Cordillera de la Costa ocurridas desde el Jurásico hasta el presente.

I.5 Organización del presente trabajo de tesis

Este documento esta dividido en seis capítulos. El capítulo I, presenta la exposición del del problema estudiado, da cuenta de los objetivos generales y específicos de esta Tesis, la metodología empleada, las hipótesis de trabajo, muestra la estructura que tiene la presente tesis y por último reseña los antecedentes del marco geodinámico del margen activo de Sudamérica durante el Jurásico-Cretácico. Los capítulos II, III y IV corresponden al núcleo central de esta Tesis. En cada uno de estos tres capítulos se presenta una pequeña introducción y fundamentación del trabajo realizado. El cuerpo central de cada uno de estos tres capítulos consta de un artículo publicado/sometido a revistas indexadas. En el capítulo V se presenta una breve discusión de aspectos que no han sido tratados en los capítulos anteriores y el capítulo VI corresponde a las conclusiones de esta tesis. Los contenidos de cada capítulo se describen brevemente a continuación:

I.- INTRODUCCION. En este capítulo se presenta la exposición del del problema estudiado, los objetivos generales y específicos de la presente Tesis, la metodología empleada, las hipótesis de trabajo, muestra además como está estructurado este documento, donde se reseñan los contenidos de cada capítulo y por último se presenta una revisión de los antecedentes geodinámicos del margen activo de Gondwana durante el Jurásico-Cretácico inferior, en la región de Antofagasta.

II.- GEOLOGIA, MINERALIZACION Y ALTERACION DEL YACIMIENTO MANTOS BLANCOS. Este capítulo describe los antecedentes metalogénicos regionales y del distrito minero de Mantos Blancos, y la fundamentación del trabajo realizado. El cuerpo central de este capítulo es un manuscrito denominado "*The Mantos Blancos copper deposit: An Upper Jurassic breccia-style hydrothermal system in the Coastal Range of northern Chile*". En el cual, se describe la geología, mineralización y alteración del yacimiento Mantos Blancos, además muestra los resultados de estudios de inclusiones fluidas, isotopía estable de azufre, carbono y oxigeno. Este trabajo fue publicado en la revista *Mineralium Deposita V 41, 246-258.*

III.- EVOLUCION MAGMATICA DEL YACIMIENTO MANTOS BLANCOS. Este capítulo describe los antecedentes del magmatismo Jurásico-Cretácico inferior en la región de Antofagasta y la fundamentación del trabajo realizado. El cuerpo central de este capítulo es un manuscrito denominado "*Magmatic evolution of the Mantos Blancos copper deposit, Coastal Range of northern Chile: insight from Sr–Nd isotope, geochemical data and silicate melt inclusions*". Describe la evolución magmática de las rocas ígneas del yacimiento y su relación con la mineralización, mediante el estudio de isótopos de Sr-Nd, geoquímica de roca total y análisis por microsonda de inclusiones fundidas (*melt inclusions*) entrampadas en cuarzos. Este trabajo fue aceptado en la revista *Resource Geology,* actualmente *en prensa.*

IV.- TECTONICA DEL YACIMIENTO MANTOS BLANCOS. Este capítulo describe los antecedentes de estructurales del Jurásico-Cretácico inferior en la región de Antofagasta y el yacimiento Mantos Blancos y la

fundamentación del trabajo realizado. El cuerpo central de este capítulo es un manuscrito denominado "*Structural-Paleomagnetic study in the Mantos Blancos copper deposit: 2D plain view restoration of a dislocated orebody in the Coastal Range of northern Chile*". Describe y caracteriza la deformación ocurrida en el distrito Mantos Blancos, donde se propone la geometría original del yacimiento. Este estudio paleomagnético-estructural fue sometido a la *Revista Geológica de Chile*, y se encuentra en proceso de revisión.

V.- DISCUSION. Se presenta una discusión con respecto a la edad de las rocas riolíticas del yacimiento, la profundidad a la cual ocurrió la mineralización y las condiciones de entrampamiento y significado de los datos de inclusiones fundidas.

VI.- CONCLUSIONES. Presenta las conclusiones que se desprenden de los resultados obtenidos en los capítulos anteriores de la presente tesis.

I.6 Geodinámica del margen activo durante el Jurásico – Cretácico inferior

La Cordillera de los Andes en el norte de Chile corresponde a la sección sur de los Andes Centrales, que ha sido considerada como un ejemplo clásico del desarrollo orogénico a lo largo de un contacto de placas convergentes (Coira et al., 1982, Mpodozis y Ramos, 1990). A comienzos del Jurásico, en el borde oeste de Sudamérica, se desarrolló la subducción de una placa oceánica bajo el supercontinente Gondwana, lo que marcó el comienzo del ciclo Andino (Coira et al., 1982), conformando una estructura de arco-cuenca de tras arco. Actualmente el arco magmático Jurásico se ubica en la Cordillera de la Costa y los depósitos marinos-continentales de la cuenca de tras arco (cuenca de Tarapacá; Mpodozis y Ramos, 1990) en la Depresión Intermedia y en la Cordillera de Domeyko (Figura 1).

Desde el Jurásico inferior, en el margen continental oeste de Sudamérica, se desarrollaron arcos magmáticos sucesivos. El frente magmático sistemáticamente cambió su posición hacia el oriente con el tiempo, y el cambio de la posición del arco magmático fue seguido de periodos de engrosamiento cortical causados por deformación compresiva, por lo que el tectonismo también migró hacia el este con el tiempo (Boric et al., 1990). Básicamente se pueden se pueden reconocer dos etapas principales en la evolución de los Andes en el norte de Chile: i) desde el Jurásico hasta fines del Cretácico inferior, cuando el arco magmático estaba flanqueado por el este por una cuenca de tras arco sedimentaria marina desarrollada en un ambiente extensional y ii) desde el Cretácico superior al presente, cuando el sistema de arco se desarrolló en un ambiente continental, bajo un marco tectónico principalmente compresivo (Maksaev et al., 2007).

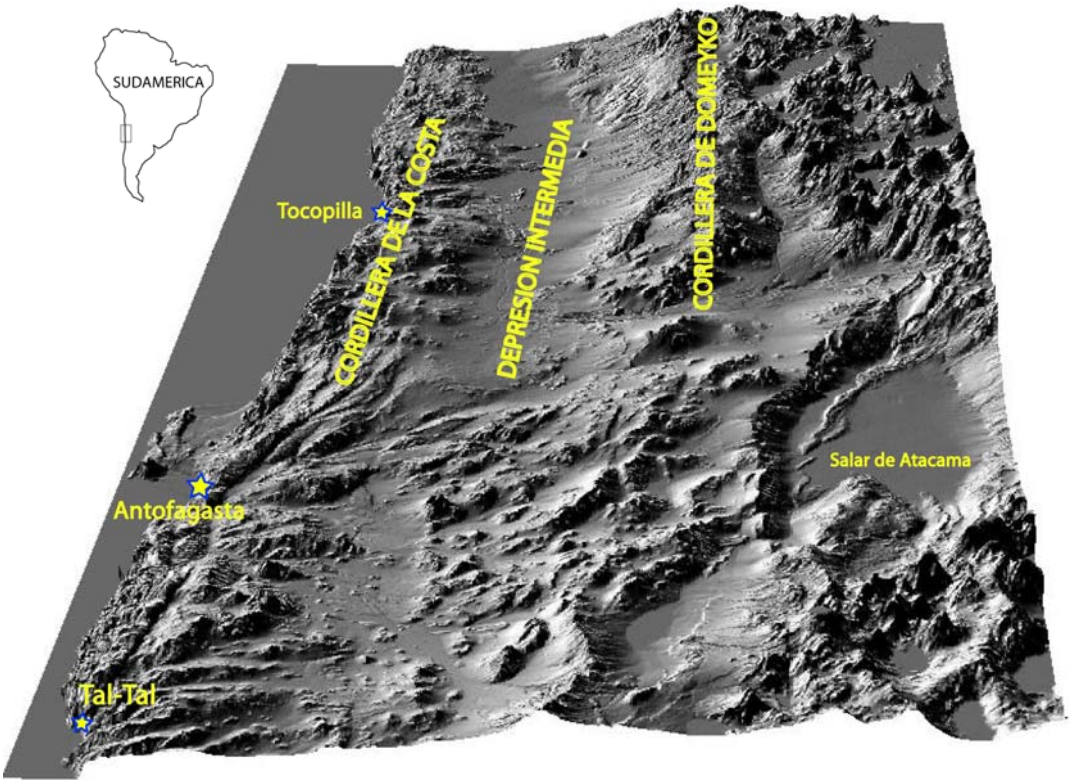

Figura 1. Modelo digital de terreno (SRTM 90m) del norte de Chile.

Gran parte de la Cordillera de los Andes en el norte de Chile se desarrolló sobre un basamento de edad Paleozoico superior - Triásico inferior. Este basamento correspondería a un prisma de acreción y a un sistema de arco relacionado a subducción pre-existente en el borde del supercontinente Gondwana (Mpodozis y Ramos, 1990). El prisma de acreción y arco magmático del Paleozoico superior-Triásico inferior fue remplazado en el Triásico medio a superior por una paleogeografía dominada por cuencas o "*grabens*" delimitados por fallas de dirección NW (Charrier, 1979, Suárez y Bell, 1993, Ramos y Aleman, 2000). La formación de estos "*grabens*" se cree que estuvo relacionada a tectónica extensional que precedió a la fragmentación del supercontinente Gondwana (Mpodozis y Ramos, 1990).

El arco magmático Jurásico-Cretácico de la Cordillera de la Costa del norte de Chile, esta cortado longitudinalmente por zonas miloníticas y cataclásticas de orientación NS, asociadas al Sistema de Fallas de Atacama (SFA), expuestas a

lo largo de la Cordillera de la Costa del norte de Chile entre los 22°S y 29°S (Hervé, 1987; Scheuber y Andriessen, 1990; Grocott et al., 1994; Scheuber y González, 1999).

Este sistema de fallas (SFA) se desarrolló durante el Jurásico al Cretácico inferior como una estructura regional intra-arco relacionada a la subducción oblicua de la placa Aluk (Phoenix) relativa al continente Sudamericano (Figura 2) (Boric et al., 1990: Scheuber y Andriessen, 1990; Scheuber y González, 1999) y posee una larga historia de deformación hasta el presente, actuando principalmente como un sistema de fallas de rumbo sinestral intra-arco (*left-lateral trench-linked fault*) en el Jurásico- Cretácico inferior.

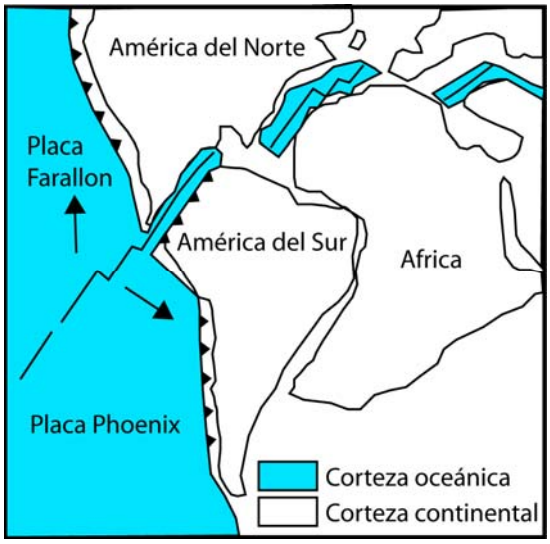

Figura 2. Reconstrucción paleo-geodinámica de la configuración durante el Jurásico-Cretácico inferior del SE de la placa Pacífico (modificado de Scheuber y González, 1999).

En el norte de Chile, durante las primeras etapas extensionales de la evolución Andina se desarrolló mineralización principalmente de cobre tipo estrato-ligado, mientras que depósitos tipo pórfidos cupríferos se desarrollaron y dominaron durante la segunda etapa. Estas dos etapas mayores revelan un cambio sustancial en las condiciones geodinámicas del margen activo durante la

formación orogénica, que también se ve reflejada en la metalogénesis Andina. (Maksaev y Zentilli, 2002).

I.7 Geología de la Cordillera de la Costa (22 - 24ºS)

La Cordillera de la Costa del Norte de Chile está formada principalmente por rocas volcánicas de edad Jurásica, intruidas por granitoides de composición intermedia emplazados entre el Jurásico Inferior y el Cretácico Inferior (Figura 3) (Boric et al., 1990). El volcanismo activo en el Jurásico inferior-medio, permitió la depositación de 5-7 km de una pila volcánica, principalmente compuesta de lavas andesítico-basálticas y tobas (Formación La Negra; García, 1967). Intercalaciones marinas de edad Bajociano dentro de la secuencia volcánica indica una depositación en una cuenca subsidente y que probablemente no se haya formado una cordillera con altos montañosos. Una topografía de bajos relieves ha sido inferida a partir de la observación de que los sedimentos de la cuenca marina de trasarco, que bordea el arco por el este, recibió solo pequeñas cantidades de detritos provenientes de éste (Maksaev y Zentilli, 2002). Ya que el magmatismo en este sector no está asociado con edificios montañosos y engrosamiento cortical, la actividad ígnea debió haber estado acompañada de una importante extensión cortical (Maksaev y Zentilli, 2002). La actividad plutónica, que comenzó cerca de 200 Ma (Boric et al., 1990) permitió la formación de numerosos cuerpos intrusivos de variadas formas y tamaños, desde gabros a granodioritas, la mayoría de los cuales se emplazaron principalmente en la corteza superior (Dallmeyer et al., 1996). De acuerdo con la información radioisotópica existente, el plutonismo tuvo su máxima expresión al fin del Jurásico-principio del Cretácico (160-120 Ma; Boric et al., 1990).

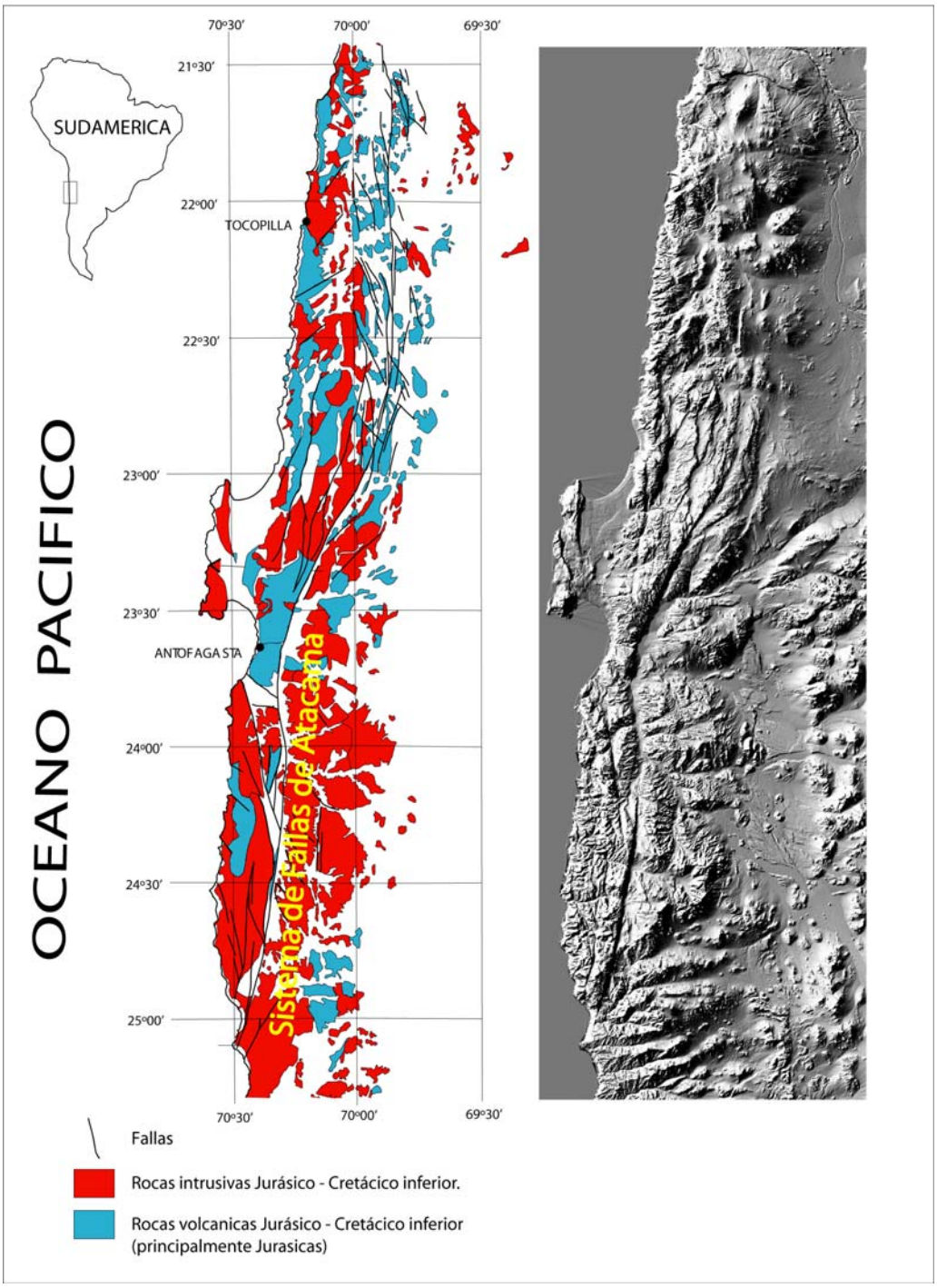

Figura 3. Mapa geológico esquemático de la Cordillera de la Costa del norte de Chile, donde se muestran los afloramientos de las rocas magmáticas que representan el arco del Jurásico-Cretácico inferior (Modificado de Maksaev y Zentilli, 2002). En la imagen de la derecha se muestra un modelo digital de terreno (SRTM 90m), donde se destacan los rasgos principales del SFA.

El arco magmático Jurásico-Cretácico inferior de la Cordillera de la Costa del norte de Chile, está cortado longitudinalmente por zonas miloníticas y cataclásticas de orientación NS asociadas al SFA (Figura 3), el cual posee una historia de deformación que abarca desde el Jurásico inferior al Cenozoico. Scheuber y González (1999) sugieren una evolución tectónica para el Jurásico-Cretácico inferior desarrollada en cuatro etapas (Figura 4): **Etapa I**: volcanismo y plutones emplazados en profundidad contemporáneos a movimientos sinestrales en un régimen de subducción de alto stress y un alto grado de acople sísmico entre las placas. **Etapa II**: intenso emplazamiento somero de plutones sin volcanismo, engrosamiento cortical y extensión normal al arco, y desacople entre las placas (baja tasa de convergencia). **Etapa III**: dilatación oblicua en el arco. **Etapa IIIa**: intrusión de diques orientados NE-SW (extensión NW-SE) indicando desacople en un regimen de subducción de bajo stress. **Etapa IIIb**: intrusión de diques orientados NW-SE (extensión NE-SW) indica un régimen de alto stress. **Etapa IV**: desplazamientos sinestrales a lo largo del Sistema de Fallas de Atacama, indicando un alto grado de acoplamiento en un régimen de subducción de alto stress. Movimientos de rumbo y en el manteo de carácter frágil continuaron intermitentemente a lo largo de SFA desde el Mioceno superior (Hervé, 1987). Desde el Neógeno, en la Cordillera de la Costa del norte de Chile, ha dominado un régimen compresivo N-S que genera estructuras EW de carácter inverso y las estructuras previamente formadas NS han sido reactivadas como normales (González et al., 2003; Allmendinger et al., 2005).

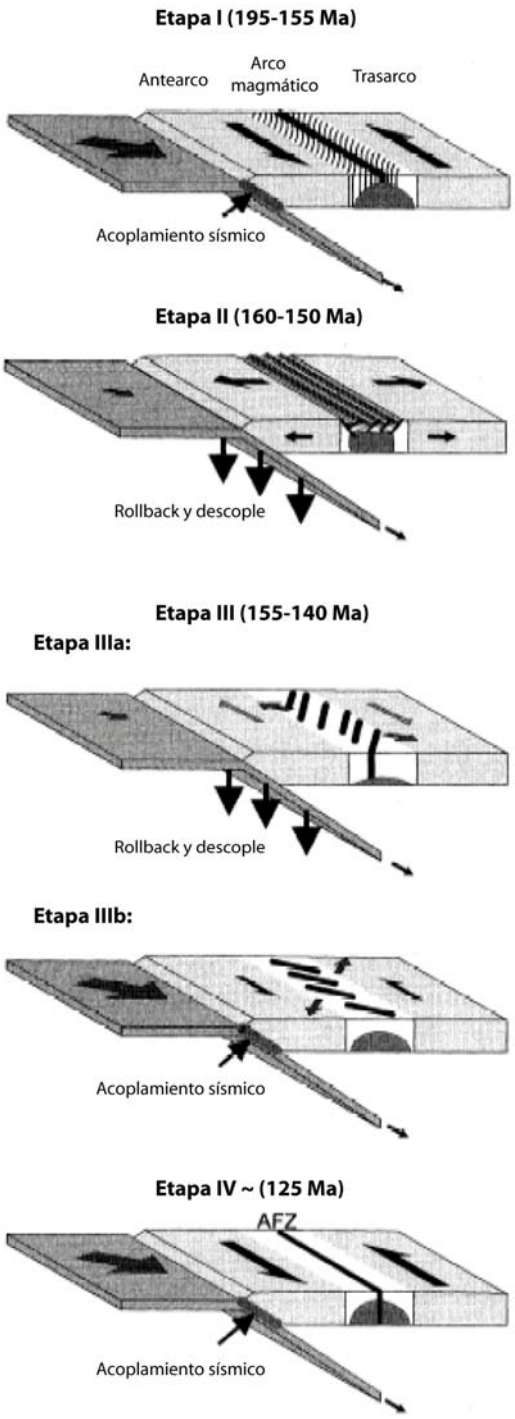

Figura 4. Modelo de evolución tectónica del arco Jurásico-Cretácico inferior y el régimen de subducción. (Modificado de Scheuber y González, 1999).

I.8 Referencias

Allmendinger, R. W., González, G., Yu, J., Hoke, G., Isacks, B., 2005. Trench – parallel shortening in the Northern Chilean Forearc: Tectonic and climatic implications. GSA Bulletin. 117: 89 – 104.

Arriagada C., Roperch P., Mpodozis C., Dupont-Nivet G., Cobbold P. R., Chavin A., Cortés J., 2003. Paleogene clockwise tectonic rotations in the forearc of central Andes, Antofagasta region, northern Chile. J Geophys Res 108 (B1), doi:10.1029/2001JB001598

Boric, R., Díaz, F. & Maksaev, V. 1990. Geología y yacimientos metalíferos de la Región de Antofagasta. Servicio Nacional de Geología y Minería, Boletín 40, Santiago, 246 p.

Coira, B., Davidson, J., Mpodozis, C. and Ramos, V. 1982. Tectonic and magmatic evolution of the Andes of northern Argentina and Chile. Earth Science Reviews, V. 18, pp. 303-332.

Charrier, R., 1979. El Triásico de Chile y regiones adyacentes de Argentina: una reconstrucción paleogeográfica y paleoclimática. Comunicaciones, Santiago, Chile, V. 26, pp.1-37.

Chávez, W. 1985. Geological setting and the nature and distribution of disseminated copper mineralization of the Mantos Blancos district, Antofagasta Province, Chile. PhD Thesis, University at California, Berkeley, USA. 142 pp

Dallmeyer, R.D., Brown, M., Grocott, J., Taylor, G.K., Treolar, P.J. 1996. Mesozoic magmatic and tectonic events within the Andean plate boundary zone, 26º - 27º30`S, North Chile: Constraints from ^{40}Ar / ^{39}Ar mineral ages. J. Geol. 104: 19 – 40

Espinoza S, Véliz H, Esquivel J, Arias J, Moraga A. 1996 The cupriferous province of the Coastal Range, Northern Chile. In: Camus F, Sillitoe RH, Petersen R (eds.) Andean Copper Deposits: New discoveries, mineralization, styles and metallogeny. Econ Geol, Spec Publ 5: 19 – 32

García, F. 1967. Geología del Norte Grande de Chile. In: Symposium sobre el Geosinclinal Andino, Soc. Geológica de Chile, Santiago, Nº 3

González, G., Cembrano, J., Carrizo, D., Macci, A., Schneider, H. 2003. The link between forearc tectonics and Pliocene – Quaternary deformation of the Coastal Cordillera, northern Chile. Journal of South American Earth Sciences, 16: 321 – 342.

Grocott, J., Brown, M., Dallmeyer, R.D., Taylor, G.K. & Treloar, P.J. 1994. Mechanism of continental growth in extensional arcs: An example from de Andean plate-boundary zone. Geology, 22, 391-394.

Hervé, M., 1987. Movimiento sinistral en el Cretácico Inferior de la Zona de Falla Atacama al norte de Paposo (24ºS), Chile. Revista Geológica de Chile, Nº 31, pp. 37-42.

Maksaev, V., Zentilli, M. 2002. Chilean stratabound Cu – (Ag) deposits: An overview. In: Potter, T. M. (ed.). Hydrothermal iron oxide copper – gold and related deposits: A global perspective. 2nd PCG Publ.: 185 – 205.

Mpodozis, C., Ramos, V. 1990. The Andes of Chile and Argentina. In : Ericksen, G. E., Cañas, M. T.., Reinemund, J. (eds.). Geology of the Andes and its relation to hydrocarbon and mineral resources. Circum – Pacific Council for Energy and Mineral Resources. Earth Science Series, 11: 59 – 90.

Munizaga F, Ramírez R, Drake R, Tassinari C, Zentilli M. 1991. Nuevos antecedentes geocronológicos del yacimiento Manos Blancos, Región de Antofagasta, Chile. Proc. 6° Congr Geol Chile 1: 221 – 224

Oliveros, V. 2005. Les formations magmatiques jurassiques et mineralisation du nord Chili, origine, mise en place, alteration, metamorphisme: etude geochronologique et geochemie. PhD Thesis. Universite de Nice-Sophia Antipolis, France. 285 pp

Palacios C. 1990. Geology of the Buena Esperanza Copper – Silver deposit, northern Chile. In: Fontbote L, Amstutz G C, Cardozo M, Cedillo E, Frutos J (eds.) Stratabound Ore Deposits in the Andes. Springer – Verlag, pp 313 – 318

Ramos, V. y Aleman, A., 2000. Tectonic evolution of the Andes. In: Cordani, U.G. et al. (editors), Tectonic Evolution of South America, Rio de Janeiro, Brazil, pp. 635-685.

Scheuber, E., Andriessen, P.A.M., 1990. The kinematic and geodynamic significance of the Atacama fault zone, northern Chile. Journal of Structural Geology, V. 12, No 2, pp. 243-257.

Scheuber, E., González, G. 1999. Tectonics of the Jurassic – Early Cretaceous magmatic arc of the North Chilean Coastal Cordillera (22º - 26ºS): A story of crustal deformation along a convergent plate boundary. Tectonics 18: 895 – 910

Tassara, A.; Roperch, P.; Pavez, A. 2000. Paleomagnetismo de los Yacimientos Mantos Blancos y Manto Verde: Implicancias Tectónicas y Cronológicas. Actas IX Congreso Geológico Chileno. V2. p. 166 – 170.

Tassinari, C., Munizaga, F., Ramírez, R. 1993. Edad y geoquímica isotópica Rb-Sr del yacimiento de cobre Mantos Blancos: relación temporal con el magmatismo jurásico. Rev Geol Chile 20: 193 – 205.

II. GEOLOGÍA, MINERALIZACIÓN Y ALTERACIÓN DEL YACIMIENTO MANTOS BLANCOS

II.1 Antecedentes metalogénicos regionales

Las rocas volcánicas e intrusivas relacionadas al arco magmático del Jurásico-Cretácico inferior en la Cordillera de la Costa del norte de Chile, hospedan numerosos depósitos de cobre y constituyen un metalotecto cuprífero distintivo. Los más importantes son los depósitos estratoligados de cobre hospedados en rocas volcánicas (Ej.: Mantos Blancos, Buena Esperanza, Michilla, Santo Domingo) y sistemas de vetas cupríferas de rumbo NE a ENE hospedadas por intrusivos granodioríticos-dioríticos del Jurásico Superior (Ej.: Minita-Despreciada, Toldo-Velarde, Naguayán-Desesperado; Boric et al., 1990). Recientemente se ha descrito la presencia de yacimientos del tipo pórfido cuprífero, en la vertiente oriental de la cordillera de la Costa (Buey Muerto-Antucoya, Puntillas- Galenosa; Boric et al., 1990; Pacci, 1991; Arellano, 2003; Perelló et al., 2003) (ver Figura 5).

En los yacimientos estratoligados de cobre hospedados en rocas volcánicas, la mineralización hipógena, está caracterizada por calcosina y bornita con cantidades menores de calcopirita, covelina y digenita. Estos yacimientos típicamente presentan contenidos subordinados de plata. La ganga incluye cuarzo, hematita, pirita, clorita y calcita (Losert 1973; Chávez 1985; Palacios 1986, 1990). Esta alteración local se cree que está sobreimpuesta sobre una alteración/metamorfismo regional (facies prehnita-actinolita) de la secuencia

volcánica, pero el contraste es pequeño o nulo entre la alteración de las rocas volcánicas mineralizadas y estériles (Boric et al., 1990).

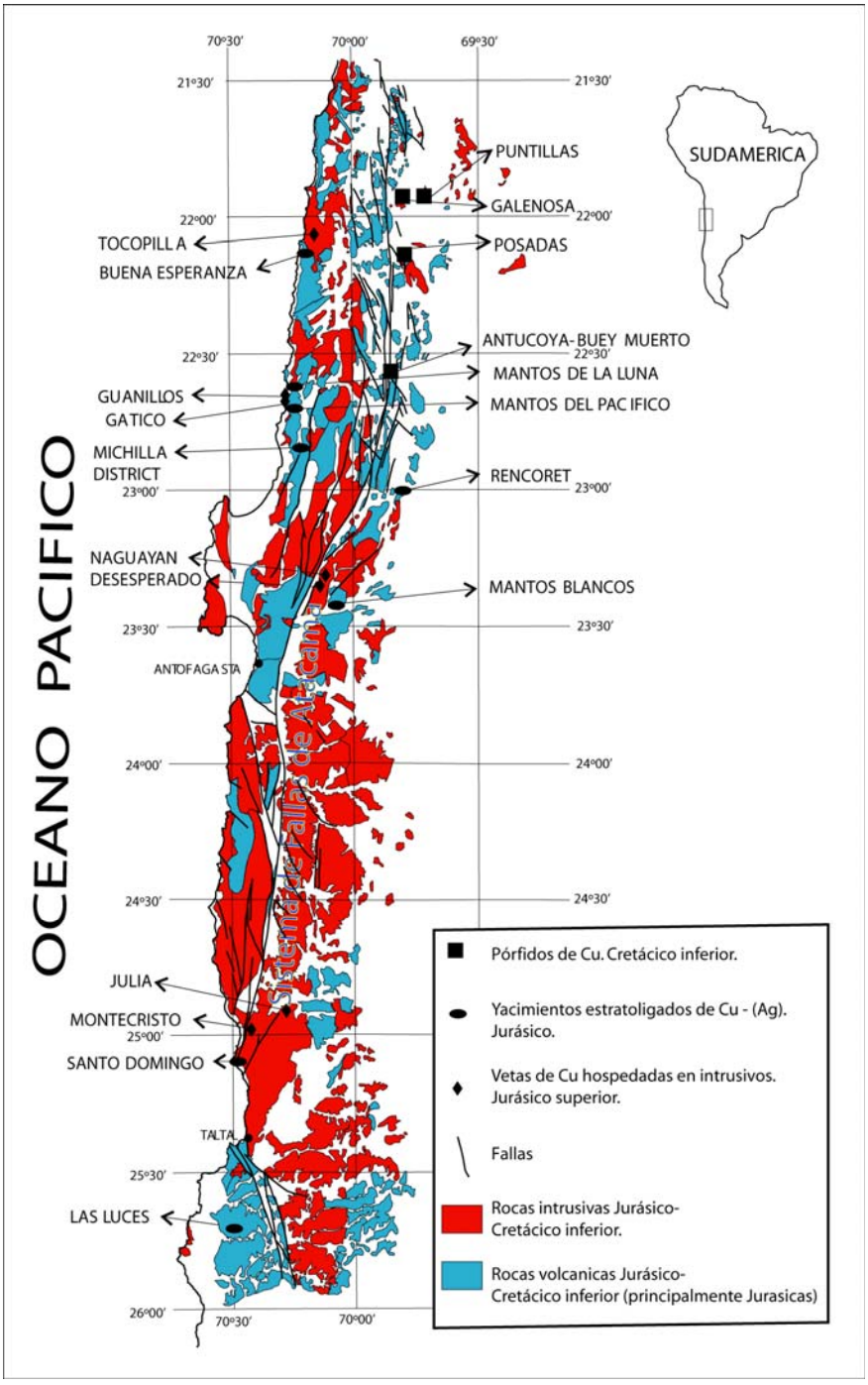

Figura 5. Mapa geológico esquemático de la Cordillera de la Costa del norte de Chile, donde se muestra la ubicación de los principales yacimientos de cobre (Modificado de Maksaev y Zentilli, 2002).

En cuanto a la edad de estos depósitos existen escasas dataciones radiométricas K-Ar y Rb-Sr, que indican que la mayoría de estos depósitos se formaron entre los 150-140 Ma (Boric et al., 1990; Venegas et al., 1991; Tassinari et al., 1993; Vivallo y Henríquez, 1998). Este rango de dataciones radiométricas es mas joven que las rocas volcánicas que albergan la mineralización, las que han sido datadas por los métodos Rb-Sr y K-Ar en el rango 186-165 Ma, pero coinciden con edades $^{40}Ar/^{39}Ar$, Rb-Sr y K-Ar de batolitos graníticos que intruyen la secuencia volcánica (compilación de edades en Oliveros, 2005). Sin embargo, dataciones recientes realizadas por el método $^{40}Ar/^{39}Ar$ (Oliveros, 2005) indican un rango de edad Jurásico superior para el volcanismo en la región de Antofagasta (ver Figura 6).

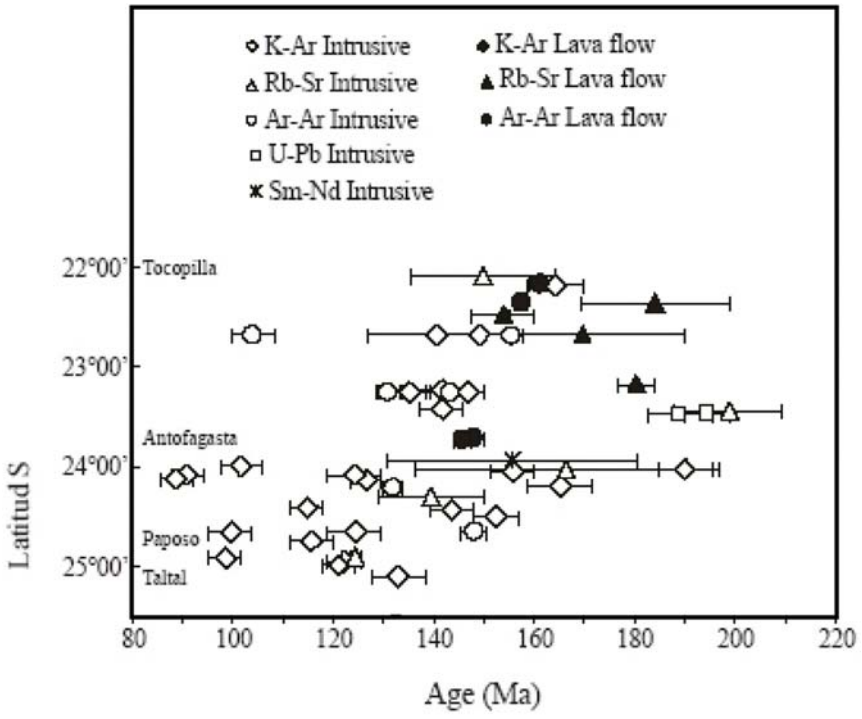

Figura 6. Compilación de edades radiométricas en la Cordillera de la Costa entre los 22° y 25,5°S (modificado de Oliveros, 2005).

Inicialmente los depósitos estratiformes fueron considerados como singenéticos y de origen exhalativo (Ruiz et al., 1971). Estudios posteriores, sugieren un origen epigenético, dado el hallazgo de cuerpos mineralizados discordantes, la relación espacial de la mineralización cuprífera en torno o dentro de stocks, diques y sills del Jurásico Superior, más una significativa alteración hidrotermal (albita, clorita, cuarzo, sericita, calcita, esfeno, escapolita, anatasa) asociada a una diseminación de sulfuros ricos en cobre (calcosina, bornita) dentro de las rocas volcánicas mineralizadas (Sato, 1984; Dreyer y Soto, 1985; Espinoza et al., 1996). Sin embargo, todavía prevalecen distintas hipótesis para el origen de estos depósitos hospedados en rocas volcánicas: a) diagenético-metamórfica (Sato 1984; Sillitoe, 1990), b) derivación hidrotermal ligada a cuerpos intrusivos subvolcánicos (Chávez, 1985; Palacios, 1986), c) formados por fluidos hidrotermales mixtos movilizados durante la intrusión y enfriamiento del batolito costero (Maksaev and Zentilli, 2002) y d) formados por fluidos no magmáticos, probablemente una mezcla de aguas meteóricas con aguas provenientes de la secuencia sedimentaria de la Formación La Negra, calentadas por una fuente magmática (Kojima et al., 2003).

Vivallo y Henríquez (1998) plantearon, en base a una comparación química e isotópica, que los depósitos estratoligados de cobre en rocas volcánicas Jurásicas tendrían un origen hidrotermal común con las vetas mesotermales de cobre del Jurásico Medio a Superior emplazadas en batolitos Jurásicos de la Cordillera de la Costa de Antofagasta (Minita-Despreciada, Toldo-Velarde, Naguayán-El Desesperado, Julia, Montecristo). Según estos autores representarían los conductos hidrotermales más profundos de los sistemas que habrían mineralizado las lavas suprayacentes.

Datos de inclusiones fluidas salinas (hasta 35 % peso NaCl eq.) de Buena Esperanza, en calcita con sulfuros de cobre y cuarzo en amígdalas han dado temperaturas de homogenización entre 65º-195ºC y 130º-235ºC, respectivamente y presiones mínimas de formación del orden de 285-315 bares (Nisterenko et al., 1973). Posteriormente, Palacios (1990) reportó la presencia de inclusiones fluidas hipersalinas en cuarzo del intrusivo gabroico de Buena

Esperanza con temperaturas de homogenización entre 440º y 500ºC, sugiriendo que este cuerpo fue la fuente del calor y fluidos mineralizadores cuya temperatura decrece hacia fuera. Los isótopos de azufre de las menas indican un rango restringido de $\delta^{34}S$ entre -0,1 y -2,1 $^{o}/_{oo}$ sugiriendo una derivación magmática de este elemento.

II.2 Antecedentes geológicos y metalogénicos del Distrito Minero de Mantos Blancos

El mayor y más importante de estos yacimientos estratoligados de cobre, en el norte grande de Chile, es Mantos Blancos que se ubica 45 km al NE de la ciudad de Antofagasta, en la Cordillera de la Costa de la II Región (Figura 5). Está emplazado en rocas de la secuencia volcánica de Mantos Blancos (SVMB; Chávez, 1985), nombre informal aplicado a un conjunto de rocas estratiformes de tipo intermedio a ácido, aparentemente restringido a las inmediaciones del Distrito minero de Mantos Blancos. Este mismo autor obtuvo edades K-Ar (en hornblenda) de 147±13 Ma 149±13 Ma en diques que cortan la secuencia volcánica, permitiendo asignar a estas una edad mínima, correspondiente al Jurásico superior. Sin embargo, otros autores han asignado estas rocas al Triásico (Espinoza et al., 1996). La mineralización primaria en Mantos Blancos corresponde a calcopirita, bornita, calcosina y pirita, diseminadas y según pequeñas vetillas (Chávez, 1985), que forman cuerpos irregulares de geometría lenticular y sigmoidal a pequeña escala, con tendencia estratoligada a nivel del yacimiento. Es posible distinguir cierta zonación, con bornita en la parte central de los cuerpos y pirita predominando en la periferia. Los óxidos de cobre también son importantes, apareciendo atacamita, crisocola, malaquita y antlerita, en ese orden de abundancia. (Orrego et al., 2000).

La alteración hidrotermal en el yacimiento Mantos Blancos ha sido descrita por Chávez (1985) y Ramírez (1991), como moderada, dejando evidencias de la textura de la roca original. Según estos autores, ésta se presenta en cuatro

tipos principales: Sódica, representada por albitización de los feldespatos y albita en venillas; cloritización; intensa hematitización que se presenta como especularita diseminada o como hematita roja y silicificación generalizada que se manifiesta en agregados microcristalinos de cuarzo en la masa fundamental de las rocas. Además, existe calcita concentrada en algunas áreas del distrito, reemplazando fenocristales y como vetillas. La ganga está limitada a escasas vetas tardías de calcita-baritina-cuarzo, que contienen diseminación gruesa de calcopirita, pirita, galena y esfalerita. La edad de la alteración hidrotermal ha sido propuesta por Tassinari et al. (1993) mediante una errorcrona Rb-Sr en torno a los ~150 Ma. Por otra parte, edades radiométricas previas realizadas por Munizaga et al. (1991) indican que la albitización ocurrió entre los 145-147 Ma ($^{40}Ar/^{39}Ar$ en albita). Inclusiones fluidas en cuarzo y calcitas con sulfuros de Mantos Blancos, poseen temperaturas de homogenización ente 225º-400ºC y salinidades entre 8 y 17 % peso NaCl eq. (Collao, 1993).

Isótopos de azufre en sulfuros de cobre en Mantos Blancos (Sasaki et al., 1984; Vivallo y Henríquez, 1998), indican un origen magmático para este elemento. Otros estudios isotópicos (Tassinari, et al., 1993), concluyen que los fluidos que dieron origen a la mena de Mantos Blancos serían magmáticos, en mezcla con fluidos meteóricos o provenientes de la roca de caja durante el proceso de mineralización.

II.3 Fundamentación del trabajo realizado

Como se expone en el Capitulo I (Exposición del problema estudiado), la mayoría de los depósitos estratoligados, en la Cordillera de la Costa de la región de Antofagasta, están asociados a brechas hidrotermales alimentadoras de la mineralización (Ej.: Buena Esperanza, Lince-Estefanía, Inán-Zar, Gimena, Santo Domingo), en los cuales dichas brechas contienen al menos el 50 % de la mineralización comercial y las mas altas leyes de Cu (Palacios, 1990). A pesar de que Chávez (1985) describe el yacimiento Mantos Blancos como un "*depósito de Cu diseminado*", en revisiones recientes ha sido considerado el

representante más grande de esta clase de depósitos (Espinoza et al., 1996; Maksaev y Zentilli, 2002; Maksaev et al., 2007).

Aunque existen varios trabajos y estudios realizados en el yacimiento (e.g. Chavéz, 1985; Munizaga et al., 1991; Tassinari et al., 1993; Pizarro, 1997; Orrego et al., 2000), aún no es clara la génesis y a que tipo de depósito corresponde Mantos Blancos, tampoco se sabe con certeza la edad de las rocas de caja ni la edad de la mineralización. El rol genético que juegan los distintos cuerpos intrusivos que afloran en el distrito, y en el depósito, en la mineralización tampoco se ha podido establecer con claridad. En este capitulo se presentan nuevos antecedentes realcionados a la geología, mineralización y alteración del yacimiento y se plantea una discusión con respecto a la génesis del depósito.

II.4 Referencias

Arellano, M. 2003. Distribución y control de la mineralización del pórfido cuprífero Antucoya, II Región. Chile. B.Sc. Thesis. Departamento de Ciencias Geológicas. Universidad Católica del Norte, Antofagasta. Chile. 81 p.

Boric, R., Díaz, F., Maksaev, V. 1990. Geología y yacimientos metalíferos de la Región de Antofagasta. Servicio Nacional de Geología y Minería, Boletín 40, Santiago, 246 p.

Chávez, W. 1985. Geological setting and the nature and distribution of disseminated copper mineralization of the Mantos Blancos district, Antofagasta Province, Chile. PhD Thesis, University at California, Berkeley, USA. 142 pp

Collao, S., 1993. Inclusiones Fluidas en el Yacimiento Mantos Blancos. Inedito, Departamento de Ciencias de la Tierra, Universidad de Concepción, Concepción, Chile, 27 p.

Dreyer, H. y Soto, H. 1985. Geología de Mina Susana, un yacimiento novedoso en Carolina de Michilla. 4° Congreso Geológico Chileno, Antofagasta, Chile, 2, 3 354-3 382.

Espinoza S, Véliz H, Esquivel J, Arias J, Moraga A. 1996 The cupriferous province of the Coastal Range, Northern Chile. In: Camus F, Sillitoe RH, Petersen R (eds.) Andean Copper Deposits: New discoveries, mineralization, styles and metallogeny. Econ Geol, Spec Publ 5: 19 – 32

Kojima, S., Astudillo, J., Rojo, J., Tristá, D., Hayashi, K. 2003. Ore mineralogy, fluid inclusion, and stable isotopic characteristics of stratiform copper deposits in the Coastal Cordillera of northern Chile. Mineralium Deposita, 38, 208–216.

Losert, J. 1973. Genesis of copper mineralization and associated alterations in the Jurassic volcanics rocks of Buena Esperanza mining area. Publicación N°40, Departamento de Geología, Universidad de Chile, Santiago, 104 p.

Maksaev, V. y Zentilli, M. 2002. Chilean strata-bound Cu-(Ag) deposits: an overview; In: Porter, T.M. (ed.) Hydrothermal iron oxide copper-gold & related deposits: a global perspective, v. 2, PGC Publishing, Adelaide, 185-205.

Maksaev, V., Townley, B., Palacios, C. and Camus, F. 2007. Metallic ore deposits. In: Moreno T. and Gibbons, W. (eds) The Geology of Chile. The Geological Society, London, p. 179-199.

Munizaga F, Ramírez R, Drake R, Tassinari C, Zentilli M. 1991. Nuevos antecedentes geocronológicos del yacimiento Manos Blancos, Región de Antofagasta, Chile. Proc. 6° Congr Geol Chile 1: 221 – 224

Nisterenko, G.V., Losert, J., Chavez, L. y Naumov, V.B. 1973. Temperaturas y presiones de formación de algunos yacimientos cupríferos de Chile. Revista Geológica de Chile, 1, 74-84.

Oliveros, V. 2005. Les formations magmatiques jurassiques et mineralisation du nord Chili, origine, mise en place, alteration, metamorphisme: etude geochronologique et geochemie. PhD Thesis. Universite de Nice-Sophia Antipolis, France. 285 pp

Orrego, M., Robles, W., Sanhueza, A., Zamora, R., Infanta, J. 2000. Mantos Blancos y Manto Verde: Depósitos del tipo Fe-Cu-Au? Una comparación con implicancias en la exploración. Actas IX Congreso Geológico Chileno. V2. p. 145 - 149

Pacci, D. 1991. El sistema de cobre porfírico Galenosa, NE de Tocopilla. Norte de Chile: Un modelo diorítico. Actas VI Congreso Geológico Chileno: p.142-145.

Palacios, C. 1986. Subvolcanic copper deposits in the Coastal Range of northern Chile. Zentralblatt für Geologie und Paläontologie, Stuttgart, Teil I, 1985, H.9/10, 1605-1615.

Palacios C. 1990. Geology of the Buena Esperanza Copper – Silver deposit, northern Chile. In: Fontbote L, Amstutz G C, Cardozo M, Cedillo E, Frutos J (eds.) Stratabound Ore Deposits in the Andes. Springer – Verlag, pp 313 – 318

Perelló, J., Martini, R., Arcos, R., Muhr, R. 2003. Buey Muerto: porphyry copper mineralization in the early Cretaceous arc of northern Chile. Proc. 10th Congreso Geológico de Chile. Electronic version.

Pizarro, J., 1997. Estudio geológico de la unidad dacita cuarcifera del yacimiento Mantos Blancos, Antofagasta-Chile. B.Sc. Thesis, Departamento de Geología, Universidad de Chile, Santiago, 87 p.

Ramírez, R., 1991. Diseño, Desarrollo e Implementación del Sistema Computacional para Manejo de Datos Geológicos en el Yacimiento Mantos Blancos. Memoria de Prueba. Facultad de Ciencias Físicas y Matemáticas, Departamento de Geología y Geofísica, Universidad de Chile.

Ruiz, C., Aguilar, A., Egert, E., Espinosa, W., Peebles, F., Quezada, R. & Serrano, M. 1971. Strata-bound copper sulphide deposits of Chile. In: Proceedings IMA-IAGOD, 7th General Meeting, Tokyo-Kyoto, Japan, 1970. Society Mining & Geology Japan, Special Issue 3, 252-260

Sasaki A, Ulriksen C, Sato K, Ishihara S. 1984. Sulphur isotope reconnaissance of porphyry copper and manto type deposits in Chile and the Philippines. Bull Geol Survey of Japan 35: 615 – 622.

Sato, T. 1984. Manto type copper deposits in Chile: a review. Bulletin of the Geological Survey of Japan. 35, 565-582.

Sillitoe, R.H. 1990. Copper Deposits and Andean Evolution. In: Ericksen, G.E., Cañas, M.T., & Reinemund, J.A. (eds) Geology of the Andes and its relation to hydrocarbon and mineral resources, Circum-Pacific Council for Energy and Mineral Resources, Earth Science Series, 11, 285-311.

Tassinari, C., Munizaga, F., Ramírez, R. 1993. Edad y geoquímica isotópica Rb-Sr del yacimiento de cobre Mantos Blancos: relación temporal con el magmatismo jurásico. Rev Geol Chile 20: 193 – 205.

Venegas, R., Munizaga, F., Tassinari, C. 1991. Los yacimientos de Cu-Ag del Distrito de Carolina de Michilla, Región de Antofagasta, Chile: nuevos antecedentes geocronológicos. 6° Congreso Geológico Chileno, Viña del Mar, Chile, 1, 452-455.

Vivallo, W. y Henriquez, F. 1998. Genesis comun de los yacimientos estratoligados y vetiformes de cobre del Jurásico Medio a Superior en la Cordillera de la Costa, Region de Antofagasta, Chile. Rev Geol Chile 25:199 – 228

II.5 Articulo 1: “The Mantos Blancos copper deposit: an upper Jurassic breccia – style hydrothermal system in the Coastal Range of northern Chile”

Ramírez, L. E., Palacios, C., Townley, B., Parada, M.A.,

Departamento de Geología, Universidad de Chile. P.O. Box 13518 - 21, Santiago. Chile.

Sial, A. N.

NEG LABISE Department of Geology, Federal University of Pernambuco. C. P. 7852, Recife-PE 50.732-970, Brazil.

Fernandez-Turiel, J. L.

Institute of Earth Sciences J. Almera, CSIC, Sole i Sabaris, 08028, Barcelona. Spain.

Gimeno, D., Garcia-Valles, M.

Faculty of Geology, University of Barcelona. Marti i Franques, 08028, Barcelona. Spain.

Lehmann, B.

Institut für Mineralogie und Mineralische Rohstoffe, Technische Universität Clausthal, Adolph Roemer Strasse 2 A, D-38678 Clausthal-Zellerfeld, Germany.

Communicating author:
L. E. Ramírez
E-mail: lramirez@cec.uchile.cl
Phone: 56 2 9784536
Fax: 56 2 6963050.

Abstract

The Upper Jurassic Mantos Blancos copper deposit (500 Mt @ 1.0 % Cu), located in the Coastal Range of northern Chile, displays two superimposed hydrothermal events. An older phyllic alteration probably related to felsic magmatic-hydrothermal brecciation at ~155 Ma, and younger (141 – 142 Ma) potassic, propylitic and sodic alterations, coeval with dioritic and granodioritic stocks and sills, and dioritic dikes. Main ore formation is genetically related to the second hydrothermal event, and consists of hydrothermal breccias, disseminations and stockwork style mineralization, associated with sodic alteration. Hypogene sulfide assemblages show distinctive vertical and lateral zoning, centered on magmatic and hydrothermal breccia bodies, which constitute the feeders to mineralization. A barren pyrite root zone is overlain by pyrite-chalcopyrite, and followed upwards and laterally by chalcopyrite-digenite or chalcopyrite-bornite. The assemblage digenite - supergene chalcocite characterizes the central portions of high-grade mineralization in the breccia bodies. Fluid inclusions show evidence of boiling during the potassic and sodic alteration events, which occurred at temperatures around 450-460ºC and 350-410ºC, and salinities between 3-53 and 13-45 wt. % NaCl eq., respectively. The hydrothermal events occurred during episodic decompression, due to fluid overpressuring, hydrofracturing, and sharp changes from lithostatic to hydrostatic conditions. Sulfur isotope results of hypogene sulfide minerals fall in a narrow range around 0 per mil, suggesting a dominance of magmatic sulfur. Carbon and oxygen isotopic data of calcites from propylitic alteration suggest a mantle-derived carbon and oxygen isotope fractionation due to low temperature alteration.

Keywords: Cu mineralization, Upper Jurassic, Coastal Range, Northern Chile.

Introduction

This paper presents the results of a comprehensive and updated study of the Mantos Blancos ore deposit, in the Coastal Range of northern Chile (Fig. 1). Pre-mining resources of this deposit are estimated at 500 million metric tons with 1.0 % Cu, of which 200 million tons were extracted between 1960 and 2002 (Maksaev and Zentilli, 2002). The remaining ore reserves stand at 142 million tons with 0.86 % Cu, and a resource of 156 million tons with 0.89 % Cu (Anglo Base Metals Report, May 2003). The Coastal Range is host to Upper Jurassic to Lower Cretaceous copper deposits of volcanic-hosted strata-bound type, and Cretaceous, generally heavily eroded porphyry type systems, which constitute a NS-trending metallogenetic province (Camus, 2003). The volcanic-hosted strata-bound orebodies are mainly associated with hydrothermal breccia feeder structures, in which the hydrothermal breccias contain at least 50% of the economic mineralization and the highest ore grades. The hydrothermal breccias are coeval with barren and generally incipiently altered stocks and sills of mainly dioritic composition, and are intruded by late mineralization dioritic dikes. Sulfide mineralization consists of chalcocite, digenite, bornite, chalcopyrite, and pyrite related to sodic hydrothermal alteration (Palacios, 1990; Wolf et al., 1990). Most of these deposits are relatively small, with resources between 10 to 50 million tons grading 1% Cu (Espinoza et al., 1996). The porphyry copper type mineralization is associated with granodioritic porphyries and hydrothermal breccias, in which the hypogene mineralization consists of chalcopyrite, pyrite, and minor bornite and molybdenite, and occurs coeval with potassic and phyllic alteration (Camus, 2003). The Mantos Blancos orebody, located 30 km NE of Antofagasta, was described in the past as disseminated copper mineralization in a bimodal rhyolite-andesite sequence by Chávez (1985), but in general has been considered as a strata-bound Cu deposit in recent reviews (Espinoza et al., 1996; Maksaev and Zentilli, 2002). No detailed studies have been performed since 1985, when Mantos Blancos comprised a series of open pits and underground mines. During the past 20 years, the mine has been transformed into a large open pit operation, which now provides much better geological exposures and more detailed information. The aim of this

paper is to present new data on the geology, hydrothermal alteration and mineralization, fluid inclusions, and stable isotopes, and to discuss the metallogeny and origin of the deposit.

Tectonic and geologic setting

During the Jurassic to Early Cretaceous, a subduction-related magmatic belt was established along the present Coastal Range of northern Chile. It is represented by a 7000 m thick basaltic to andesitic volcanic pile (La Negra Formation) and granitic to dioritic plutonic rocks. The volcanic sequence evolved with time from an initial stage of tholeiitic affinity to a calc-alkaline composition (Palacios, 1984; Rogers and Hawkesworth, 1989; Pichowiak et al., 1990; Kramer et al., 2005). Based on radiometric age data and paleontological arguments, the extrusive event occurred between the Lower Jurassic to the Oxfordian (Rogers and Hawkesworth, 1989; Gelcich et al., 2004; Kramer et al., 2005). The Jurassic volcanic pile was deposited without significant relief building, indicating considerable crustal subsidence, probably related to crustal thinning in an extensional setting (Dallmeyer et al., 1996; Maksaev and Zentilli, 2002). The intrusive rocks, also of calc – alkaline composition, include granites, tonalites, granodiorites and diorites of Lower Jurassic to Early Cretaceous age (200 – 130 Ma; Scheuber and González, 1999; Oliveros, 2005). Tectonic evolution of the Coastal Range during the Jurassic is interpreted in terms of coupling and decoupling between the subducting oceanic and overriding continental plates (Scheuber and González, 1999). From 195 to 155 Ma, an intra-magmatic belt was widespread, spatially related to the north–south–trending, sinistral strike-slip dominant Atacama Fault Zone. However, at the end of Jurassic time, due to foundering of the subducting plate, subduction rollback and decoupling, an east-west - trending extensional regime developed. At the end of the Jurassic to the Early Cretaceous seismic coupling of the subducted plate is suggested by the return of the sinistral strike – slip style of deformation (Scheuber and González, 1999).

Geology of the deposit

Rock units recognized within the Mantos Blancos ore deposit consist of a rhyolitic dome and its magmatic-hydrothermal breccias, intruded by dioritic and granodioritic stocks and sills. The dioritic and granodioritic stocks locally grade upwards into magmatic-hydrothermal breccias. These rock units are all mineralized to variable degrees. Late mafic dikes crosscut all previously mentioned rock units and are essentially barren. All the above rock units are informally grouped as the Mantos Blancos Igneous Complex (MBIC; Fig. 2). The local structural framework at deposit scale is characterized by three groups of faults: 1) NE - and NW - trending subvertical faults with evidence of sinistral and dextral movements respectively, 2) NS / 50º - 80º W normal faults, and 3) NS / 50º - 80º E normal faults. The MBIC consists of the following major rock units:

Rhyolitic porphyry dome

The central part of the deposit consists of a rhyolitic dome (Figs. 2 and 3). The dome structure is partially preserved in the open pit walls, but its geometry has been roughly defined from drill core logs and samples of the early stages of exploitation of the ore deposit (Chávez 1985), and later lithological modeling. Due to pervasive alteration, the contacts between different internal flows are very difficult to observe, however near-horizontal and vertical flow laminations are typical, varying between 1 to 4 cm in thickness. West of the pit, the felsic dome is intercalated with felsic tuffs and andesitic lava flows, and is intruded by dioritic and granodioritic sills. The rhyolitic dome consists of a rhyolite porphyry with fragments of corroded quartz and feldspar phenocrysts (1-5 mm) in an intensively altered felsic groundmass.

Rhyolitic Magmatic-Hydrothermal breccia system

Several sub-vertical monomictic and matrix-supported rhyolitic magmatic and hydrothermal breccia bodies, have been recognized within the felsic dome intrusion (Figs. 2 and 3). They consist of irregular bodies, about 100 to 250 m in vertical extent, and semi-oval to circular sections, 50 to 100 m in diameter.

The matrix is composed of rhyolitic rock flour with intense alteration and disseminated sulfide minerals (Fig.4 A). The fragments are altered, irregular in shape, poorly sorted and vary in size between 1 cm and several m. In the centre of the ore deposit, the rhyolitic magmatic and hydrothermal breccias are intruded by late dioritic to granodioritic magmatic-hydrothermal breccias.

Bimodal stock and sill system

The rhyolite dome is intruded by a subvolcanic complex of porphyritic dioritic and granodioritic stocks and sills. At least five gently dipping sills of both rock types occur in the mine, varying in thickness between 10 and 50 m. The feeder relationship between the stocks and sills has been locally observed (Fig. 3). The granodiorite porphyry is composed of 10 to 30% phenocrysts of hornblende, plagioclase, quartz and biotite, in a groundmass of quartz, feldspars, biotite, and hematite microlites. The diorite porphyry has 5 to 10% pyroxene and minor amphibole phenocrysts in a groundmass of fine-grained pyroxene, plagioclase and magnetite. In both rock types the porphyritic texture grades to aphanitic near the intrusive margins. The diorite porphyry has mm-size amygdules filled with quartz and quartz-sulfide. Mutual intrusive relationships between both granodioritic and dioritic rocks are common, and enclaves of one in the other have been frequently observed. The dioritic enclaves show convolute to flame-like contacts (Fig. 4 B) with the host granodiorite, whereas the granodioritic enclaves exhibit sharp or brecciated contacts with the surrounding diorite. Backveining between the two lithological types is also observed. Recent $^{40}Ar/^{39}Ar$ data on amphibole provide ages of 142.18 ± 1.01 Ma for the granodiorite, and 141.36 ± 0.52 Ma for the diorite (Oliveros, 2005).

Dioritic to granodioritic Magmatic-Hydrothermal breccia system

Two polymictic and matrix-supported pipe-like magmatic-hydrothermal breccias hosted within the ryolitic dome, at the top of some dioritic and granodioritic stocks and spatially related with NS-trending faults, are recognized (Figs. 3 and 4 C, D, E). The central and largest breccia body is cross cut by at least three metric-size sills; two dioritic and one granodioritic in composition. The breccias form near-vertical bodies, with a vertical extent of about 700 m, and diameters

between 100 and 500 m. It is likely that these bodies did not reach the upper levels of the ore deposit, as they were not observed and described in the earlier study by Chávez (1985). The upper part of the breccia pipes exhibit hydrothermal characteristics as evidenced by the presence of a matrix mainly composed of hydrothermal gangue and ore minerals. The breccia consists of altered angular and subrounded fragments of the rhyolitic dome, and the granodioritic and dioritic porphyries. They are poorly sorted and range in size from 1 cm to 15 m. Downwards in the breccia bodies, magmatic features are progressively evident with granodioritic fragments in an altered and mineralized dioritic matrix, as well as dioritic fragments in a granodioritic matrix (Fig. 4 F).

Mafic dyke swarm

Intruding all the rock units in Mantos Blancos deposit, partially altered late-ore dioritic dikes were emplaced. They are subvertical and have orientations preferentially NNE, and subordinate NS-NNW. The dikes are 1 to 12 m wide and represent about 15% of the total rock volume in the deposit. They exhibit porphyritic texture, composed of 10 – 25% phenocrysts of altered plagioclase, amphibole and minor pyroxene, in a very fine-grained groundmass of feldspar, amphibole, and minor biotite and magnetite. An $^{40}Ar/^{39}Ar$ date on amphibole from a late-mineral dike in the mine has an age of 142.69 ± 2.08 Ma (Oliveros, 2005).

Hydrothermal Alteration and Mineralization

Two hydrothermal events have been recognized, based on superimposition of alteration minerals and relationship between different stages of veinlets. The first event is represented by the rhyolitic magmatic – hydrothermal brecciation hosted by the rhyolitic dome. The second event, which represents the main stage of mineralization, is hosted mostly within the dioritic to granodioritic magmatic – hydrothermal breccias, dioritic sills and the rhyolitic dome, and may be genetically associated with the intrusion of dioritic and granodioritic stocks.

First hydrothermal event

The first hydrothermal event is characterized by the assemblage chalcopyrite, bornite, pyrite, quartz and sericite. This assemblage occurs: 1) disseminated in the matrix of irregular and sub-vertical bodies of rhyolitic magmatic-hydrothermal breccias, 2) planar veinlets, 3) disseminated within the rhyolitic dome and in fragments of the hydrothermal breccias, and 4) as isolated crystals or as rim assemblages within and on quartz phenocrysts of the rhyolitic dome. In the rhyolitic magmatic-hydrothermal breccias, chalcopyrite and bornite are the most abundant sulfides. Around these bodies the sulfides are chalcopyrite and pyrite. The phyllic veinlets contain the sulfide minerals as open space filling within fractures, and often display weak alteration halos of sericite and quartz. Due to the intense and widespread superimposition of the main (second) hydrothermal event, it was not possible to establish the extent and intensity of this first event. It probably extended to all rocks of the rhyolitic dome. An $^{40}Ar/^{39}Ar$ age on sericite from this first hydrothermal event yields an age of 155.11 ± 0.786 Ma (Oliveros, 2005).

Second hydrothermal event

The main hydrothermal alteration and mineralization event at Mantos Blancos is centered on the dioritic to granodioritic magmatic-hydrothermal breccias and is considered syngenetic with both breccia formation and emplacement of the granodioritic and dioritic stocks and sills. The mineralized zone extends discontinuously for 3 km in an EW-direction, has a width of up to 1 km, and depth of 600 m. The hypogene mineralization occurs between the elevations of 720 and 450 m.a.s.l. (Fig. 3). Primary mineralization developed mainly within and around the magmatic-hydrothermal breccia pipes, yet the ore deposit exhibits a discontinuous lateral ore grade distribution. The highest Cu grades occur within the breccias with lateral zoning to progressively lower concentrations. This fact suggests that the magmatic-hydrothermal breccia pipes served as the feeder bodies of the main mineralization. In the second hydrothermal event, the early alteration stage was potassic and propylitic, followed by sodic alteration. The potassic and propylitic mineral assemblages

are centered on the dioritic to granodioritic magmatic-hydrothermal breccias, affecting all lithologies of the deposit. These alteration types developed pervasively, disseminated, filling amygdules within the dioritic sills, and as weak halos around flame-like veinlets that cross-cut the the first generation phyllic veinlets in the rhyolitic dome. The potassic alteration is characterized by K-feldspar, quartz, tourmaline, biotite-chlorite, magnetite, chalcopyrite, digenite and minor pyrite (Fig. 5). Relicts of K-feldspar, tourmaline, and biotite are observed in most locations, suggesting that potassic alteration was initially widespread, but was subsequently overprinted and obliterated by later alteration stages. Dioritic and granodioritic sills, that contain amygdules filled with quartz, chlorite, digenite, chalcopyrite and traces of K-feldspar and tourmaline, intruded the magmatic–hydrothermal breccias. Propylitic alteration occurs extensively in the whole deposit, affecting all of the rocks (including sills and dikes), and overprinting and obliterating the potassic alteration assemblage. It occurs as disseminations and veinlets of quartz, chlorite, epidote, calcite, albite, sericite, hematite and minor chalcopyrite, galena and pyrite. These minerals also fill amygdules within dioritic sills and dikes. Laterally, propylitic alteration consists of quartz, chlorite, epidote and pyrite, forming a ring around the orebody at least 2 km wide. From elevations of 600 m to the upper part of the deposit, a swarm of N 25º-30º E striking and sub-vertical pebble-dikes have been observed. These pebble-dikes are 10 to 20 cm thick and consist of rounded fragments of the rhyolitic dome, dioritic and granodioritic rocks, set in a matrix of quartz, epidote, calcite, galena and pyrite (Fig. 4 G). Both potassic and propylitic alteration were followed by sodic alteration, containin albite (replacing feldspar), hematite, pyrite, chalcopyrite, and Ag-rich digenite, with minor amounts of quartz. This mineral assemblage is very extensive, centered on the magmatic and hydrothermal breccias, and occurs as disseminations, cavity fillings, and sharp veinlets. Sodic alteration and mineralization affected all lithological types between elevations of 500 m to the surface and spatially coinciding with the current commercial ore zone. Above the elevation of 500 m, the dioritic sills that intruded the magmatic–hydrothermal breccias exhibit intense stockwork with a sodic alteration mineral assemblage. As the syn-mineralization granodioritic and

dioritic stocks and sills have been dated at 142.18 ± 1.01 and 141.36 ± 0.52 Ma (Oliveros, 2005), respectively, and a late-ore dike yields an age of 142.69 ± 2.08 (Oliveros, 2005), the age of the main hydrothermal event is constrained between 141-142 Ma.

Supergene oxide mineralization has been mined, with only patches of atacamite, chrysocolla and malachite remaining. This supergene mineralization was described in detail by Chávez (1985). Although he reported primary chalcocite (late within the hypogene assemblage), our data indicates the presence of only secondary chalcocite (Fig. 6). The secondary sulfides are mainly chalcocite (forming zones of high-grade copper mineralization centered over the magmatic - hydrothermal breccia bodies, with bornite-digenite), and weak layers of covellite, together with cuprite-native copper and tenorite.

Fluid inclusions studies

Fluid inclusion studies were carried out on quartz crystals of the second hydrothermal event. Samples include quartz crystals from potassic, propylitic and sodic veinlets, and from potassic and propylitic amygdules of the dioritic sills and stocks. A total of 23 samples were taken from the central part of the deposit (Fig. 7), from which 153 microthermometric measurements of primary inclusions were done. Vertical sampling extends to a depth of 850 m. Heating and freezing experiments were conducted on a Linkam THMS600 stage for homogenization temperatures (T_h) up to 450ºC and on a Linkam TS1500 stage for T_h above 450ºC. The uncertainty for heating runs is about ± 2ºC at 400ºC. Three fluid inclusion types were recognized, following the classification scheme of Nash (1976): I (liquid-dominant inclusions without halite daughters), II (vapor-dominant inclusions without halite daughters), and IIIb (vapor-dominant inclusions with halite daughters). All fluid inclusions types have mostly rounded shapes and ranged from 5 to 15 µm. No evidence was observed for either liquid CO_2 or clathrate formation, freezing point depression measurements rule out the presence of significant CO_2. Apparent salinities are reported in weight

percent NaCl equivalent (wt% eq.), based on the halite solubility equation for halite-saturated inclusions and on the final ice melting temperature for halite-undersaturated inclusions (Bodnar and Vityk, 1994). The fluid inclusion microthermometric data are presented in Table 1 and Fig. 8. The highest temperatures were measured in types II and IIIb inclusions trapped in quartz from veinlets of the potassic alteration assemblage within the matrix of the magmatic-hydrothermal breccia at elevations between 239 and 260 m. The type II inclusions, homogenize between 550º and 608ºC and have salinities of 9.9 to 10.1 wt% NaCl eq., whereas the IIIb-type inclusions have T_h values between 530º and 590ºC and salinities ranging from 52 to 74 wt% NaCl eq. The coexistence of both types of inclusions within the same growth zone of a quartz crystal, is considered as indicative of deposition from boiling fluids. In these brines, T_h (halite) values are at least 60ºC greater than T_h (l-v) values in the same samples (Fig. 9). Fluid inclusions observations of samples from potassic alteration assemblages at elevation of 684 m also display evidence of boiling: Type IIIb inclusions have T_h values between 449º to 464ºC and salinities between 52.4 to 53.5 NaCl eq., and co-exist with vapor-rich type II inclusions (with T_h between 462º and 415ºC, and salinities between 2.5 and 3.3 wt% NaCl eq.). Also in these brines, T_h (halite) values are at least 65ºC greater than T_h (l-v) values in the same samples. Quartz crystals from potassic alteration assemblage in amygdules and veinlets from sills in the diorite contain type I and II inclusions. In these samples, T_h values decrease systematically with an increase in elevation (from an average of 515ºC at 360 m to 365ºC at 720 m). In contrast, salinities remain relatively constant (19 - 22 wt% NaCl eq.). Fluid inclusions associated with propylitic alteration assemblages have been measured in samples from elevations of 720 to 816 m. They correspond to type-I inclusions, in which T_h values vary between 340º and 150ºC and salinities between 9 and 22 wt% NaCl eq.

Fluid inclusions in quartz related to the sodic assemblage were difficult to measure due to the limited amounts of albite-bearing quartz veinlets. Fluid inclusions in quartz obtained from these veinlets in the matrix of the magmatic-hydrothermal breccia at elevations between 696 and 768 m, are mainly of the

types II and IIIb. Evidence of boiling has been recognized at elevations of 696 to 720 m.a.s.l., in which both types of inclusions coexist in growth zones of similar hydrothermal quartz crystals. The brines have T_h values between 349º and 423ºC and salinities ranging between 42 and 48 wt% NaCl eq., whereas the vapor-rich-two phase inclusions have T_h values between 313º and 364ºC and salinities between 13 and 14 wt% NaCl eq. Brines in the same sample exhibit halite dissolution temperatures greater than the vapor homogenization temperatures.

Stable Isotope Studies

Sulfur

Seventeen sulfides samples from the second hydrothermal event were analyzed for $\delta^{34}S$ at the Scientific-Technical Services of the University of Barcelona. Sulfide samples were separated mechanically to obtain splits with 50-80 µg of sulfur. Between 100 and 300 µg of pure sulfide were mixed with V_2O_5 (1:1), homogenized and packed into high purity tin cups. The sulfur isotopic composition was analyzed using a Continuous Flow-Isotope Ratio Mass Spectrometry (CF-EA-IRMS). Samples were combusted in an elemental analyzer (Carlo Erba EA 1108) connected to a Finnigan MAT Delta C gas mass spectrometer via a Finnigan MAT Conflo II interface. Results are expressed in the per mil notation relative to the international Vienna-Canyon Diablo troilite (VCDT) standard. The reproducibility of measurements was ± 0.3‰. The $\delta^{34}S$ values of 11 samples of pyrite, 5 samples of chalcopyrite and 1 sample of digenite are reported in Table 2 and Fig. 10. All samples were taken in the central part of the deposit, between elevations of 450 and 780 m.a.s.l. The analyzed sulfides exhibit $\delta^{34}S$ values ranging from -5 to 1.2 per mil, with a mean value of -1.4‰ and a standard deviation of 1.8‰. Results are similar to those previously reported by Sasaki et al (1984) and Vivallo and Henriquez (1998). Pyrite shows the widest sulfur isotope range in comparison to the Cu-sulfides

and the variation is independent of alteration types or host rock lithology (Fig. 10).

Carbon and Oxygen

Eighteen calcite samples were analyzed for $\delta^{13}C$ and $\delta^{18}O$ at the stable isotope laboratory (LABISE) of the Department of Geology, Federal University of Pernambuco, Brazil. CO_2 gas was extracted from micro-drilled powder, in a high vacuum line after reaction with 100% orthophosphoric acid at 25ºC for one day. CO_2 released, after cryogenic cleaning, was analyzed in a double inlet, triple collector SIRA II mass spectrometer. Results are reported relative to PDB, in per mil notation. The uncertainties of the isotope measurements were better than 0.1‰ for carbon and 0.2‰ for oxygen, based on multiple analyses of an internal laboratory standard (BSC). Values of $\delta^{13}C$ and $\delta^{18}O$ of calcite samples from propylitic alteration stage (of the second hydrothermal mineralization event) are reported in Table 3 and Fig. 11. All samples were taken in the central part of the deposit, between elevations of 172 and 900 m.a.s.l. The carbon isotope values of calcites vary between -4.37 to -6.71 ‰, whereas the $\delta^{18}O$ values fluctuate between 13.08 to 23.49 ‰.

Discussion

Based on available radiometric ages and geological observations described in this study, the Mantos Blancos ore deposit was formed by two superimposed Upper Jurassic hydrothermal events. The older event occurred at ~155 Ma, coeval with the rhyolitic magmatic-hydrothermal brecciation and phyllic alteration. The younger event represents the main hydrothermal mineralization (~141-142 Ma) and is genetically related to dioritic and granodioritic stocks and sills and coeval magmatic-hydrothermal brecciation. Probably, both hydrothermal events contributed to extensive but irregularly-distributed ore grades of hypogene mineralization. High ore grade mineralization is restricted to the upper part of the magmatic-hydrothermal breccias from the second hydrothermal event. The radiometric ages for the two hydrothermal events

reported by Oliveros (2005), agree with previous $^{40}Ar/^{39}Ar$ (total gas in albite) and whole rock Rb–Sr (errorchrons in strongly altered samples) radiometric ages (150-146 Ma; Munizaga et al., 1991; Tassinari et al., 1993).

The younger event is characterized by three types of alteration and mineralization: an early potassic, a propylitic and a late sodic stage. The potassic and propylitic alteration stages occurred coeval with dioritic and granodioritic porphyry stock intrusions, magmatic-hydrothermal breccias and late sill and dike emplacements. The late sodic alteration developed centered around the magmatic-hydrothermal breccias, associated with intense fracturing and brecciation (including in the sills) and the main mineral deposition. The ore grade, alteration and the copper sulfide mineral zoning indicate that the magmatic-hydrothermal breccia bodies represent the feeders to the hydrothermal system. The hydrothermal activity, was followed by the intrusion of a dioritic dike swarm. An indication of local subsidence is the common occurrence of sills intruded by vertical dikes as part of the same magmatic event. Because the magmatic pressure must exceed the least main horizontal stress and the tensile strength of the rock cover in order to form discordant intrusions, these intrusive relationships between sills and dikes are an indication that sufficiently thick magmatic overburden was progressively formed to produce a change of the least principal stress from vertical to horizontal (Parada et al., 1997). As this sill-dike relationship has been observed at Mantos Blancos, it is suggested that the tectonic setting during mineralization corresponded to a local extensional regime, probably related to a transtensional faulting within the Atacama Fault System.

Evidence of boiling associated with potassic alteration has been found in samples up to an elevation of 684 m.a.s.l. At this elevation fluid inclusions T_h values exceed 450ºC. At such temperatures, rocks in the hydrothermal system behave in a ductile manner: with strain rates smaller than 10^{-14}/s, rocks of dioritic or granodioritic compositions behave quasiplastically, making brittle fracturing difficult and allowing fluid pressure to approach lithostatic values (Fournier, 1991; 1999). As a consequence, the magmatic-hydrothermal

breccias most likely did not reach the paleosurface, and the hydrothermal system mostly formed at lithostatic pressure. The hydrothermal fluids within the magmatic-hydrothermal breccias evolved along a cooling trend, as indicated by the fluid inclusion data in quartz of the propylitic assemblage.

The emplacement of dioritic and granodioritic sills crosscutting the magmatic-hydrothermal breccias at different levels, sealed the hydrothermal system, over pressured the fluids, hydrofractured the rocks and produced the sodic boiling. The thermodynamic evolution of brine into the field of gas + solid salt at 350 - 400ºC (conditions under which sodic alteration associated boiling occurred), has important implications regarding the concentration of HCl that may be transported when and if steam escapes into the overlying rocks. Fournier and Thompson (1993) noted an abrupt increase in the concentration of HCl^o in steam when NaCl begins to precipitate at pressures below 300 bars. This increase occurs because hydrolysis reactions that produces HCl^o and NaOH by the reaction of NaCl with H_2O become important only at pressures sufficiently low for halite (and probably also NaOH) to precipitate (Fournier and Thompson, 1993). In addition, an order of magnitude higher HCl^o concentration is obtained at comparable pressures and temperatures when quartz is present. This occurs because quartz reacts with NaOH to form albite at the expense of K-feldspar or plagioclase (Fournier and Thompson, 1993). The limited amounts of quartz-bearing albite veinlets in the deposit support this model.

In addition, as fluids migrated away from the early heat source (the magmatic - hydrothermal breccias) and down a thermal gradient, K-feldspar was the stable alteration mineral, as reflected by potassic alteration. The reverse reaction operated when fluids migrated away from a second heat source (intrusion of sills), conditions under which the albite stability field expanded at the expense of K-feldspar (Hezarkhani et al., 1999; Simmons and Browne, 2000). Both processes probably occurred at Mantos Blancos, in which the entire evolution points to a prograde (potassic and propylitic) - retrograde (sodic) hydrothermal sequence. These results can be interpreted as boiling events and associated

decompression occurring episodically due to fluid over pressuring, hydrofracturing, and sharp changes from lithostatic to hydrostatic conditions.

The sulfur isotopic results from hypogene sulfides suggest a largely magmatic source for sulfide sulfur, and indicate a co-genetic relationship for the analyzed sulfide minerals. C-O isotopes in fresh calcite crystals reported in this paper suggest C of magmatic origin, probably of mantle provenance (Cartigny et al., 1998), and fractionation of O following the trend of low temperature alteration caused by magmatic-hydrothermal fluids.

Acknowledgements

This study was funded by a FONDEF (CONICYT, Chile), grant DO1–1012, awarded to the authors and the Mantos Blancos division of Anglo American Chile. Permission for publication was granted by the University of Chile, the Chilean Government and AngloAmerican Chile. We thank the Mantos Blancos mine geology staff, in special to Jorge Pizarro, with whom we had the pleasure of working. Special acknowledgement to Jens Wittenbrink for his constructive comments to the manuscript. Finally, this paper was improved through the valuable reviews of Shoji Kojima, Robert King and Larry Meinert.

References

Bodnar RJ, Vityk MO (1994) Interpretation of microthermometric data for H2O-NaCl fluid inclusions. In: De Vivo B, Frezzotty ML (eds.) Fluid Inclusion in Minerals: Methods and Applications. VPI Press, Blackburg, Virginia, pp 117 – 130. Camus F (2003) Geología de los sistemas porfíricos en los Andes de Chile. SERNAGEOMIN, Chile, 267 pp

Cartigny P, Harris JW, Javoy M (1998) Eclogitic diamond formation at Jwaneng: No room for a recycled component. Science 280: 1421 – 1424

Chávez W (1985) Geological setting and the nature and distribution of disseminated copper mineralization of the Mantos Blancos district, Antofagasta Province, Chile. PhD Thesis, University at California, Berkeley, USA. 142 pp

Deines P (1989) Stable isotope variations in carbonatites. In: Bell K (ed). Carbonatites – Genesis and Evolution. Unwin Hyman, London, pp. 301 – 359

Dallmeyer, RD, Brown M, Grocott J, Taylor GK, Treolar PJ (1996) Mesozoic magmatic and tectonic events within the Andean plate boundary zone, 26º - 27º30`S, North Chile: Constraints from ^{40}Ar / ^{39}Ar mineral ages. J Geol 104: 19 – 40

Espinoza S, Véliz H, Esquivel J, Arias J, Moraga A (1996) The cupriferous province of the Coastal Range, Northern Chile. In: Camus F, Sillitoe RH, Petersen R (eds.) Andean Copper Deposits: New discoveries, mineralization, styles and metallogeny. Econ Geol, Spec Publ 5: 19 – 32

Fournier RO (1991) The transition from hydrostatic to greater than hydrostatic fluid pressure in present active continental hydrothermal systems in crystalline rock. Geophys Res Lett 18: 955 – 958

Fournier RO (1999) Hydrothermal processes related to movement of fluid from plastic into brittle rock in the magmatic – epithermal environment. Econ Geol 94: 1193 – 1212

Fournier RO, Thompson JM (1993) Composition of steam in the System NaCl – KCl – H2O – quartz at 600ºC. Geochim Cosmochim Acta 57: 4365 – 4375

Gelcich S, Davis DW, Spooner ET (2004) Onset of Early Jurassic magmatism in northern Chile: Precise U – Pb zircon ages for the La Negra Formation and the Flamenco Pluton in the Coastal Cordillera of Chañaral. Proc. IAVCEI General Assembly, Pucón, Chile. Electronic version

Hezarkhani A, Williams – Jones AE, Gammons CH (1999) Factors controlling copper solubility and chalcopyrite deposition in the Sungun porphyry copper deposit, Iran. Mineralium Deposita 34: 770 – 783

Keller J, Hoefs J (1995) Stable isotope characteristics of recent carbonatites. In: Bell K, Keller J (eds). Carbonatite Volcanism. Proc. Volc. 4: 113 – 123

Kramer W, Siebel W, Romer R L, Haase G, Zimmer M, Ehrlichmann R (2005) Geochemical and isotopic characteristics and evolution of the Jurassic volcanic arc between Arica (18º30´S) and Tocopilla (22ºS), North Chilean Coastal Range. Chemie der Erde, Geochemistry 65: 47 – 78

Maksaev V, Zentilli M (2002) Chilean stratabound Cu – (Ag) deposits: An overview. In: Porter TM (ed.) Hydrothermal iron oxide copper – gold and related deposits: A global perspective, 2. PCG Publishing, pp 185 – 205

Munizaga F, Ramírez R, Drake R, Tassinari C, Zentilli M (1991) Nuevos antecedentes geocronológicos del yacimiento Manos Blancos, Región de Antofagasta, Chile. Proc. 6° Congr Geol Chile 1: 221 – 224

Nash JT (1976) Fluid-inclusion petrology. Data from porphyry copper deposits and applications to exploration. USGS Prof Pap 907D, 16 pp

Oliveros, V. (2005) Les formations magmatiques jurassiques et mineralisation du nord Chili, origine, mise en place, alteration, metamorphisme: etude geochronologique et geochemie. PhD Thesis. Universite de Nice-Sophia Antipolis, France. 285 pp

Palacios C (1984) Considerations about the plate tectonic models, volcanism, and continental crust in the Southern part of the Central Andes. Tectonophysics 108: 205 – 214

Palacios C (1990) Geology of the Buena Esperanza Copper – Silver deposit, northern Chile. In: Fontbote L, Amstutz G C, Cardozo M, Cedillo E, Frutos J (eds.) Stratabound Ore Deposits in the Andes. Springer – Verlag, pp 313 – 318

Parada M, Palacios C, Lahsen A (1997) Jurassic extensional tectono-magmatism and associated mineralization of the El Faldeo polymetallic district, Chilean Patagonia: geochemical and isotopic evidence of crustal contribution. Mineralium Deposita 32: 547 – 554

Pichowiak S, Buchelt M, Damm KW (1990) Magmatic activity and tectonic setting of early stages of Andean cycle in northern Chile. Geol Soc Am. Spec Pap 241: 127 – 144

Rogers G, Hawkesworth CJ (1989) A geochemical traverse across the North Chilean Andes: evidence for crust generation from the mantle wedge. Earth and Planet Sci Lett 91: 271 – 285

Sasaki A, Ulriksen C, Sato K, Ishihara S (1984) Sulphur isotope reconnaissance of porphyry copper and manto type deposits in Chile and the Philippines. Bull Geol Survey of Japan 35: 615 – 622

Scheuber E, González G (1999) Tectonics of the Jurassic – Early Cretaceous magmatic arc of the North Chilean Coastal Cordillera (22º - 26ºS): A story of crustal deformation along a convergent plate boundary. Tectonics 18: 895 – 910

Simmons SF, Browne PR (2000) Hydrothermal minerals and precious metals in the Broadlands – Ohaaki geothermal system: Implications for understanding low – sulfidation epithermal environments. Econ Geol 95: 971 – 1000

Tassinari C, Munizaga F, Ramírez R (1993) Edad y geoquímica isotópica Rb-Sr del yacimiento de cobre Mantos Blancos: relación temporal con el magmatismo jurásico. Rev Geol Chile 20: 193 - 205

Taylor HP, Frechen J, Degens ET (1967) Oxygen carbon isotope studies of carbonatites from the Laachersee district West Grmany and Alno district, Sweden. Geochim Cosmochim Acta 31: 407 – 430

Vivallo W, Henriquez F (1998) Genesis comun de los yacimientos estratoligados y vetiformes de cobre del Jurásico Medio a Superior en la Cordillera de la Costa, Region de Antofagasta, Chile. Rev Geol Chile 25:199 – 228

Wolf FB, Fontboté L, Amstutz GC (1990) The Susana copper (- silver) deposit in northern Chile, hydrothermal mineralization associated with a Jurassic volcanic arc. In: Fontbote L, Amstutz G C, Cardozo M, Cedillo E, Frutos J (eds.) Stratabound Ore Deposits in the Andes. Springer – Verlag, pp 319 – 338

Figure captions

Figure 1.- Geological map of the Coastal Cordillera, Northern Chile, and location of the Mantos Blancos ore deposit (star) and the Upper Jurassic volcanic-hosted copper deposits (diamonds) In grey are the Middle to Upper Jurassic volcanic rocks of the La Negra Formation, crosses represent Jurassic plutonic rocks. Modified after Maksaev and Zentilli (2002).

Figure 2.- Geological map of the Mantos Blancos ore deposit.

Figure 3.- E - W profile of the Mantos Blancos ore deposit. For symbols, and location of profile see Fig. 2.

Figure 4.- Photographs of (A) rhyolitic magmatic-hydrothermal breccia, (B) dioritic enclave within the granodiorite showing convolute contacts, (C, D and E) dioritic to granodioritic magmatic-hydrothermal breccias in which hydrothermal features dominate, (F) dioritic to granodioritic magmatic-hydrothermal breccia with dominating magmatic features, and (G) pebble dike.

Figure 5.- Hypogene mineral assemblage of the hydrothermal events at the Mantos Blancos ore deposit.

Figure 6.- Microphotographs of (A) digenite relict in chalcocite, (B and C) digenite with hematite flakes replaced by chalcocite, (D) chalcocite with inclusions of hematite flakes, (E) chalcopyrite replaced by covellite (blue), and (F) native copper in cuprite (red internal reflections in grey) with replacement rim of tenorite.

Figure 7.- N - S profile of the Mantos Blancos deposit showing the location samples used in the fluid inclusions study. For symbols, and location of profile see Fig. 2.

Figure 8.- Homogenization temperature versus salinity of fluid inclusions.

Figure 9.- Halite dissolution temperature versus liquid-vapor homogenization temperature of boiled fluid inclusion samples from potassic and sodic alteration.

Figure 10.- $\delta^{34}S$ (‰) values of sulfides from the main hydrothermal event at the Mantos Blancos ore deposit (A). Diagrams B and C show the types of alteration and host rock, with which the sulfides are related.

Figure 11.- $\delta^{13}C$ (‰) versus $\delta^{18}O$ (‰) diagram showing the distribution of calcites from the Mantos Blancos ore deposit. Fields and arrows after Taylor et al. (1967) and Keller and Hoefs (1995).

Table captions

Table 1.- Microthermometry data of fluid inclusions from the second hydrothermal event.

Table 2.- Sulfur Isotope of sulfides from the main hydrothermal event at the Mantos Blancos ore deposit.

Table 3.- C and O isotope analyses (‰) of calcites from the Mantos Blancos ore deposits.

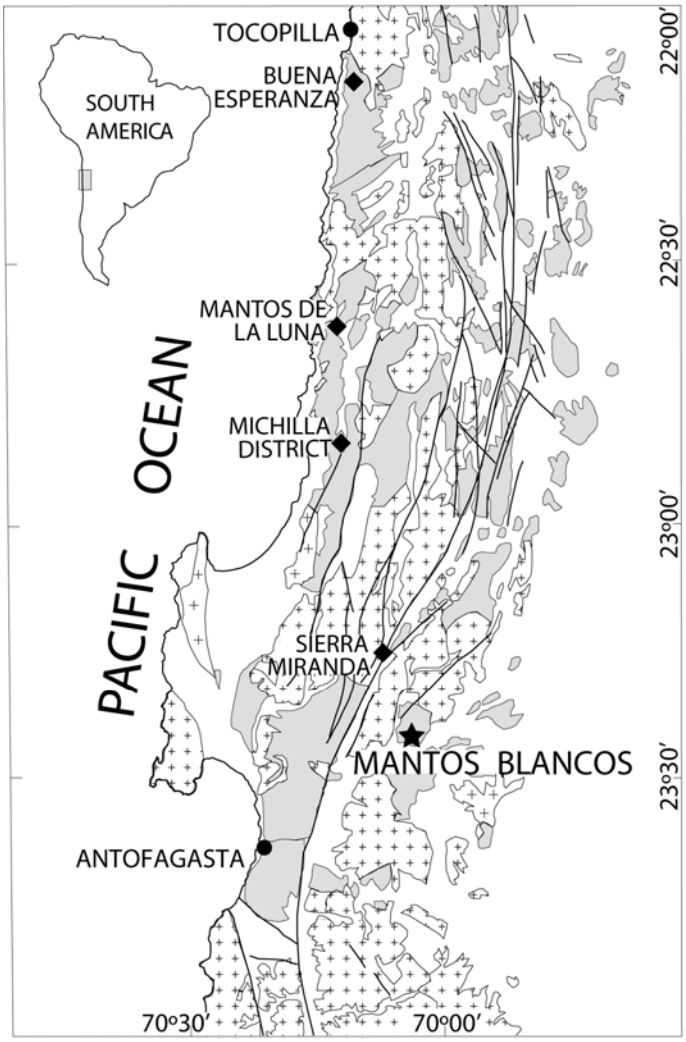
TOCOPILLA
BUENA ESPERANZA
SOUTH AMERICA
MANTOS DE LA LUNA
MICHILLA DISTRICT
PACIFIC OCEAN
SIERRA MIRANDA
MANTOS BLANCOS
ANTOFAGASTA
22°00′
22°30′
23°00′
23°30′
70°30′
70°00′

FIGURE 1

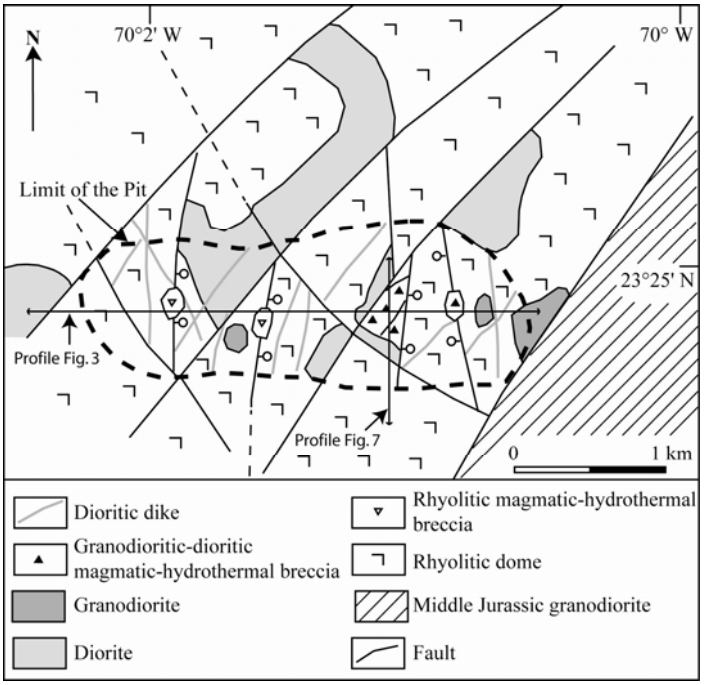
N
70°2' W
70° W
Limit of the Pit
23°25' N
Profile Fig. 3
Profile Fig. 7
0
1 km
Dioritic dike
Granodioritic-dioritic magmatic-hydrothermal breccia
Granodiorite
Diorite
Rhyolitic magmatic-hydrothermal breccia
Rhyolitic dome
Middle Jurassic granodiorite
Fault

FIGURE 2

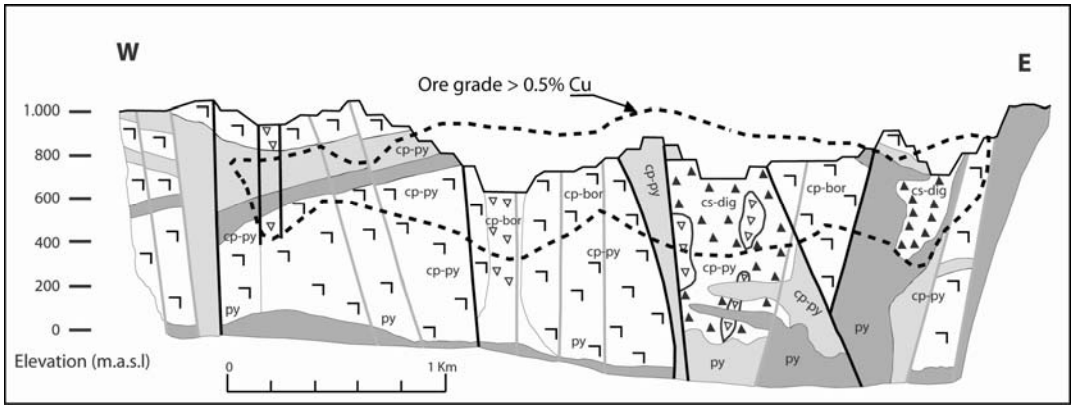
W
E
Ore grade > 0.5% Cu
1.000
800
600
400
200
0
Elevation (m.a.s.l)
0
1 Km
cp-py
cp-bor
cs-dig
py

FIGURE 3

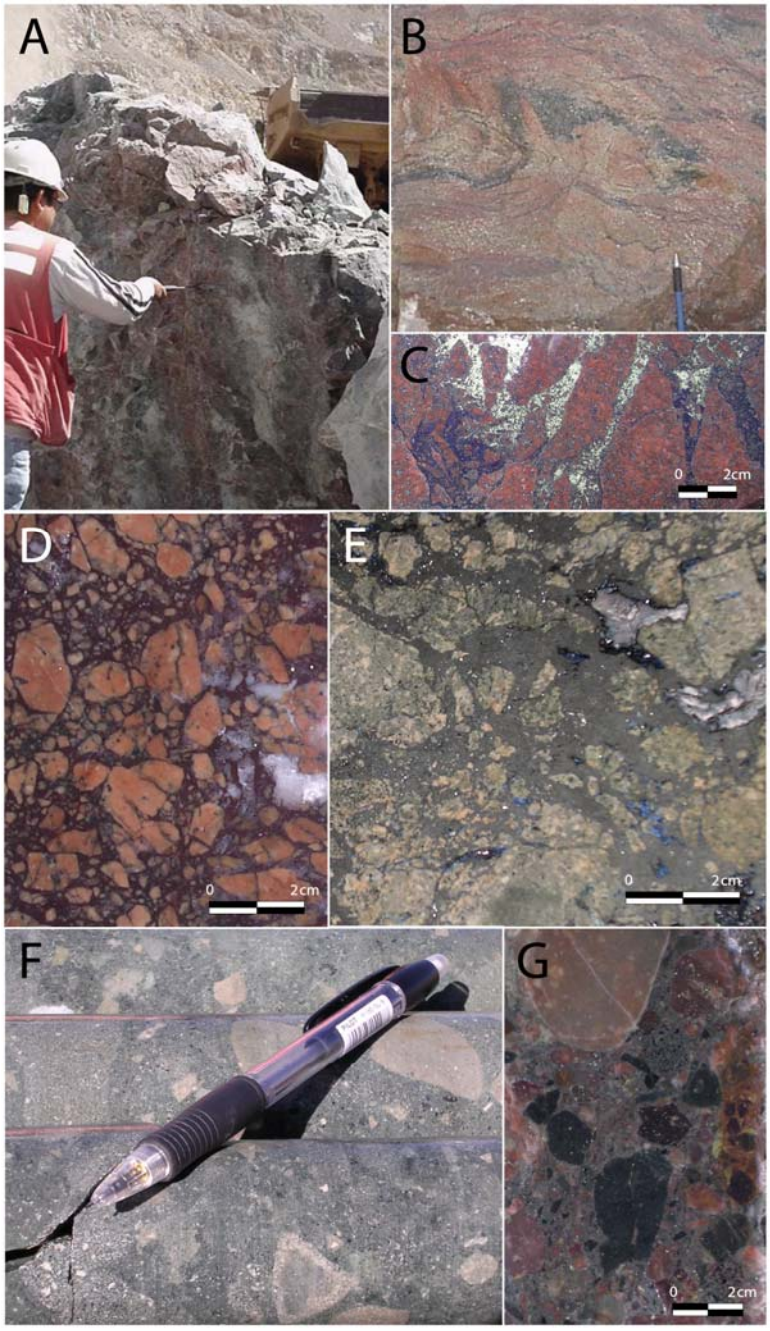

FIGURE 4

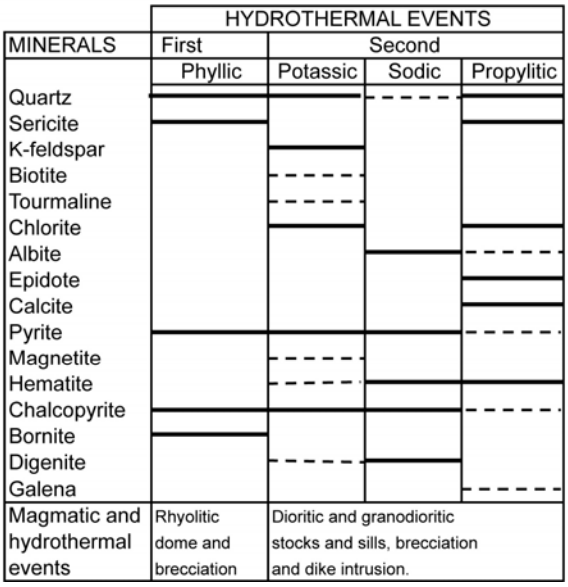
HYDROTHERMAL EVENTS
MINERALS
First
Second
Phyllic
Potassic
Sodic
Propylitic
Quartz
Sericite
K-feldspar
Biotite
Tourmaline
Chlorite
Albite
Epidote
Calcite
Pyrite
Magnetite
Hematite
Chalcopyrite
Bornite
Digenite
Galena
Magmatic and hydrothermal events
Rhyolitic dome and brecciation
Dioritic and granodioritic stocks and sills, brecciation and dike intrusion.

FIGURE 5

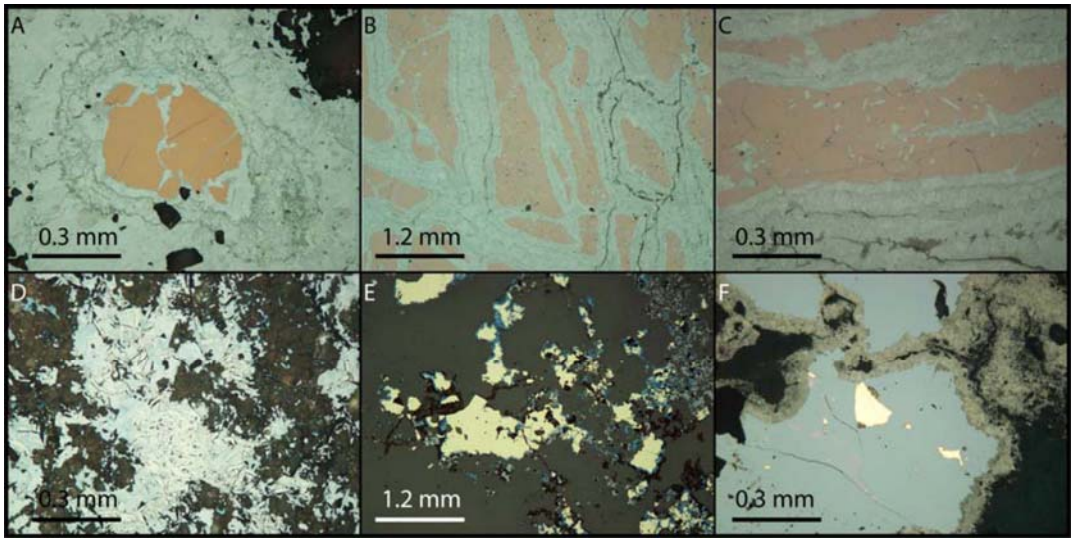

FIGURE 6

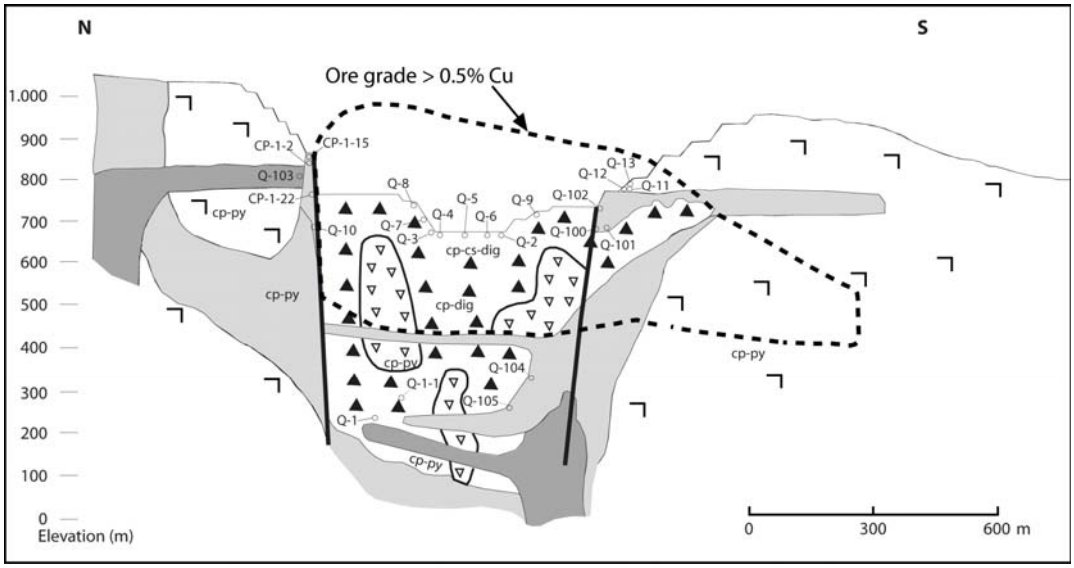
N
S
Ore grade > 0.5% Cu
1.000
900
800
700
600
500
400
300
200
100
0
Elevation (m)
CP-1-2
CP-1-15
Q-103
CP-1-22
cp-py
Q-8
Q-5
Q-9
Q-102
Q-12
Q-13
Q-11
Q-4
Q-6
Q-7
Q-3
Q-10
Q-2
Q-100
Q-101
cp-cs-dig
cp-dig
cp-py
cp-py
cp-py
Q-104
Q-1-1
Q-105
Q-1
cp-py
0
300
600 m

FIGURE 7

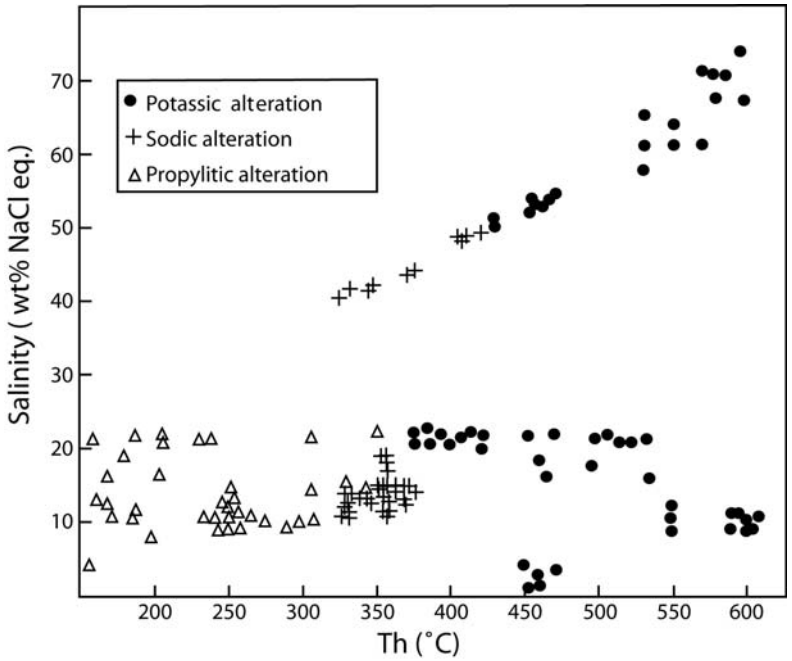
Potassic alteration
Sodic alteration
Propylitic alteration
Salinity (wt% NaCl eq.)
70
60
50
40
30
20
10
200
250
300
350
400
450
500
550
600
Th (˚C)

FIGURE 8

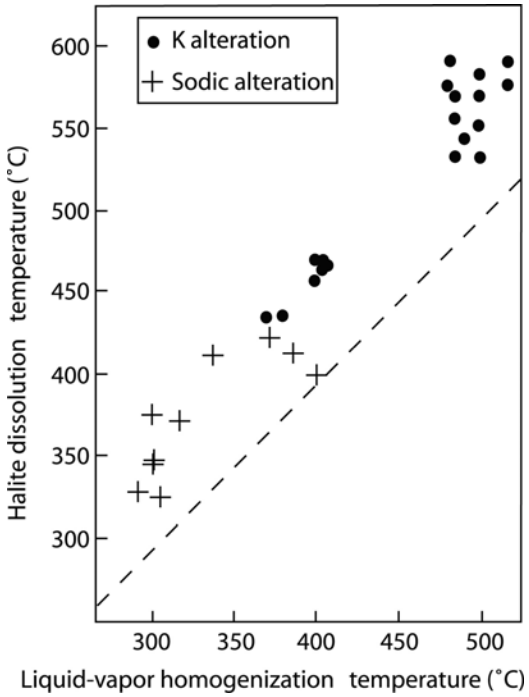
K alteration
Sodic alteration
Halite dissolution temperature (°C)
600
550
500
450
400
350
300
300
350
400
450
500
Liquid-vapor homogenization temperature (°C)

FIGURE 9

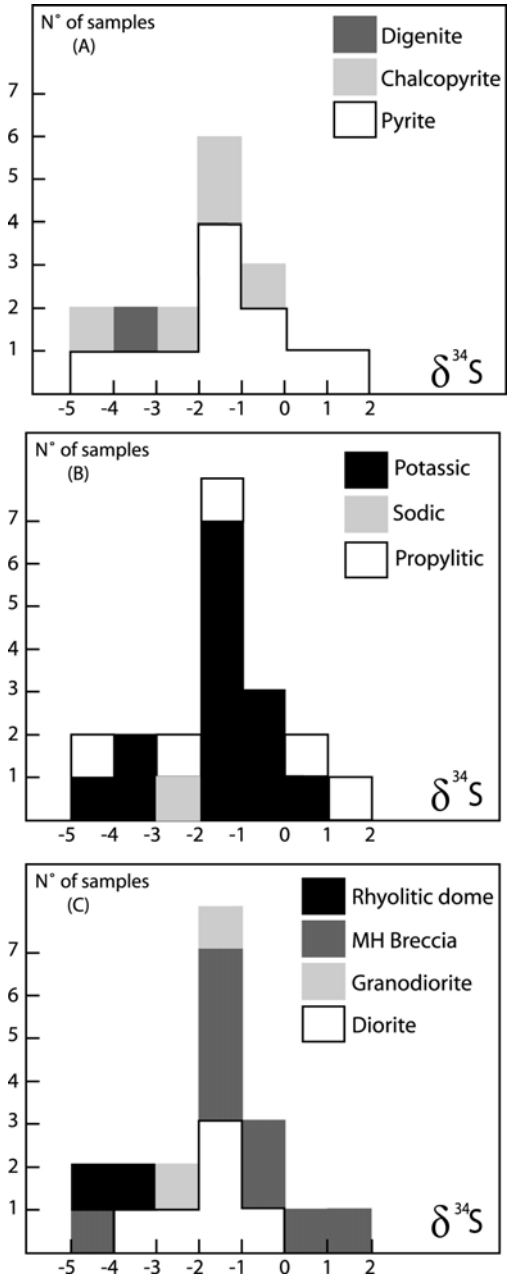
N° of samples
(A)
Digenite
Chalcopyrite
Pyrite
δ34S
N° of samples
(B)
Potassic
Sodic
Propylitic
δ34S
N° of samples
(C)
Rhyolitic dome
MH Breccia
Granodiorite
Diorite
δ34S

FIGURE 10

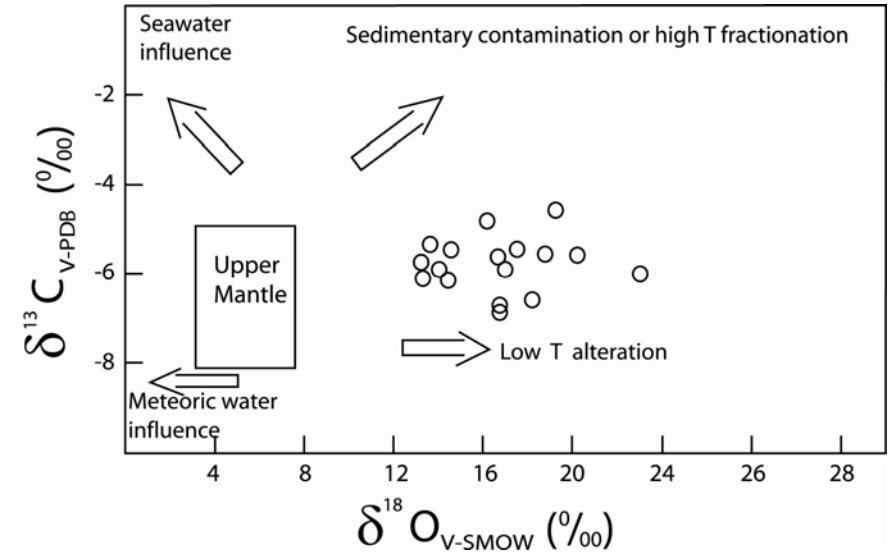
Seawater influence
Sedimentary contamination or high T fractionation
Upper Mantle
Low T alteration
Meteoric water influence
-2
-4
-6
-8
4
8
12
16
20
24
26
28
δ13 CV-PDB (‰)
δ18 OV-SMOW (‰)

FIGURE 11

TABLE 1 MICROTHERMOMETRY DATA OF FLUID INCLUSIONS FROM THE MAIN HYDROTHERMAL EVENT

Sample	elevation (m.a.s.l)	Size (μm)	Th (L-v) (°C)	Th (Halite) (°C)	%L	%V (%in)	% Halite	Tm (ice) (°C)	Salinity (wt% NaCl equiv)	Remarks	N° of inclusions
Q-1	239	5-8	601 ± 7		24 ± 9	76 ± 9		-6.5 ± 0.5	9.9 ± 0.7	Veinlets of K-assemblage in MHB	5
	239	5-9	500 ± 20	580 ± 10	10 ± 5	30 ± 4	60 ± 5		71 ± 3.0		5
Q-104	247	8-10	505 ± 15		20 ± 5	20 ± 5		-18.0 ± 2	19.4 ± 3.0	Veinlets of K-assemblage in sill of dioritic porphyry	9
Q-1-1	260	5-10	564 ± 14	550 ± 20	23 ± 8	77 ± 8		-6.7 ± 0.8	10.1 ± 1.0	Veinlets of K-assemblage in MHB	5
	260	5-10	490 ± 10		20 ± 10	20 ± 10	60 ± 10		62 ± 10.0		7
Q-105	260	8-10	465 ± 12		19 ± 6	81 ± 5		-15.0 ± 3.5	18.5 ± 3.0	Veinlets of K-assemblage in sill of dioritic porphyry	5
Q-2	684	5-10	390 ± 12	449 ± 20	11 ± 4	51 ± 6	38 ± 4		52.4 ± 1.6	Veinlets of K-assemblage in MHB	5
		6-10	462 ± 8		15 ± 10	85 ± 10		-1.5 ± 0.5	2.5 ± 0.8		3
Q-3	684	5-8	404 ± 6	464 ± 6	10 ± 2	50 ± 10	40 ± 8		53.5 ± 0.5	Veinlets of K-assemblage in MHB	3
		10	455 ± 6		10 ± 5	90 ± 5		-2.0 ± 1	3.3 ± 2.5		2
Q-100	720	5-10	413 ± 13		20 ± 10	80 ± 10		-19.4 ± 1.4	22.2 ± 10	Amygdules filled by K-assemblage in dioritic sill	5
Q-101	720	10-15	380 ± 15		25 ± 10	75 ± 10		-19.4 ± 1.4	22.1 ± 10	Amygdules filled by K-assemblage in dioritic sill	5
Q-4	696	8-10	302 ± 16	349 ± 26	15 ± 6	50 ± 5	35 ± 8		42.2 ± 1.9	Veinlets of Albitic assemblage in matrix of MHB	6
		8-10	357 ± 23		10 ± 6	90 ± 6		9.9 ± 0.9	13.9 ± 1.1		5
Q-5	696	8	349 ± 20	349 ± 20	6 ± 5	60 ± 10	35 ± 5		42.3 ± 1.6	Veinlets of Albitic assemblage in MHB	2
		8-15	346 ± 6		9 ± 3	90 ± 7		-9.4 ± 1.2	13.4 ± 1.4		5
Q-6	696	7-10	362 ± 8		10 ± 5	90 ± 5			13.2 ± 1.8	Veinlets of Albitic assemblage in MHB	5
Q-7	708	7-10	356 ± 11		8 ± 2	92 ± 2		-9.7 ± 1.2	14.0 ± 1.4	Veinlets of Albitic assemblage in MHB	5
Q-8	720	8-10	376 ± 25	413 ± 2	10 ± 4	50 ± 2	40 ± 6		47.8 ± 0.3	Veinlets of Albitic assemblage in MHB	3
		5-15	351 ± 23		10 ± 5	90 ± 5		-8.8 ± 1.8	12.6 ± 2.2		3
Q-9	720	8	371	423	8 ± 2	50 ± 4	42 ± 5		48.7	Veinlets of Albitic assemblage in MHB	1
		8-10	313 ± 15		11 ± 7	89 ± 4		-8.5 ± 1.0	12.3 ± 1.3		5
Q-103	768	5-10	358 ± 3		75 ± 10	25 ± 10		-12.5 ± 5.0	15.3 ± 2.5	Veinlets of K-assemblage in sill of dacitic porphyry	6
Q-10	720	8-10	301 ± 1		90 ± 5	10 ± 5		7.1 ± 0.1	10.6 ± 1.0	Veinlets of Propylitic assemblage in sill of dioritic porphyry	2
CP-1-22	760	8-12	218 ± 25		65 ± 8	35 ± 8		-19 ± 6.8	20 ± 2.4	Amygdules in dioritic porphyry filled by Propylitic assemblage	11
Q-11	780	8-15	269 ± 11		70 ± 10	30 ± 10		-6.6 ± 0.6	9.8 ± 0.9	Veinlets of Propylitic assemblage in RPD	4
Q-12	780	7-12	249 ± 5		68 ± 12	32 ± 12		-7.9 ± 1.3	12.0 ± 2.4	Veinlets of Propylitic assemblage in RPD	5
Q-102	792	8-10	335 ± 5		90 ± 4	10 ± 6		-10.5 ± 0.5	14.5 ± 0.5	Veinlets of Propylitic assemblage in sill of dioritic porphyry	2
Q-13	792	8-10	247 ± 3		70 ± 5	30 ± 5		-6.5 ± 0.5	9.8 ± 0.7	Veinlets of Propylitic assemblage in RPD	6
CP-1-15	816	7-11	187 ± 35		65 ± 10	35 ± 10		-8.8 ± 5.6	12 ± 5.1	Amygdules in dioritic porphyry filled by Propylitic assemblage	6
CP-1-22	816	6-9	318 ± 15		80 ± 10	20 ± 10		-10.1 ± 1.3	14.1 ± 1.2	Veinlets of Propylitic assemblage in dioritic porphyry	2

Th (L+v) = L-V homogenization temperature; Th (Halite) = Halite dissolution temperature; Tm (ice) = melting temperature of ice; % L,V, Halite = abundance of phases at room conditions; MHB = Magmatic and hydrothermal breccia; RPD = Rhyolitic porphyry dome

Table 2. Sulfur Isotope data of sulfides from the main hydrotermal event at the Mantos Blancos ore deposit.

Sample Nº	Mineral	$\delta^{34}S_{CDT}$(‰)	Hydrothermal Alteration (1)	Lithology (2)
M-25	Pyrite	-2.0	Propylitic	Granodiorite
CPM-54	Pyrite	-1.9	Potassic	Diorite
CP-122	Pyrite	-2.6	Sodic	Diorite
CPM-53	Pyrite	-4.0	Potassic	Rhyolitic dome
M-3	Pyrite	1.2	Propylitic	MHB
M-4-A	Pyrite	0.7	Propylitic	MHB
BC-708	Pyrite	-0.1	Potassic	MHB
P-2-1	Pyrite	-0.3	Potassic	MHB
C-684	Pyrite	-1.1	Potassic	MHB
N-684	Pyrite	-1.2	Potassic	MHB
M-24	Pyrite	-5.0	Propylitic	MHB
M-25	Chalcopyrite	-2.1	Propylitic	Granodiorite
CPM-54	Chalcopyrite	-0.5	Potassic	Diorite
CPM-54a	Chalcopyrite	-2.0	Potassic	Diorite
CPM-53	Chalcopyrite	-4.5	Potassic	Rhyolitic dome
BC-708	Chalcopyrite	-1.3	Potassic	MHB
CPM-54a	Digenite	-3.2	Potassic	Diorite

(1) Hydrothermal alteration stage associated with the analyzed sulfide.
(2) Host rock of the sulfide.
MBH=Magmatic Hydrothermal Breccia.

Table 3.- C and O isotope analyses of calcites from the Mantos Blancos ore deposit.

Sample	$^{18}O_{SMOW}$ (‰)	$^{18}O_{PDB}$ (‰)	$^{13}C_{PDB}$ (‰)
56-585	14.98	-15.40	-6.16
56-590	17.42	-13.04	-6.69
56-628	16.44	-13.99	-6.71
VB-1	18.74	-11.71	-5.50
97-230	23.49	-7.14	-6.58
VB-2	17.60	-12.86	-5.36
06-268	13.27	-16.44	-5.13
06-335	15.87	-14.54	-6.27
BC-1	13.91	-16.44	-5.13
33-200	16.72	-13.71	-6.91
33-257	20.81	-9.75	-5.72
33-288	19.87	-10.66	-4.37
33-298	13.08	-17.25	-6.02
DV-1	14.59	-15.78	-5.09
1-14B	16.51	-13.92	-6.02
696-41	13.88	-16.47	-6.17
1-14C	16.68	-13.75	-5.42
CPM1-21	16.85	-13.60	-4.75

III. EVOLUCIÓN MAGMÁTICA DEL YACIMIENTO MANTOS BLANCOS

III.1 Magmatismo del arco Jurásico-Cretácico inferior de la Cordillera de la Costa del norte de Chile

La Cordillera de la Costa del Norte de Chile está formada principalmente por rocas volcánicas de edad Jurásica, intruidas por granitoides emplazados entre el Jurásico Inferior y el Cretácico Inferior (Boric et al., 1990; compilación edades Oliveros, 2005). El conjunto de estas rocas ígneas representan un arco magmático ligado a subducción desarrollado en el margen continental activo de Sudamérica, sobre un basamento de rocas Paleozoicas, interpretadas como un prisma de acreción ligado a un sistema de subducción más antiguo (Mpodozis y Ramos, 1990).

El arco magmático Jurásico-Cretácico inferior se desarrolló principalmente en un ambiente tectónico transtensional (Scheuber y Adriessen, 1990; Reutter et al., 1991; Scheuber y Reutter, 1992, Lucassen y Franz, 1994), probablemente inducido por un movimiento oblicuo de la Placa Alud (Phoenix) en dirección SSE, respecto al margen continental de Sudamérica (Scheuber y Reutter, 1992; Lucassen y Franz, 1994). Esto derivó en movimientos de rumbo sinestrales paralelos al arco y extensión normal al mismo, conduciendo a un adelgazamiento extremo de la corteza continental pre-Jurásica (Lucassen y Franz, 1994), cuya parte inferior pudo ser reemplazada por material derivado del manto durante la evolución del arco (Reutter et al., 1991; Scheuber y Reutter, 1992). La distribución longitudinal del magmatismo, junto con la

instalación de una cuenca marina en la posición oriental del arco son características de este dominio extensional (Reutter et al., 1991; Scheuber y Reutter, 1992).

Durante este dominio extensional, en el Jurásico inferior a medio se depositó una gruesa pila volcánica (5-7 km), compuesta principalmente de andesitas basálticas, basaltos, andesitas y dacitas subordinadas (Palacios, 1978; Naranjo y Puig, 1984; Rogers and Hawkesworth, 1989; Marinovic et al., 1995; Kramer et al., 2005), de composición calcoalcalina, con etapas iniciales de afinidad toleítica (Pichowiak et al., 1990). Estas rocas volcánicas (Formación La Negra, García, 1967) se formaron en condiciones principalmente subaéreas, sin embargo intercalaciones menores de rocas calcáreas de origen marino y *pillow* lavas, sugieren una depositación cercana al nivel del mar (Naranjo y Puig, 1984; Gröschke et al. 1988; Grocott et al. 1994; Marinovic et al. 1995). Esta potente secuencia volcánica Jurásica ha sido interpretada de distintas maneras: como arco de islas (Palacios, 1984), arco magmático continental (Rogers, 1985; Oliveros 2005), cuenca marginal ensiálica (Buchelt y Zeil, 1986).

La actividad plutónica, que comenzó cerca de 200 Ma (Boric et al., 1990) permitió la formación de numerosos cuerpos intrusivos, desde gabros a granodioritas, la mayoría de los cuales se emplazaron en la corteza superior (Dallmeyer et al., 1996). Esta actividad tuvo su máxima expresión a fines del Jurásico-principio del Cretácico (160-120 Ma; Boric et al., 1990).

Las rocas volcánicas e intrusivas de la región tienen bajas razones isotópicas iniciales de $^{87}Sr/^{86}Sr$, las que sugieren una afinidad mantélica y prácticamente nula contaminación cortical (Rogers, 1985; Hervé y Marinovic, 1989; Lucassen y Franz, 1994).

Datos de trazas de fisión indican que los cuerpos intrusivos del Jurásico Medio a Superior en gran medida se enfriaron bajo el rango de temperatura de borrado ("annealing") de trazas de fisión en apatitos (70-125ºC) durante el Cretácico Inferior (129 a 92 Ma) contemporáneamente con la actividad

plutónico-volcánica más tardía del arco magmático y cizalle sinistral a lo largo del Sistema de Falla de Atacama (Maksaev, 2000).

III.2 Fundamentación del trabajo realizado

Los yacimientos tipo pórfido cuprífero reciben su nombre a partir de el hecho que están asociados genéticamente a plutones porfídicos, los cuales son por lo general calcoalcalinos, relacionados a subducción, y varían en composición desde granodioritas a monzonitas cuarcíferas (Guilbert y Parks, 1986). Nuestro conocimiento actual de la formación de estos depósitos supone que el cobre y otros metales son extraídos desde fundidos silicatados como fluidos magmático/hidrotermales exueltos durante la cristalización y procesos de despresurización del magma (Hedenquist y Lowerstern, 1994; Burnham, 1997). Los metales son precipitados posteriormente dentro y a los alrededores de estos plutones, mientras los fluidos de origen magmático se enfrían y se mezclan con aguas externas al sistema magmático (Beane y Tiley, 1981).

En décadas pasadas, numerosos estudios de detalle, han caracterizado el ambiente físico y químico asociado con la actividad hidrotermal, mineralización y alteración en este tipo de depósitos (ej. Lowell y Guilbert, 1970; Beane y Tiley, 1981; Roedder y Bodnar, 1997). Sin embargo, existe escasa información con respecto a las etapas magmáticas tempranas (pre-mineralización) debido a que las rocas comúnmente han sido alteradas por fluidos hidrotermales sobreimpuestos, remplazando las fases ígneas originales. Adicionalmente, en la mayoría de estos depósitos, la estratigrafía volcánica sobre las intrusiones mineralizadas ha sido removida por erosión, eliminando cualquier información magmática previa relacionada a los procesos mineralizadores.

Las inclusiones fundidas (o vítreas) silicatadas (*melt inclusions*) son pequeñas muestras de fundido que han sido entrampadas durante el crecimiento de cristales a presiones y temperaturas magmáticas. Estas inclusiones vítreas representan muestras de fundidos que han sido aislados del magma durante la cristalización y crecimiento de su mineral huésped y pueden estar compuestas

de una fase única vítrea o contener múltiples fases (burbujas de vapor y cristales) que se han nucleado desde el fundido dentro de la inclusión durante el enfriamiento, o producidas por desvitrificación posterior a su entrampamiento (Roedder, 1984). Estas inclusiones fundidas han sido usadas exitosamente para estudiar la evolución magmática de sistemas ígneos (Lowerstern, 1995; Sobolev, 1996). En los sistemas volcánicos en los cuales las rocas se enfrían rápidamente, las inclusiones vítreas son comúnmente preservadas como un vidrio homogéneo, y son fácilmente reconocibles y analizables (Anderson, 1991; Sobolev, 1996). Por el contrario, en los sistemas ígneos más profundos (plutones) las inclusiones fundidas son preservadas como vidrio parcialmente desvitrificado o como cristales de distintas fases minerales, los cuales usualmente son envueltos por fases volátiles. Estas inclusiones vítreas cristalizadas son características de rocas ígneas enfriadas lentamente (Roedder, 1984; Lowerstern, 1995). Estudios relacionados a la composición de estas inclusiones fundidas y al contendido de metales (ej. Cu, Zn, Pb, Mo, Ag, Au) han sido desarrollados para comprender el comportamiento magmático durante la cristalización y degasificación, y su contribución a la mineralización metalifera primaria (e.g. Lehmann et al., 2000; Campos et al., 2002; Harris et al., 2003; Halter et al., 2005).

La mayoría de los depósitos de Cu en la Cordillera de la Costa del norte de Chile, se localizan alrededor de cuerpos intrusivos subvolcánicos porfídicos que incluyen gabros, dioritas, monzodioritas y granodioritas que constituyen diques, filones-mantos y stocks. Generalmente estos intrusivos son estériles y en algunos de los depósitos cortan cuerpos mineralizados (Buena Esperanza, Lince-Estefanía, Santo Domingo). Sin embargo, también existen filones-mantos mineralizados en Mantos Blancos, Santo Domingo y Rencoret (Boric et al., 1990).

Clásicamente el yacimiento Mantos Blancos se ha considerado como un deposito estratoligado (e.g. Espinoza et al., 1996; Maksaev y Zentilli, 2002), sin embargo, en el Capitulo II de esta tesis se describen nuevos antecedentes relacionados a la geología, alteración y mineralización del yacimiento, y se

postula que origen volcanico de las rocas que hospedan la mineralización (SVMB de Chávez, 1985), corresponde a una actividad intrusiva somera. Mediante el estudio de inclusiones fundidas, geoquímica y análisis isotópicos de Sr-Nd, en este capítulo se determina la evolución magmática de las rocas del distrito de Mantos Blancos y se discute el rol de los procesos magmáticos y su relación con la mineralización - alteración hidrotermal.

III.3 Referencias

Anderson, A.T. 1991. Hourglass inclusions: Theory and application to the Bishop rhyolitic Tuff. Am. Mineral. 76, 530-547.

Beane, R.E., and Titley, S.R. 1981. Porphyry copper deposits. Part II. Hydrothermal alteration and mineralization. Economic Geology, 75th Anniversary Volume: 235-263

Boric, R., Díaz, F. and Maksaev, V., 1990. Geología y yacimientos metalíferos de la Región de Antofagasta. Servicio Nacional de Geología y Minería, Boletín Nº 40, Santiago, 246 p.

Buchelt, M. y Zeil, W. 1986. Petrographische und geochemische Undersurchungen an Jurassischen Vulkaniten der Porphyrit Formation in der Kustenkordillere nord-Chile. Berliner Geowissenschaft, Vol. 66, p. 191-204.

Burnham, C.W. 1997. Magmas and hydrothermal fluids, *in* Barnes, H.L., ed., Geochemistry of Hydrothermal Ore Deposits, 3rd edition. New York, J. Wiley and Sons. p. 63-124.

Campos, E., Touret, J.L.R., Nikogosian, I., and Delgado, J. 2002. Overheated, Cu-bearing magmas in the Zaldivar porphyry-Cu deposit, Northern Chile. Geodynamic consequences. Tectonophysics, 345, 229–251.

Chávez, W. 1985. Geological setting and the nature and distribution of disseminated copper mineralization of the Mantos Blancos district, Antofagasta Province, Chile. PhD Thesis, University at California, Berkeley, USA. 142 pp

Dallmeyer, R.D., Brown M., Grocott J., Taylor G.K., Treolar P.J. (1996). Mesozoic magmatic and tectonic events within the Andean plate boundary zone, 26º - 27º30`S, North Chile: Constraints from ^{40}Ar / ^{39}Ar mineral ages. The Journal of Geology 104: 19 – 40.

Espinoza S, Véliz H, Esquivel J, Arias J, Moraga A. 1996 The cupriferous province of the Coastal Range, Northern Chile. In: Camus F, Sillitoe RH, Petersen R (eds.) Andean Copper Deposits: New discoveries, mineralization, styles and metallogeny. Econ Geol, Spec Publ 5: 19 – 32

García, F. 1967. Geología del Norte Grande de Chile. In: Symposium sobre el Geosinclinal Andino, Soc Geológica de Chile, Santiago, Nº 3

Grocott, J., Brown, M., Dallmeyer, R.D., Taylor, G.K. & Treloar, P.J. 1994. Mechanism of continental growth in extensional arcs: An example from de Andean plate-boundary zone. Geology, 22, 391-394.

Gröschke, M., Von Hillebrandt, A., Prinz, P., Quinzio, L.A., and Wilke, H.-G. 1988. Marine Mesozoic Paleogeography in Northern Chile between 21º and 26ºS. In: Bahlburg, H., Breitkreutz, C., and Giese, P., (editors) The Southern Central Andes. Lecture Notes in Earth Sciences, 17, p. 105-117.

Guilbert, J.M., and Parks, C.F., Jr. 1986. The geology of ore deposits. W.H. Freeman and Company, New York. p. 985.

Halter W.E., Heinrich, C.A., Pettke T. 2005. Magma evolution and the formation of porphyry Cu–Au ore fluids: evidence from silicate and sulfide melt inclusions. Mineralium Deposita 39: 845–863.

Harris AC, Kamenetsky VS, White NC, van Achterbergh E, Ryan CG (2003) Melt inclusions in veins: linking magmas and porphyry Cu deposits. Science 302:2109–2111.

Hedenquist, J.W., y Lowenstern, J.B. 1994. The role of magmas in the formation of hydrothermal ore deposits. Nature, v. 370, p. 519-526.

Hervé, M. y Marinovic, N. 1989. Geocronología y evolución del Batolito Vicuña Mackenna, Cordillera de la Costa, sur de Antofagasta (24 -25°S). Revista Geológica de Chile, 16, 31-49.

Kramer, W., Siebel, W., Romer, R., Haase, G., Zimmer M. and Ehrlichmann, R., 2005. Geochemical and isotopic characteristics and evolution of the Jurassic volcanic arc between Arica (18º30'S) and Tocopilla (22ºS), North Chilean Coastal Cordillera. Chemie der Erde (65), 47–68.

Lehmann, B., Dietrich, A., Wallianos, A., 2000. From rocks to ore. International Journal Earth Sciences <Geologische Rundschau> 89: 284-294.

Lowell J.D. and Guilbert, J.M. 1970. Lateral and vertical zonation in porphyry ore deposits. Economic Geology, v. 65, p. 373-408.

Lowenstern, J.B. (1995) Application of silicate-melt inclusions to the study of magmatic volatiles. In Magmas, fluids and ore deposition, Vol. 23 (ed. J.F.H. Thompson), pp. 71-98. Mineralogical Assoc. of Canada, Short Course Series.

Lucassen, F., Franz, G. 1994. Arc – related Jurassic igneous and metaigneous rocks in the Coastal Cordillera of northern Chile. Antofagasta Region. Lithos. 32: 273 – 298.

Maksaev, V., 2000. Significado tectónico y metalogénico de datos de trazas de fisión en apatitas de plutones de la Cordillera de la Costa de la región de Antofagasta. IX Congreso Geológico Chileno, Actas, vol 2, 129-134.

Maksaev, V. y Zentilli, M. 2002. Chilean strata-bound Cu-(Ag) deposits: an overview; In: Porter, T.M. (ed.) Hydrothermal iron oxide copper-gold & related deposits: a global perspective, v. 2, PGC Publishing, Adelaide, 185-205.

Marinovic, N., Smoje, I., Maksaev, V., Hervé, M., Mpodozis, C., 1995. Hoja Aguas Blancas, Región de Antofagasta. Servicio Nacional de Geología y Minería, Carta Geológica de Chile N° 70, 150 p.

Mpodozis, C., Ramos, V. 1990. The Andes of Chile and Argentina. In : Ericksen, G. E., Cañas, M. T., Reinemund, J. (eds.). Geology of the Andes and its relation to hydrocarbon and mineral resources. Circum – Pacific Council for Energy and Mineral Resources. Earth Science Series, 11: 59 – 90.

Naranjo, J.A. and Puig, A., 1984. Hojas Taltal y Chañaral, Regiones de Antofagasta y Atacama. Carta Geológica de Chile, Escala 1:250.000, SERNAGEOMIN, Santiago, Chile, Nº 62-63, 140 p.

Oliveros, V. 2005. Les formations magmatiques jurassiques et mineralization du nord Chili, origine, mise en place, alteration, metamorphisme: etude geochronologique et geochemie. PhD Thesis. Universite de Nice – Sophia Antipolis, France. 285 p.

Palacios, C., 1978. The Jurassic paleovolcanism in northern Chile. PhD Thesis. Tubingen University, Germany. 99 p.

Palacios, C. 1984. Considerations about the plate tectonic models, volcanism, and continental crust in the southern part of the Central Andes. Tectonophysics 108: 205–214.

Pichowiak S., Buchelt M., Damm K.W. (1990) Magmatic activity and tectonic setting of early stages of Andean cycle in northern Chile. Geol Soc Am. Special Paper 241: 127 – 144.

Ramírez L.E., Palacios C., Townley B., Parada M.A., Sial A.N., Fernandez-Turiel J. L., Gimeno D., Garcia-Valles M., Lehmann, B. (2006) The Mantos Blancos copper deposit: an Upper Jurassic breccia–style hydrothermal system in the Coastal Range of Northern Chile. Mineraluim Deposita V 41, 246-258.

Reutter, K., Scheuber, E. & Helmcke, D. 1991. Structural evidence of orogen-parallel strike-slip displacements in the Precordillera on northern Chile. Geologische Rundschau, 80, 135-153.

Roedder, E. 1984. Fluid Inclusions, Min. Soc. Am. Rev. in Min. v. 12, 646 pp. 101

Roedder, E. and Bodnar, R.J. 1997. Fluid Inclusion Studies of Hydrothermal Ore Deposits. In Geochemistry of Hydrothermal Ore Deposits, 3rd ed., H.L. Barnes, ed., Wiley & Sons, Inc, New York, 657-698.

Rogers, G., 1985. A geochemical traverse across the North Chilean Andes. Ph.D. Thesis, Dept. of Earth Sciences, The Open University, Milton Keynes, U.K., 333 p.

Rogers G, Hawkesworth CJ (1989) A geochemical traverse across the North Chilean Andes: evidence for crust generation from the mantle wedge. Earth and Planet Sci Lett 91: 271 – 285.

Scheuber, E. and Andriessen, P., 1990. The kynematic and geodynamic significance of the Atacama fault zone, northern Chile. Journal of Structural Geology (12), 243– 257. Scheuber y Reutter, 1992

Scheuber, E. & Reutter, K.-J. 1992. Magmatic arc tectonics in the Central Andes between 21° and 25° S.- Tectonophysics, 205: 127-140.

Sobolev A.V. 1996. Melt inclusions in minerals as a source of principal petrologic information. Petrology, 4:228-239.

III.4 Articulo 2: “Magmatic evolution of the Mantos Blancos copper deposit, Coastal Range of northern Chile: insight from Sr–Nd isotope, geochemical data and silicate melt inclusions”

Luis Ernesto Ramírez, Miguel Angel Parada, Carlos Palacios

Departamento de Geología, Universidad de Chile. P.O. Box 13518-21, Santiago, Chile.

Jens Wittenbrink

Institut für Mineralogie und Mineralische Rohstoffe, Technische Universität Clausthal, Adolf Roemer Strasse 2 A, D-38678 Clausthal-Zellerfeld, Germany.

Shortened title for header: Magmatic evolution of Mantos Blancos Cu deposit.

Keywords: Cu mineralization, Sr-Nd isotopes, magma mixing, Coastal Range, Chile.

Corresponding author:

Luis Ernesto Ramírez

e-mail: lramirez@cec.uchile.cl

Phone: (56) – 2- 9780233.

Fax: (56) – 2- 6963050.

Abstract

The Mantos Blancos copper deposit (500 Mt @ 1.0% Cu) was affected by two superimposed hydrothermal events: (1) phyllic alteration related to a rhyolitic dome emplacement and brecciation at ~155 Ma, (2) potassic, sodic and propylitic alteration at ~142 Ma, coeval with stocks and sills emplacement of dioritic and granodioritic porphyries, that locally grade upwards into polymictic magmatic–hydrothermal breccias. Major hypogene copper sulfide mineralization is related to the second event. A late-ore mafic dyke swarm crosscuts all rocks in the deposit. Two types of granodioritic porphyries can be distinguished from petrographic observations and geochemical data: granodiorite porphyry I (GP I) and granodiorite porphyry II (GP II) that resulted from two different trends of magmatic evolution. The concave shape of the REE distribution pattern together with the weak or absence of negative Eu anomalies in mafic dykes, dioritic and GP I porphyries, suggest hornblende-dominated fractionation for this magmatic suite. On the other hand, distinct negative Eu anomalies and the flat REE patterns suggest plagioclase-dominated fractionation, at low oxygen fugacity, for the GP II porphyry suite. However, shallow mixing and mingling between silicic and dioritic melts are also likely for the formation of the GP II and polymictic breccias, respectively. Sr-Nd isotopic compositions suggest that the rhyolitic dome rocks were generated from a dominantly crustal source, while the GP I has mantle affinity. The composition of melt inclusions (MI) in quartz crystals from the rhyolitic dome is similar to the bulk composition of their host rock. The MIs analyzed in quartz from GP II and in the polymictic magmatic-hydrothermal breccia of the deposit are compositionally more evolved than their host rocks. Field, geochemical and petrographic data provided here point to dioritic and siliceous melt interaction as an inducing mechanism for the release of hydrothermal fluids to form the Cu mineralization.

Introduction

The Coastal Range of northern Chile hosts numerous copper deposits, constituting a NS–trending Late Jurassic–Early Cretaceous metallogenic belt, which extends for more than 200 km (22° to 24° S; Fig. 1). Two main types of ore deposits occur in this copper province: volcanic-hosted strata-bound orebodies (Espinoza et al., 1996; Maksaev and Zentilli, 2002) and porphyry copper deposits (Camus, 2003). Other ore deposits are hosted in intrusive rocks and were described by Espinoza et al. (1996) as vein type deposits. The volcanic-hosted strata-bound ore deposits are characterized by magmatic and hydrothermal breccias that form feeder structures to the flat-lying peripheral stratiform mineralization. The hydrothermal breccias contain a major portion of the commercial mineralization and have the highest ore grade in these deposits. The pipes-like hydrothermal breccias are genetically related to coeval stocks and sills of mainly dioritic composition, and are intruded by post-mineralization basaltic dykes (Maksaev and Zentilli, 2002). The porphyry copper mineralization in the belt is associated with granodioritic porphyries and hydrothermal breccias (Perelló et al., 2003). The Mantos Blancos deposit produces about 50% of all copper of the belt, and had pre-mining resources of 500 million tons with 1.0% Cu (Ramírez et al., 2006). The ore deposit formed by two main hydrothermal events: i) a first event (~155 Ma) related to rhyolitic magmatism and magmatic-hydrothermal monomictic breccias of rhyolitic composition and ii) a second event (~142 Ma) related to dioritic and granodioritic porphyries and magmatic-hydrothermal polymictic breccias (Ramírez et al., 2006). We here present new geochemical, isotopic and silicate melt inclusion data of the Mantos Blancos district, in order to better understand its magmatic evolution. Additionally, the role of the magmatic processes in the associated hydrothermal alteration will be discussed.

Geological setting

During the Jurassic to Early Cretaceous, a subduction-related magmatic belt developed along the present Coastal Range of northern Chile. It is represented by 7000 m thick basaltic to andesitic volcanic pile (La Negra Formation) and granitic to dioritic plutonic rocks. The volcanic sequence has mantle affinity (Rogers and Hawkesworth, 1989; Lucassen et al. 2002) and evolved with time from an initial stage of tholeiitic affinity to calc-alkaline composition (Palacios, 1984; Rogers and Hawkesworth, 1989; Pichowiak et al., 1990; Kramer et al., 2005). Three main plutonic events have been described in the Coastal Range of northern Chile (Pichowiak, 1994; Andriessen and Reutter, 1994; Scheuber, 1994; Dallmeyer et al., 1996; Scheuber and González, 1999): Early Jurassic (200–180 Ma) granitic to tonalitic rocks, Middle Jurassic (170–160 Ma) granodioritic rocks, and Late Jurassic to Early Cetaceous (155-140 Ma) granodioritic to dioritic rocks. The tectonic evolution of the Coastal Range during the Jurassic is interpreted in terms of coupling and decoupling between the down-going and overriding plates, in a transtensional regime due to oblique subduction (Scheuber and González, 1999). Between 200 and 155 Ma an intra-magmatic belt, controlled by the NS-trending sinistral strike-slip Atacama Fault Zone was developed. However, at the end of the Jurassic, and due to foundering of the subducting plate, subduction rollback and decoupling, the emplacement of the magmatic belt was controlled by an EW-trending extensional regime (Scheuber and González, 1999).

Geology of the deposit

The lithological units recognized within the Mantos Blancos ore deposit consist of a rhyolitic dome and magmatic-hydrothermal monomictic breccias of the same composition, intruded by stocks and sills of dioritic and granodioritic porphyries. The dioritic and granodioritic stocks locally grade upwards into magmatic-hydrothermal polymictic breccias. These rock units are all

mineralized to variable degree. Late mafic dyke swarms crosscut all previously mentioned rock units and are essentially barren (Ramírez et al., 2006; Fig.2).

Rhyolitic dome and associated magmatic-hydrothermal rhyolitic breccias

The dome structure has been identified by the restoration of its pre-mining geometry by studying drill core logs of the early stage of exploitation (Chávez, 1985). Drill cores located in the vicinity of the mine also provide evidence of an outward decreasing thickness, compatible with a dome structure, from the main rhyolitic body of the pit. The rhyolitic dome occupies the most important parts of the deposit, and it is hosted by felsic tuffs and mafic to intermediate lava flows of the La Negra Formation and intruded by stocks and sills of dioritic and granodioritic porphyries. The rhyolitic dome is exposed over 350 m depth along the walls of the current open pit, however information from drill cores indicates a vertical extent to at least 800 m. Due to pervasive alteration, the contacts between internal flows are very difficult to observe, however, near-horizontal and vertical flow laminations of 1-4 cm thickness are recognized. The rhyolitic dome consists of rhyolitic porphyry with 30-60% of feldspar and corroded quartz phenocrysts (1-5 mm) in a highly altered felsic groundmass. Magnetite and zircon are common accessory minerals. Sub-vertical bodies of magmatic-hydrothermal breccia hosted in the rhyolitic dome have been recognized. They are matrix supported monomictic (rhyolite) breccias about 100 to 250 m in vertical view, and with sub-circular horizontal sections of 50 to 100 m in diameter. The matrix is composed of rhyolitic rock flour with intense alteration and disseminated sulfides. The rhyolitic fragments are altered, irregular in shape, poorly sorted and vary in size between 1 cm and several m. Although the age of the rhyolitic dome is not known, the age of the hydrothermal event affecting the dome is ~155 Ma ($^{40}Ar/^{39}Ar$ in sericite; Oliveros, 2005) and is probably close to the dome emplacement age.

Granodioritic and dioritic porphyries, and associated magmatic-hydrothermal polymictic breccias

Granodiorite porphyries. Two granodioritic porphyries have been recognized: granodiorite porphyry I (GP I) and granodiorite porphyry II (GP II). Rocks of the GP I are mainly located west and south of the pit, but also recognized from drill cores in the mine. It commonly exhibits 35 to 50% of 0.5-5 mm large phenocrysts of hornblende, oscillatory-zoned plagioclase and biotite, in a groundmass of quartz, feldspars and minor biotite. The GP II is restricted to the ore deposit domain. It contains 10 to 30% of phenocrysts of 0.5-3 mm large plagioclase (albitized), embayed β-quartz and chloritized hornblende in a groundmass of quartz, feldspars and hematite intergrowth (see Fig. 3 E, F). Minor amounts of magnetite and zircon have been observed in both GPI and GPII.

Diorite porphyry. The diorite porphyry has 5 to 10% of 2-5 mm large phenocrysts of pyroxene (and minor hornblende) in a groundmass of fine-grained pyroxene, plagioclase and magnetite. The diorite porphyry exhibits mm-sized spherical miarolitic cavities with quartz and sulfide infill (Fig. 3 A) and chlorite sulfide infill (Fig. 3 B). Mutual intrusive relationships between both GP II and diorite porphyries are common (Ramírez et al., 2006), and metric to centimetric enclaves of one in the other have been frequently observed (Fig. 3 G, H). Recent $^{40}Ar/^{39}Ar$ data on amphibole give ages of 142.2 ± 1 Ma for GP I, and 141.4 ± 0.5 Ma for the diorite porphyry (Oliveros, 2005). Although the age of GP II is not known, the mutual intrusive relationships with the dioritic porphyry suggest that both are coeval.

Polymictic magmatic-hydrothermal breccias. Two polymictic and matrix supported pipe-like magmatic-hydrothermal breccias are recognized in the pit of the mine. They are spatially-related with N-S faults and hosted within the rhyolitic dome. The largest breccia body, located in the central part of the pit, is cross-cut by metric-sized sills of dioritic porphyry and GP I. The breccias form near-vertical bodies, with a vertical extent of about 700 m, and have sub-spherical sections with diameters between 100 and 500 m. The upper part of

the breccia pipes exhibits hydrothermal characteristics as evidenced by the presence of a matrix composed by hydrothermal and ore minerals (Fig. 3 C, D). The breccia fragments include angular and sub-rounded altered rocks of the rhyolitic dome and of granodioritic and dioritic porphyries. They are poorly sorted and range in size from 1 cm to 15 m. Downwards in the breccia bodies, magmatic features are progressively more evident. It is common to observe magma mingling as evidenced by granodioritic enclaves in a dioritic matrix, as well as dioritic enclaves in a granodioritic matrix (Fig. 3 G, H).

Mafic dyke swarm

Most mafic dykes are sub-vertical oriented in NNE direction, although NS and NNW sub-vertical dykes also occur. The dykes are 1 to 12 m thick and represent about 15% of the total rock volume in the deposit. They exhibit porphyritic texture, with 10-25% of 3-10 mm sized altered plagioclase, hornblende and minor pyroxene phenocrysts, in a very fine-grained groundmass of feldspar, hornblende, and subordinately biotite and magnetite. A hornblende $^{40}Ar/^{39}Ar$ age determination of 142.7 ± 2.1 Ma was obtained for a weak late-mineralized dyke in the mine (Oliveros, 2005).

Hydrothermal alteration and mineralization

The deposit was affected by two overprinted hydrothermal events: (1) a phyllic alteration event related to the rhyolitic dome emplacement and rhyolitic magmatic-hydrothermal brecciation that took place at ~155 Ma, (2) a potassic-propylitic-sodic alteration event developed at ~141-142 Ma, coeval with the stocks and sills intrusion of dioritic and granodioritic porphyries. This second hydrothermal event is related to the main mineralization pulse, which occurs disseminated and in stockworks centered in the polymictic magmatic-hydrothermal breccias (Ramírez et al., 2006). Hypogene sulfide assemblages show a vertical and lateral zoning within polymictic breccia bodies. A barren pyrite root zone is overlain by pyrite-chalcopyrite, and followed upwards and laterally by chalcopyrite-digenite or chalcopyrite-bornite. The assemblage digenite - supergene chalcocite characterizes the central portions of high-grade mineralization in the polymictic breccia bodies (Ramírez et al., 2006).

Whole rock geochemistry

Major oxide, trace, and REE contents of 52 representative samples from the Mantos Blancos ore deposit are listed in Table 1. Geochemical analyses were carried out using ICP-AES (Perkin Elmer P-430) at the Departamento de Geología, Universidad de Chile. The USGS standards BCR-2, AGV-2 and G-2 were used for calibration. Because of the widespread hydrothermal alteration, the rock classification is by immobile elements according to Floyd and Winchester's (1978) diagram for volcanic rocks. Figure 4 indicates that samples of the dioritic and granodioritic porphyries fall in the fields of its volcanic counterparts (andesite and dacite), respectively. Most rocks of the felsic dome are rhyolitic in composition and rocks of the mafic dyke swarm plot in the basaltic field. The REE chondrite-normalized patterns for different rock units are shown in Fig. 5. The rhyolite samples show strongly fractionated LREE patterns with distinct negative Eu anomalies and flat HREE patterns. The GP I samples have concave REE patterns and no Eu anomaly. The GP II samples differ from the GP I samples in their negative Eu anomalies and in the less fractionated HREE patterns. The rocks of the dioritic porphyries and late-ore basaltic dykes exhibit similar gently-dipping slightly fractionated REE patterns with a small Eu depletion.

Sr-Nd isotopes and the nature of the magma sources

The analyzed samples of Mantos Blancos district (Table 2) have different isotopic signatures. The analytical isotope procedure is presented in appendix 1. Two samples from GP I have initial $^{87}Sr/^{86}Sr$ ratios of 0.70362 and 0.70395 and εNd values of +3.5 and +3.2, respectively. These data suggest a dominantly mantle source and are similar to the reference data for La Negra Formation (Rogers and Hawkesworth, 1989; Lucassen et al., 2002; Fig. 6). The rhyolitic dome has an initial $^{87}Sr/^{86}Sr$ ratio of 0.70592 and an εNd value of -2.0, suggesting more crustal involvement. A sample from the igneous matrix of the Mantos Blancos polymictic breccia has an initial $^{87}Sr/^{86}Sr$ ratio of 0.70591,

similar to that of the rhyolitic dome, and an εNd of +0.15, suggesting a mixed source in between the rhyolitic dome and the GP I. Three samples of the dioritic porphyry (unpublished data; F. Munizaga, written communication) from the open pit have intermediate isotopic composition between the GP I porphyry (and the field of volcanic rocks of the La Negra Formation) and the rhyolitic dome ($^{87}Sr/^{86}Sr$ initial ratios range between 0.70455 and 0.70573 and εNd values between 0.0 and +2.5; see Fig. 6). No isotope data exist for the basaltic dykes of the deposit. However because the chemical compositional similarities between the basaltic dykes and mafic lavas of the La Negra Formation (Rogers and Hawkesworth, 1989; Lucassen et al, 2002) and Cretaceous dykes in the region (Lucassen et al., 2002), it is possible to assume a depleted isotopic signature for the Mantos Blancos dykes.

Silicate melt inclusions hosted in quartz

Silicate melt inclusions (MI) hosted in quartz phenocrysts of the GP II, and quartz crystals of the polymictic breccia were analyzed using a Cameca SX 100 electron microprobe (TU Clausthal, Germany). An accelerating voltage of 15 kV, beam current of 8 nA, beam diameter of 3 μm and a counting time of 6 s were chosen for major elements, and 20 kV, beam current of 40 nA, and a counting time of 20 s for trace elements.

The sample preparation by remelting can introduce contamination by silica from the host quartz. Webster et al. (2004) discussed in detail the difficulties to determine appropriate heating times and temperatures for remelting of MI characterized by variable compositions. Based on the empirical results obtained in the laboratory, the best conditions for the experiments in quartz are 950ºC and 1 atm external pressure during 24 hours (Dietrich, 1999; Wittenbrink, 2006). After the heating experiments, the samples were quenched to produce a silicate glass. The homogenized MIs are small (15 to 40 μm), in some cases with a vapor bubble (1 to 10 μm) of 5 to 15% in volume relative to the MI. Although the heating temperature (950ºC) seems to be high, after 24 hours only in very small

inclusions (<10 μm) the host quartz walls were partially melted, and few larger inclusions were not entirely re-homogenized.

MIs are located towards the central portions of their host embayed β-quartz crystals, phenocrysts formed early in the crystallization of Mantos Blancos acidic magmas. At least three individual analyses were carried out on each MI, hence the reported values in Table 3 are averages of several analytical spots. Our analytical data of MI, within each lithological unit, have relatively low dispersion in silica content, and we use the average data for major elements (Table 3, Fig. 7). In general, the SiO_2 concentrations of the MI trapped in quartz phenocrysts of the rhyolitic dome (Wittenbrink, 2006) resemble the bulk-rock composition. In contrast, the MIs from the GP II and the polymictic breccia have higher SiO_2 contents than their host rocks. An intriguing feature of the MI is their copper concentrations. Extremely high copper contents have been detected in MI from the rhyolitic dome (323-13400 ppm; Wittenbrink, 2006). Cu contents between 60 and 1665 ppm have been measured in the GP II, whereas low Cu contents (55-150 ppm) have been obtained in MI from the polymictic breccia. Although, heating experiments show that copper could diffuse into melt inclusions during heating (Kamenetsky and Danyushevsky, 2005) the high Cu contents in the analyzed MI may represent a heterogeneous entrapment.

Discussion

Origin of the rhyolitic melts

The high-silica rhyolite composition of the dome represents an oddity within the large volume of mafic to intermediate Jurassic magmatism of the coastal range, which is strongly dominated by mantle-derived andesitic and basaltic volcanic rocks of the La Negra Formation. The enriched Sr-Nd isotopic signatures of the rhyolitic dome are consistent with a provenance from a crust-dominated source. A crustal melt, with a near thermal-minimum composition like that of the rhyolitic dome, should have consistent near-solidus temperature of formation. To

estimate the maximum temperature of rhyolite dome we use zircon saturation thermometry (Watson and Harrison, 1983; Miller et al., 2003). Zircon saturation temperatures (T_{Zr}), calculated from bulk rock compositions, provide maximum estimates of temperature if the magma is oversaturated in zircon. Because solubility of zircon is sensitive to temperature but insensitive to pressure, the zircon saturation temperature allows inferring the magma temperature at the source if the magma has abundant inherited zircon (oversaturated). A temperature of about 750º C (Fig. 8) has been obtained for the rhyolitic dome. At this temperature a rhyolitic melt is unlikely to have resulted from significant crystal fractionation of a more mafic (and high temperature) parental melt. Moreover, considering that hornblende fractionation has been invoked as an efficient mechanism to yield felsic magmas from a basic to intermediate parental liquid, the REE patterns of the rhyolitic dome (Fig. 5) preclude hornblende participation in the magma fractionation. It is likely, therefore, that the rhyolites formed by partial melting of quartz-feldspatic rocks of crustal origin. Advanced fractionation of a more primitive parental magma or partial melting of mafic source material equilibrated under lower crust (garnet-amphibolite facies) conditions is less likely. The compositional similarities among the rhyolitic dome and the melt inclusions in quartz, regardless of the host rock, may indicate that both represent evolved magmas generated through similar processes. Therefore, the crustal signature in the Sr-Nd isotopic composition and in the REE patterns of the rhyolitic dome can be extrapolated to the melt inclusions.

The coeval development of mafic magmatism and felsic magmatism in the Mantos Blancos ore deposit suggests a cause-and-effect relationship, in which the heat source for the generation of the rhyolite melts would be the mafic magma injected into the felsic crust. In this scenario the participation of two contrasting magma sources (crust and mantle) could be highly variable and deserves to be assessed. Simple mixing models (Faure, 1986) are shown in Fig. 6 in order to test the degree of involvement of felsic crust and mantle in the Sr-Nd isotopic signatures of the rhyolitic magmas. The boundary conditions for the modeling are defined by the starting compositions, which are represented by the average composition of the mantle-derived mafic volcanic rocks of the La

Negra Formation (Lucassen et al., 2002; Rogers and Hawkesworth, 1989) and by the composition of the felsic Paleozoic granitoids of the Coastal Range near Mantos Blancos (Lucassen et al., 1999). Despite the wide range of the calculated crust/mantle ratios in the source (Fig. 7), a crustal-dominated source can best explain the isotopic signatures of the rhyolitic magmas.

Origin of the intermediate rocks (GP I and GP II): crystal fractionation and magma mixing

The REE patterns indicate two distinct fractionation paths for the Mantos Blancos intermediate rocks. The concave shape of the HREE distribution, and the absent or subtle negative Eu anomalies in mafic dykes, diorites and GP I, suggest hornblende-dominated fractionation for this magmatic suite, which in turn, is consistent with the hornblende fractionation vector shown in the Fig. 9. These data suggest a GP I derivation from a dioritic parental magma. On the other hand, the negative Eu anomalies in the GP II suggest plagioclase-dominated fractionation, probably at low oxygen fugacity. However, the distribution of GP II samples in figure 9 differs from the plagioclase fractionation vector, suggesting an overprinting of magma mixing effects (Fig. 9). In fact, shallow-depth magma interaction should explain both the GP II formation by magma mixing (Fig. 3G-H) and the polymictic breccia by magma mingling. It is possible to infer that the invariably rhyolitic composition of the melt inclusions in quartz phenocrysts, regardless of the composition of the host rock, would represent the felsic end member composition of the mixing, whereas the dioritic porphyry would represent the mafic end member composition. This hypothesis is supported by: (i) the presence of abundant mingled fragments of mafic (dioritic porphyry) and felsic (granodioritic porphyries) rocks observed in polymictic magmatic breccia drill core samples (Fig. 3 G, H) and (ii) the commonly observed disequilibrium textures in the GP II, such as corroded quartz phenocrysts (Fig 3 F). Although the disequilibrium textures can be explained preferably by mechanisms of decreasing pressure and/or increasing temperature in the magma chamber, we prefer the second alternative because the GP II exhibits the highest T_{Zr} (780-810ºC; Fig. 8), consistent with a thermal

input derived from the diorite intrusion into the felsic magma system. A scheme of the petrogenetic model for the Mantos Blancos system is given in Fig. 10. It consists of two magmatic suites with distinct origin: a mantle-dominated suite represented by diorites, mafic dikes and GP I, and a crustal-dominated suite represented by the rhyolitic magmas. Magmas from the two suites interacted to give rise to GP II and polymictic magmatic breccias.

Metallogenic considerations

Considering that (i) the Jurassic- early Cretaceous magmatism in the Coastal Range of northern Chile is characterized by mantle-dominated volcanism (Rogers and Hawkesworth, 1989; Lucassen et al. 2002), (ii) the volume of high-silica rocks (like the rhyolitic dome), of probably crustal-dominated source, is very restricted in a regional scale and (iii) the mineralization in numerous copper deposits (including Mantos Blancos) hosted in Jurassic volcanic rocks of the Coastal Range, is coeval with stocks and sills of mainly dioritic composition, and are intruded by post-mineralization basaltic dykes (Maksaev and Zentilli, 2002), the hydrothermal fluids and associated mineralization in the Mantos Blancos system, were probably derived from mafic to intermediate magmas like the basaltic dykes and diorites. Basaltic dykes have also been described in the Bingham porphyry copper, where they have been considered as the potential metal source for the mineralization (Keith et al. 1997). A similar case has been described by Halter et al. (2005) in Bajo La Alumbrera Cu-Au porphyry. In these two deposits the ore is hosted by more felsic rocks (Halter et al., 2005).

In the Mantos Blancos Cu deposit, the second magmatic-hydrothermal event was temporal and spatially associated with the dioritic and granodioritic porphyries emplacement, and thus, consistent with a magma mingling process. In this scenario, the intrusion of porphyry diorite magma within a colder and shallow rhyolitic magma chamber, could supply not only heat and volatiles during quenching but also metals. In fact, magma mingling processes may have induced the early release of copper-bearing fluids from the quenched mafic hydrous magma, contributing to the mineralization in the polymictic magmatic-hydrothermal breccias, porphyries and rhyolitic dome of the Mantos Blancos

deposit. Although the proportion of felsic/mafic magma in the interaction process is unknown, the mixing line in figure 9 suggests larger volume of felsic magma, which is consistent with the quartz phenocrysts preservation in it.

The slightly radiogenic Sr initial ratios of altered rocks in Mantos Blancos (see Figure 6) resemble those obtained in hydrothermal calcites of the deposit (Tassinari et al., 1993). According to Tassinari et al. (1993), this high Sr initial ratios suggests that hydrothermal fluids were not entirely magmatic and/or isotopic equilibrium between host rocks and the ore bearing hydrothermal fluids occurred.

Conclusions

In the Mantos Blancos copper deposit, the emplacement of dioritic and granodioritic porphyries during the early Cretaceous, was related to the major hypogene copper sulfide mineralization. Two different trends of magma evolution were recognized in these rocks, which resulted in two types of granodioritic porphyries: granodiorite porphyry I (GP I) and granodiorite porphyry II (GP II). The first trend is represented by mafic dykes, dioritic and GP I porphyries, that evolved by hornblende-dominated fractionation, from a mantle dominated source. The second trend is represented by dioritic porphyries and GP II. Low pressure mixing and mingling of dioritic magmas and rhyolitic melts of crustal origin, are likely for the formation of the GP II and polymictic breccias, respectively. The melt inclusions (MI) analyzed in quartz from GP II and in the polymictic magmatic-hydrothermal breccia of the deposit are compositionally more evolved than their host rocks, reinforcing the hypothesis of magma interaction as a genetic mechanism. Field, geochemical and petrographic data in Mantos Blancos deposit point to an interaction between dioritic and siliceous magmas. This interaction may cause the release of hydrothermal fluids from the higher temperature component, during quenching.

Acknowledgements

This study was funded by FONDEF (CONICYT, Chile), grant DO1-1012, assigned to the authors and to the Mantos Blancos division of Anglo American Chile. Permission for publication was established between the University of Chile, the Chilean Government and the Company grant-related contract. Thanks to the geologists of the Mantos Blancos mine with whom we had the pleasure to work. Special acknowledgement to J. Martinez and J. Schneider who made geochemical and isotopic analyses, respectively, and to K. Herrmann for help with the EMPA data acquisition. The first author benefited from the MECESUP program of the Chilean Government to support PhD studies. Special thanks to Bernd Lehmann, Alcides Sial and Francisco Munizaga for helpful comments that greatly improved the manuscript. The manuscript was largely improved by comments and suggestions of W. Halter and I. Miyagi, as well as from the careful editorial handling.

References

Andriessen, P.A., Reutter, K-J. (1994). K-Ar and fission track mineral age determination of igneous rocks related to multiple magmatic arc systems along the 23ºS latitude of Chile and NW Argentina. 141-153. In: Reutter, K-J., Scheuber, E., Wigger, P.J. (eds.). Tectonics of the Southern Central Andes. Structure and evolution of an active continental margin. Springer Verlag. Stuttgart.

Birck, J. L., 1986, Precision K-Rb-Sr isotopic analyses: Application to Rb-Sr chronology, Chemical Geology, 56, 73-83.

Camus F. (2003). Geología de los sistemas porfíricos en los Andes de Chile. SERNAGEOMIN, Chile. 267 p.

Dallmeyer, R.D., Brown M., Grocott J., Taylor G.K., Treolar P.J. (1996). Mesozoic magmatic and tectonic events within the Andean plate boundary zone, 26º - 27º30`S, North Chile: Constraints from ^{40}Ar / ^{39}Ar mineral ages. The Journal of Geology 104: 19 – 40.

Dietrich, A. (1999). Metallogenie, Geochemie und Schmelzeinschluss-Untersuchungen von tin porphyry und copper porphyry Lagerstätten in den zentralen Anden (Bolivien, Chile). PhD Thesis, Clausthal University of Technology, Clausthal-Zellerfeld, pp 198.

Espinoza S, Véliz H, Esquivel J, Arias J, Moraga A (1996) The cupriferous province of the Coastal Range, Northern Chile. In: Camus F, Sillitoe RH, Petersen R (eds.) Andean Copper Deposits: New discoveries, mineralization, styles and metallogeny. Society of Economic Geologists, Special Publ. 5: 19 – 32.

Faure, G. (1986). Principles of isotope geology [2nd edition]: New York, John Wiley & Sons, 589 p., ISBN 0-471-86412-9.

Floyd, P.A. and Winchester, J.A. (1978): Identification and Discrimination of Altered and Metamorphosed Volcanic Rocks Using Immobile Elements. -Chemical Geology 21: 291-306.

Halter, W.E., Heinrich, C.A., Pettke, T. (2005). Magma evolution and the formation of porphyry CU-Au ore fluids: Evidence from silicate and sulfide melt inclusions. Mineralium Deposita 39: 845–863

Hattori, K.H. and Keith, J.D. (2001). Contribution of Mafic melt to porphyry copper mineralization: Evidence from Mount Pinatubo, Philippines, and Bingham Canyon, Utah, USA. Mineralium Deposita 36: 799-806.

Kamenetsky, V.S. and Danyushevsky L.V. (2005) Metals in quartz-hosted melt inclusions: Natural facts and experimental artifacts. American Mineralogist; v. 90; 1674-1678.

Keith, J.D., et al., (1997). The role of magmatic sulfides and mafic alkaline magmas in the Bingham and Tintic mining districts, Utah. Journal of Petrology 38 (12), 1679–1690.

Keskin, M. (2002). FC-Modeler: a Microsoft® Excel© spreadsheet program for modeling Rayleigh fractionation vectors in closed magmatic systems, Computers & Geosciences, 28/8, 919-928.

Kramer W, Siebel W, Romer R L, Haase G, Zimmer M, Ehrlichmann R (2005) Geochemical and isotopic characteristics and evolution of the Jurassic volcanic arc between Arica (18º30´S) and Tocopilla (22ºS), North Chilean Coastal Range. Chemie der Erde, Geochemistry 65: 47 – 78.

Lucassen, F., Franz, G., Thirlwall, M.F. and Mezger K. (1999). Crustal recycling of metamorphic basement: Late Paleozoic granites of the Chilean Coast Range and Precordillera at – 22°S. Journal of Petrology, 40: 1527- 1551

Lucassen, F., Escayola, M., Romer, R.L., Viramonte, J., Koch, K., Franz, G. (2002). Isotopic composition of Late Mesozoic basic and ultrabasic rocks from the Andes (23-32ºS) - implications for the Andean mantle. Contrib. Mineral Petrol. 143: 336-249.

Ludwig, K. R., 1980, Calculation of uncertainties of U-Pb isotope data, Earth and Planetary Science Letters, 46, 212-220.

Maksaev V., Zentilli M. (2002) Chilean stratabound Cu – (Ag) deposits: An overview. In: Porter TM (ed.) Hydrothermal iron oxide copper – gold and related deposits: A global perspective, 2. PCG Publishing, p 185 – 205.

Miller C.F., McDowell S.M., and Mapes R.W. (2003) Hot and cold granites?: Implications of zircon saturation temperatures and preservation of inheritance: Geology, 31, 529-532.

Oliveros, V. (2005) Les formations magmatiques jurassiques et mineralisation du nord Chili, origine, mise en place, alteration, metamorphisme: etude geochronologique et geochemie. PhD Thesis. Universite de Nice-Sophia Antipolis, France. 285 p.

Palacios C (1984) Considerations about the plate tectonic models, volcanism, and continental crust in the Southern part of the Central Andes. Tectonophysics 108: 205 – 214.

Perelló, J., Martini, R., Arcos, R., Muhr, R. (2003). Buey Muerto: porphyry copper mineralization in the early Cretaceous arc of northern Chile. Proc. 10th Congreso Geológico de Chile.

Pichowiak S., Buchelt M., Damm K.W. (1990) Magmatic activity and tectonic setting of early stages of Andean cycle in northern Chile. Geol Soc Am. Special Paper 241: 127 – 144.

Pichowiak, S. (1994). Early Jurassic to Early Cretaceous magmatism in the Coastal Cordillera and the Central Depression of North Chile. 203-217. In: Reutter, K-J., Scheuber, E., Wigger, P.J. (eds.) Tectonics of the Southern Central Andes. Structure and evolution of an continental margin. Springer Verlag. Stuttgart.

Pin, C. and Zalduegui, J. F. S., 1997, Sequential separation of light rare-earth elements, thorium and uranium by miniaturized extraction chromatography: application to isotopic analyses of silicate rocks, Analytica Chimica Acta, 339, 79-89.

Ramírez L.E., Palacios C., Townley B., Parada M.A., Sial A.N., Fernandez-Turiel J. L., Gimeno D., Garcia-Valles M., Lehmann, B. (2006) The Mantos Blancos copper deposit: an Upper Jurassic breccia–style hydrothermal system in the Coastal Range of Northern Chile. Mineraluim Deposita.,41, 246-258.

Rogers G, Hawkesworth CJ (1989) A geochemical traverse across the North Chilean Andes: evidence for crust generation from the mantle wedge. Earth and Planet Sci Lett 91: 271 – 285.

Scheuber E, González G (1999) Tectonics of the Jurassic – Early Cretaceous magmatic arc of the North Chilean Coastal Cordillera (22º - 26ºS): A story of crustal deformation along a convergent plate boundary. Tectonics 18: 895 – 910.

Scheuber, E. (1994). Tektonische Entwicklung des nordchilenischen aktiven Kontinentalrandes: Der Einfluss von Plattenkonvergenz und Rheologie. Geotekton. Forsch. 81: 1-131.

Tassinari C, Munizaga F, Ramírez R (1993). Edad y geoquímica isotópica Rb-Sr del yacimiento de cobre Mantos Blancos: relación temporal con el magmatismo jurásico. Rev. Geol. Chile 20: 193-205.

Watson E.B, Harrison T.M. (1983). Circón saturation revisited: temperaturas and composition effects in a variety of cristal magma types. Earth and Planetary Science Letters 64: 295-304.

Webster J.D, Thomas R., Förster HJ., Seltmann R., Tappen C. (2004). Geochemical evolution of halogen-enriched granite magmas and mineralizing fluids of the Zinnwald tin-tungsten mining district, Erzgebirge, Germany. Mineralium Deposita 39: 452–472.

Wittenbrink, J. (2006). Geochemische, metallogenetische und Bor-Isotopen Untersuchungen an Schmelzeinschluessen und Gesteinen bolivianischer und chilenischer *porphry*-Lagerstätten der zentralen Anden. Ph.D. thesis, Clausthal University of Technology, 217 pp.

Appendix 1

Analytical method of Sr-Nd isotopes

Powdered rock samples were weighed into clean Teflon screw-top beakers and spiked with mixed ^{87}Rb-^{84}Sr and ^{149}Sm-^{150}Nd tracers. The samples were completely dissolved in a 3:1 mixture of 22 N HF/14 N HNO_3 on a hotplate @ ~ 110°C. All solutions were evaporated to dryness and redissolved in aqua regia, evaporated again and then rewetted with 2 N HNO_3. Rb, Sr, Sm and Nd were chemically separated using a tandem column elution scheme, modified from Pin and Zalduegui (1997). The sample solutions were transferred to preconditioned small-size (50 µl) Teflon columns containing EICHROM Sr Resin®, coupled with a second set of 50 µl columns containing EICHROM TRU Resin® to adsorb the REE. After collecting the Rb during the first elution step and further washing with 2 N HNO_3, Sr and REE were stripped from the decoupled columns with 1.3 ml of DDW. The REE cut was directly eluted onto 1 ml columns containing EICHROM Ln Resin® and washed with 9.5 ml of 0.25 N HCl. Nd was then eluted with 4 ml of 0.25 N HCl prior to elution of Sm with 2 ml of 0.75 HCl.

For mass spectrometry, Sr was loaded with $TaCl_5$-HF-H_3PO_4 solution (Birck, 1986) onto W single filaments, and Rb, Sm and Nd loaded with DDW onto the evaporation ribbon of double-Ta and double-Re filament assemblages, respectively. All isotopic measurements were performed on a six-collector FINNIGAN MAT 261 solid-source mass spectrometer running in static multicollection mode. Sr isotopic ratios were normalized to $^{88}Sr/^{86}Sr = 0.1194$ and Nd isotopic ratios normalized to $^{146}Nd/^{144}Nd = 0.7219$. Repeated static measurements of the NBS 987 Sr isotope standard and the La Jolla Nd standard over the duration of this study yielded $^{87}Sr/^{86}Sr = 0.71025 \pm 0.00004$ (2σ mean, n = 12) and $^{143}Nd/^{144}Nd = 0.511848 \pm 0.000009$ (2σ mean, n = 8). Maximum total procedure blanks (n = 6) amounted to 30 pg Sr, 5 pg Rb, and 50 pg Sm and Nd. They were found to be negligible with respect to the analyzed sample amounts.

Figure captions

Figure 1. Geological map of the Coastal Cordillera, Northern Chile, and location of the Mantos Blancos ore deposit (*star*) and other Late Jurassic volcanic-hosted copper deposits (*diamonds*). Modified after Maksaev and Zentilli (2002).

Figure 2. Geological map of the Mantos Blancos district. In the map at deposit scale RB: Rhyolitic breccia, PB: polymictic breccia.

Figure 3. Microphotographs of different rock units in the Mantos Blancos district: A) Miarolitic cavity with quartz and sulfide (Cpy) infill in diorite porphyry (cross-polarized light, sample CPM-1-2); B) Miarolitic cavity with sulfide (Cpy±Bo) infill with a border zone of chlorite, calcite, epidote and chalcopyrite in diorite porphyry (cross-polarized light, sample CPM-1-15); C) Mineralized polymictic magmatic-hydrothermal breccia with cross-polarized light and D) with plane-polarized light (sample P-4-1); E) Oscillatory-zoned plagioclase phenocryst in GP I (cross-polarized light, sample MB-2-3); F) Reabsorbed quartz phenocryst in GP II (cross-polarized light, sample 11497-320); G) and H) Pictures of dioritic micro-enclaves in GP II. From A to F, the size of the scale bar is 1 mm, and in G and H is 1 cm. Qz: quartz, Chl: chlorite, Plg: plagioclase, Cpy: chalcopyrite, Bo: bornite, Cc:calcite, Ep: epidote.

Figure 4. Immobile element classification of mayor rocks units of the Mantos Blancos deposit. After Floyd and Winchester (1978).

Figure 5.Chondrite-normalized REE patterns of rock samples from Mantos Blancos.

Figure 6. εNd and $^{87}Sr/^{86}Sr_i$ isotope data from Mantos Blancos, with reference data from Late Jurassic volcanic rocks of the La Negra Formation, Cretaceous dykes of the Coastal Range (Rogers and Hawkesworth 1989; Lucassen et al. 2002) and Paleozoic granitoids (Lucassen et al., 1999). Lines with tick marks represent a simple mixing model. The gray vertical field represents the $^{87}Sr/^{86}Sr$ ratio of calcites from the propylitic assemblage of Mantos Blancos (Tassinari et

al. 1993). All isotope data are recalculated to age of emplacement and Paleozoic granitoids to 150 Ma, see text for details.

Figure 7. Selected major element variation diagrams of; A) melt inclusions and B) whole rock analyses of Mantos Blancos rocks. The average of melt inclusions data is also plotted forcomparison with their host rocks.

Figure 8. Zircon saturation temperature (T_{Zr}) of felsic-intermediate rocks in the Mantos Blancos district. The shaded area represents the transition of cold and hot granites of Miller et al. (2003).

Figure 9. La versus La/Yb diagram. The data define two trends: one dominated by hornblende fractionation (dashed grey line) and the other dominated by magma mixing (solid line with tick marks) over imposed to plagioclase fractionation. Because no REE data is available from GP II melt inclusions, we chose melt inclusion data from the rhyolitic dome (Wittenbrink, 2006) as endmember of the mixing model. The mafic endmember corresponds to the average of the diorite samples. Rayleigh fractionation vectors of different minerals are shown according to crystal-melt partitioning data for basic and intermediate magma by Keskin (2002). The size of the vectors is equal to 50% of crystallization. Note that small vertical apparent trend does not constitute necessarily an evolution trend.

Figure 10. Schematic diagram showing the Mantos Blancos petrogenetic model. See text for details.

Table captions

Table 1. Whole rock analyses from Mantos Blancos magmatic rocks.

Table 2. Sr-Nd isotope data from Mantos Blancos ore deposit.

Table 3. Melt inclusions analyses from Mantos Blancos ore deposit.

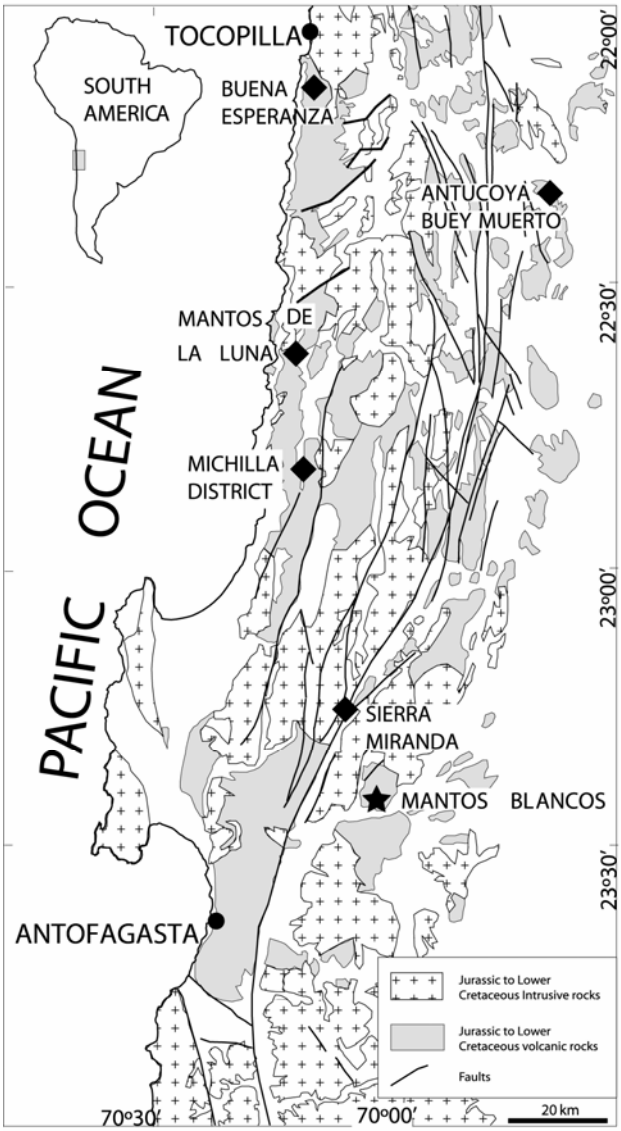
TOCOPILLA
SOUTH AMERICA
BUENA ESPERANZA
ANTUCOYA
BUEY MUERTO
MANTOS DE LA LUNA
MICHILLA DISTRICT
PACIFIC OCEAN
SIERRA MIRANDA
MANTOS BLANCOS
ANTOFAGASTA
22°00′
22°30′
23°00′
23°30′
70°30′
70°00′
20 km
Jurassic to Lower Cretaceous Intrusive rocks
Jurassic to Lower Cretaceous volcanic rocks
Faults

FIGURE 1

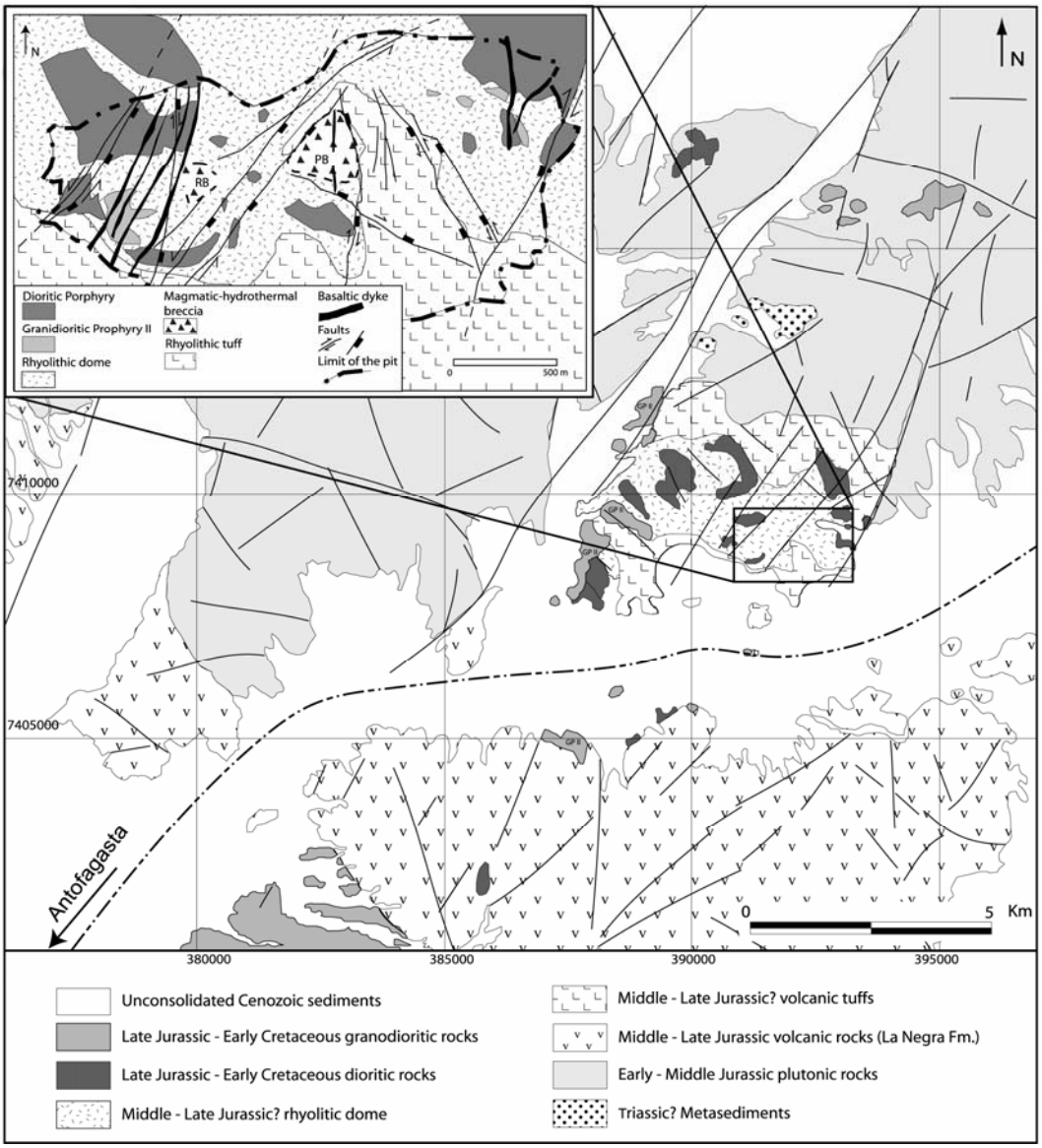
N
PB
RB
Dioritic Porphyry
Granidioritic Prophyry II
Rhyolithic dome
Magmatic-hydrothermal breccia
Rhyolithic tuff
Basaltic dyke
Faults
Limit of the pit
0
500 m
7410000
7405000
Antofagasta
0
5 Km
380000
385000
390000
395000
Unconsolidated Cenozoic sediments
Late Jurassic - Early Cretaceous granodioritic rocks
Late Jurassic - Early Cretaceous dioritic rocks
Middle - Late Jurassic? rhyolitic dome
Middle - Late Jurassic? volcanic tuffs
Middle - Late Jurassic volcanic rocks (La Negra Fm.)
Early - Middle Jurassic plutonic rocks
Triassic? Metasediments

FIGURE 2

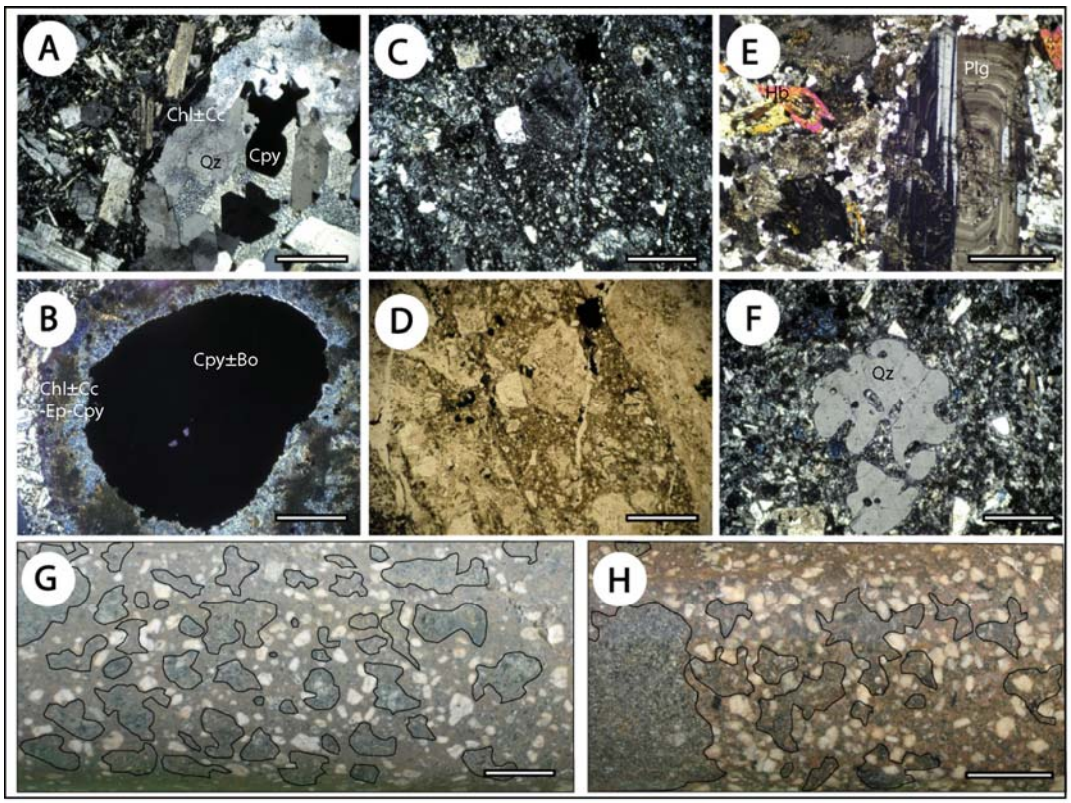

FIGURE 3

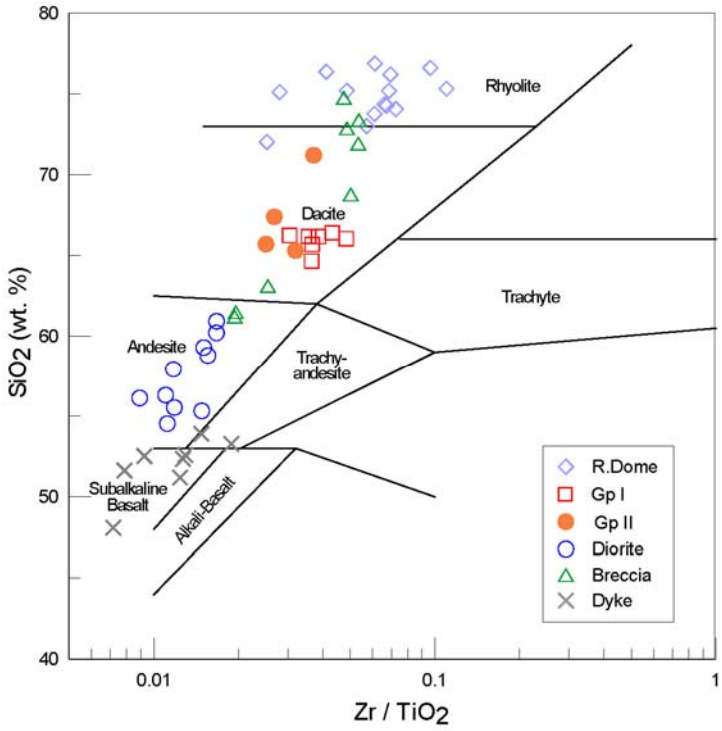
80
70
60
50
40
SiO2 (wt. %)
0.01
0.1
1
Zr / TiO2
Rhyolite
Dacite
Trachyte
Andesite
Trachy-
andesite
Subalkaline
Basalt
Alkali-Basalt
R.Dome
Gp I
Gp II
Diorite
Breccia
Dyke

FIGURE 4

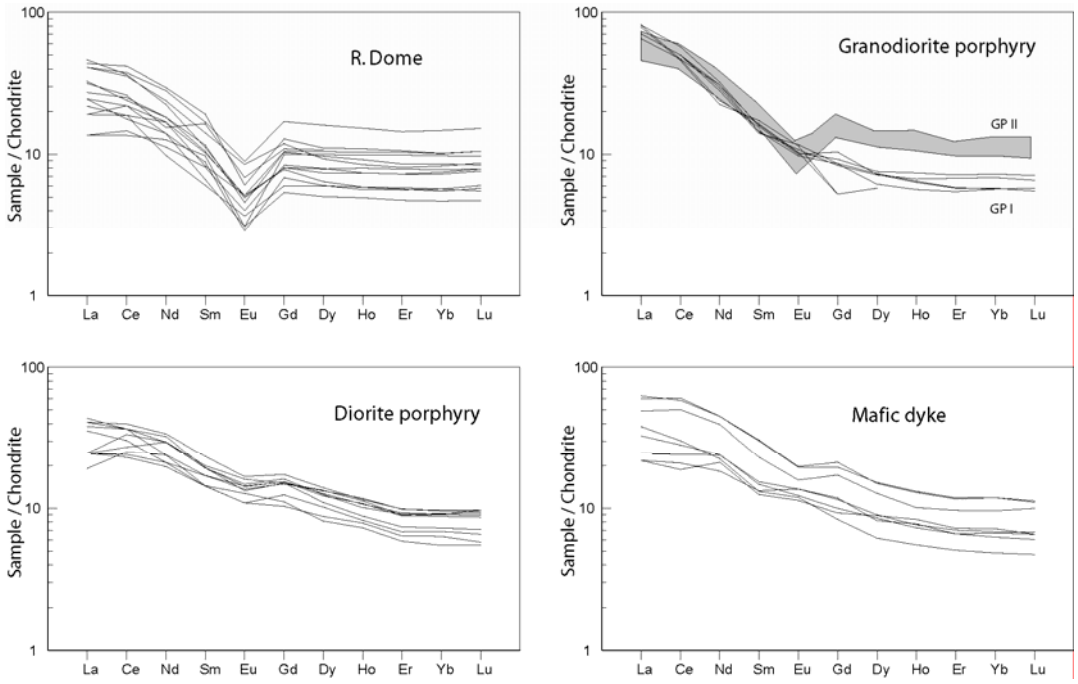
R. Dome
Granodiorite porphyry
GP II
GP I
Diorite porphyry
Mafic dyke
Sample / Chondrite
100
10
1
La Ce Nd Sm Eu Gd Dy Ho Er Yb Lu

FIGURE 5

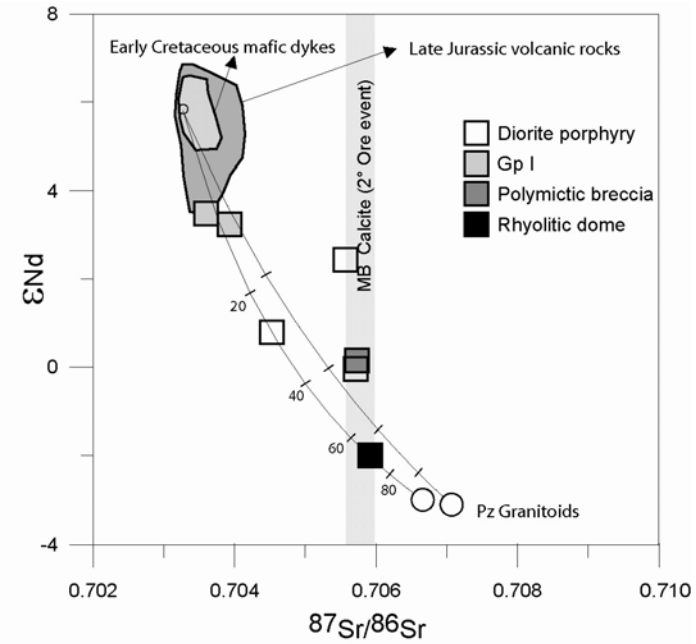
8
4
0
-4
εNd
0.702
0.704
0.706
0.708
0.710
87Sr/86Sr
Early Cretaceous mafic dykes
Late Jurassic volcanic rocks
MB Calcite (2° Ore event)
Diorite porphyry
Gp I
Polymictic breccia
Rhyolitic dome
20
40
60
80
Pz Granitoids

FIGURE 6

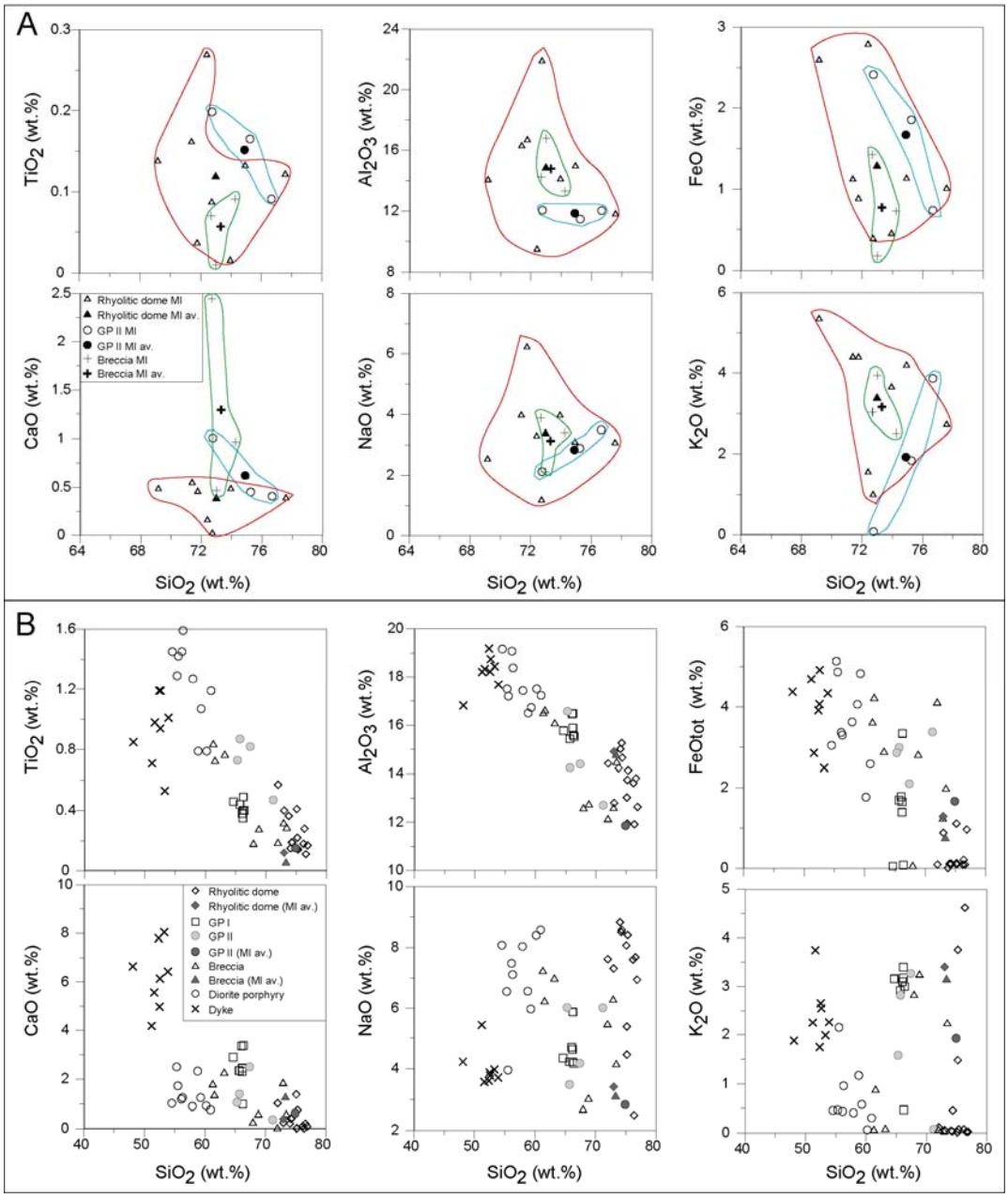
A
TiO2 (wt.%)
Al2O3 (wt.%)
FeO (wt.%)
CaO (wt.%)
NaO (wt.%)
K2O (wt.%)
SiO2 (wt.%)
Rhyolitic dome MI
Rhyolitic dome MI av.
GP II MI
GP II MI av.
Breccia MI
Breccia MI av.
B
TiO2 (wt.%)
Al2O3 (wt.%)
FeOtot (wt.%)
CaO (wt.%)
NaO (wt.%)
K2O (wt.%)
SiO2 (wt.%)
Rhyolitic dome
Rhyolitic dome (MI av.)
GP I
GP II
GP II (MI av.)
Breccia
Breccia (MI av.)
Diorite porphyry
Dyke

FIGURE 7

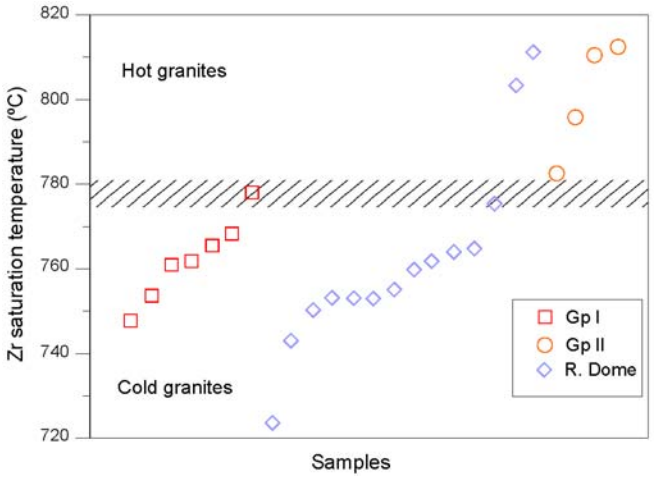
820
800
780
760
740
720
Zr saturation temperature (ºC)
Hot granites
Cold granites
Samples
Gp I
Gp II
R. Dome

FIGURE 8

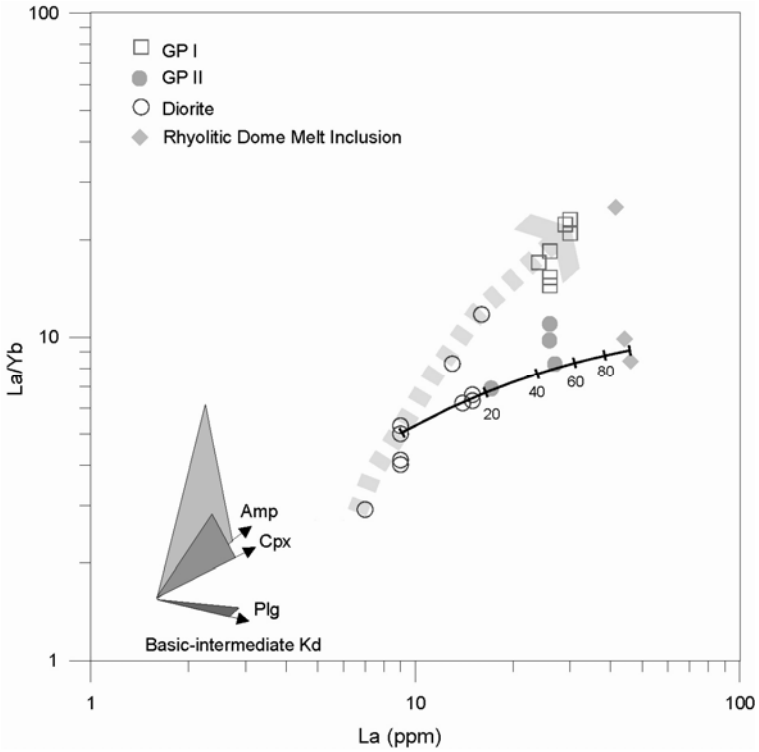
100
10
1
La/Yb
1
10
100
La (ppm)
GP I
GP II
Diorite
Rhyolitic Dome Melt Inclusion
Amp
Cpx
Plg
Basic-intermediate Kd
20
40
60
80

FIGURE 9

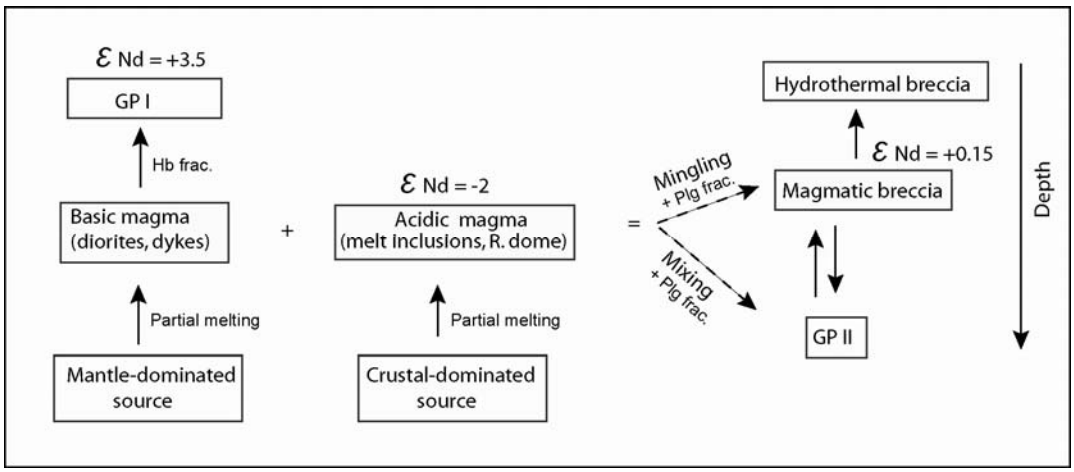
ε Nd = +3.5
GP I
Hb frac.
Basic magma
(diorites, dykes)
Partial melting
Mantle-dominated
source
+
ε Nd = -2
Acidic magma
(melt inclusions, R. dome)
Partial melting
Crustal-dominated
source
=
Mingling
+ Plg frac.
Mixing
+ Plg frac.
Hydrothermal breccia
ε Nd = +0.15
Magmatic breccia
GP II
Depth

FIGURE 10

TABLE 1. Whole rock analyses from Mantos Blancos magmatic rocks.

	Rhyolitic Dome														
Sample	CPM-1.1	CPM-1.12	CPM-1.16	CPM-1.17	CPM-1.18	CPM-1.20	CPM-1.24	CPM-1.28	CPM-1.4	CPM-1.6	CPM-1.8	CPM-1.9	MB-2.6	MB1**	MB5**
SiO2	75.19	76.36	72.02	74.27	74.35	76.60	76.87	76.20	75.31	73.00	74.05	75.10	75.18	73.76	74
TiO2	0.22	0.28	0.57	0.19	0.19	0.11	0.17	0.18	0.14	0.40	0.15	0.41	0.15	0.36	0.19
Al2O3	13.75	11.92	14.42	15.26	14.66	13.81	12.64	13.62	14.13	12.80	15.02	13.02	11.94	14.23	13.6
Fe2O3	0.45	1.58	1.35	0.23	<0.1	0.37	0.20	0.74	<0.1	1.44	0.34	0.25	1.64	1.25	1.67
FeO	0.12	0.20	0.08	<0.1	<0.1	0.08	0.96	0.08	<0.1	0.88	<0.1	<0.1	1.08	-	-
MnO	0.01	0.01	0.01	0.01	0.01	0.01	0.01	0.01	0.01	0.01	0.01	0.01	0.04	0.01	0.02
MgO	0.18	0.32	0.14	0.01	0.05	0.01	0.65	0.07	0.02	0.82	0.10	0.02	1.22	0.08	0.04
CaO	0.02	0.01	1.02	0.40	0.45	0.20	0.09	0.11	0.75	0.24	0.21	1.38	0.01	0.08	0.58
Na2O	4.46	2.50	7.62	8.50	8.57	7.68	6.94	7.60	8.40	7.31	8.82	8.07	5.38	7.65	7.87
K2O	3.76	4.62	0.12	0.04	0.46	0.03	0.03	0.08	0.08	0.06	0.05	0.02	1.48	0.04	0.13
P2O5	0.01	0.04	0.07	0.06	0.04	N/D	0.04	0.05	0.02	N/D	0.03	0.08	0.06	0.08	0.07
LOI %	1.61	1.86	2.36	0.60	0.79	0.57	0.95	0.99	0.80	1.98	0.82	1.40	1.40	1.80	1.54
Total	99.78	99.70	99.78	99.57	99.57	99.47	99.55	99.73	99.66	98.94	99.60	99.76	99.58	99.34	99.7
Ba	475	654	23	22	43	21	21	22	26	21	25	17	126	8	12
Sr	85	106	54	41	39	27	36	80	27	39	60	28	47	39	36
Nb	5.6	5.6	5.6	5.0	5.0	5.0	3.8	4.4	3.8	5.6	4.4	5.6	3.8	6.0	7
Hf	2.5	4.6	4.8	3.7	3.5	3.7	2.4	2.7	4.2	6.4	3.6	3.6	1.3	5.1	2.8
Zr	107	115	144	128	126	106	104	125	154	229	109	115	103	222	129
Y	9	23	18	14	19	22	9	16	21	32	12	23	14	29	26
Th	13.0	12.0	10.0	13.0	15.0	9.3	11.0	11.0	12.0	14.0	13.0	13.0	13.0	11.6	9.4
Cr	21	34	23	16	15	20	18	19	12	21	25	17	13	<1	<1
Co	3	6	6	4	3	2	4	2	2	4	4	3	6	1	2
Sc	4	6	6	3	3	4	2	4	5	7	2	5	3	5	5
V	28	24	38	12	11	6	18	12	18	27	7	13	16	25	11
Cu	96	485	470	880	66	1540	29	730	35	5700	155	83	920	1103	2185
Zn	3	2	8	2	2	3	52	2	2	53	3	6	40	11	14
Ni	4	6	6	2	6	4	2	2	3	2	1	2	5	7	2
La	9	16	15	12	10	5	9	17	5	15	7	7	8	12	8.2
Ce	21	40	34	23	24	13	17	35	14	36	18	21	18	25	18
Nd	10	21	17	13	13	9	10	16	8	20	7	12	12	11	8
Sm	2.04	4.45	3.28	2.43	2.69	2.26	1.54	2.59	1.88	3.91	1.40	2.37	1.92	3.80	2.9
Eu	0.25	0.53	0.74	0.43	0.40	0.27	0.27	0.44	0.35	0.78	0.32	0.45	0.45	0.60	0.4
Gd	2.10	3.94	3.64	2.47	3.17	3.05	1.65	2.46	2.57	5.22	1.84	3.21	2.40	-	-
Dy	2.30	4.22	3.54	2.82	3.69	3.80	1.92	3.01	3.03	6.12	2.28	3.98	2.45	-	-
Ho	0.48	0.93	0.72	0.63	0.78	0.84	0.42	0.68	0.63	1.30	0.50	0.88	0.50	-	-
Er	1.42	2.64	2.01	1.81	2.13	2.46	1.18	1.96	1.81	3.60	1.45	2.58	1.40	-	-
Yb	1.36	2.51	2.05	1.80	2.12	2.42	1.16	1.93	1.85	3.65	1.41	2.50	1.41	2.70	2
Lu	0.22	0.40	0.33	0.29	0.32	0.37	0.18	0.30	0.30	0.58	0.23	0.40	0.21	0.41	0.3
TempZr	760	775	755	761	750	753	753	764	765	803	743	724	753	812	750

				GP I					GP II				Diorite porphyry		
Sample	MB-2.1	MB-2.3	MB-2.7	MB-2.8	1301-208*	MB3**	MB4**	CPM-1.14a	1301-350*	1301-363*	11497-320*	CPM-1.11	CPM-1.15	CPM-1.2
SiO2	66.17	66.05	65.69	66.18	66.25	64.66	66.40	71.20	67.39	65.70	65.30	59.30	56.12	54.53
TiO2	0.35	0.38	0.44	0.40	0.49	0.46	0.40	0.47	0.82	0.87	0.73	1.07	1.45	1.45
Al2O3	15.88	16.47	15.43	16.48	15.59	15.77	15.53	12.71	14.40	14.25	16.57	16.73	19.07	19.16
Fe2O3	2.02	1.60	2.14	1.82	1.26	3.88	3.42	0.93	2.25	3.58	1.09	1.23	2.15	3.24
FeO	1.36	1.72	1.64	1.60	3.24	-	-	3.32	2.04	2.80	2.80	4.76	3.32	3.00
MnO	0.04	0.07	0.06	0.06	0.11	0.06	0.08	0.06	0.07	0.21	0.07	0.08	0.05	0.05
MgO	1.48	1.20	1.69	1.28	2.82	1.61	1.25	1.61	0.72	2.61	2.22	4.98	4.44	4.60
CaO	2.45	3.36	2.35	2.31	0.99	2.90	3.37	0.36	2.50	1.40	1.06	1.25	1.19	1.02
Na2O	4.63	4.70	4.23	4.23	5.87	4.35	4.18	6.01	4.18	3.49	6.02	5.97	7.48	8.08
K2O	3.18	3.10	2.92	3.40	0.47	3.16	3.00	0.08	3.27	2.82	1.58	0.58	0.44	0.46
P2O5	0.17	0.15	0.18	0.15	0.13	0.20	0.17	N/D	0.19	0.19	0.18	0.19	0.17	0.17
LOI %	1.86	1.11	2.79	1.90	2.54	2.67	1.15	1.77	2.02	1.96	2.12	3.40	3.67	3.88
Total	99.59	99.91	99.56	99.81	99.76	99.72	98.96	98.52	99.85	99.88	99.74	99.54	99.55	99.64
Ba	615	580	462	642	60	649	625	26	376	540	209	68	42	48
Sr	352	373	291	382	132	389	389	53	98	121	100	82	115	110
Nb	3.8	5.0	3.8	3.8	4.2	4.0	4.0	5.0	6.5	6.1	6.0	6.3	5.6	5.0
Hf	3.6	3.8	2.7	3.3	8.6	3.5	2.9	5.7	11.0	11.0	11.0	4.5	3.9	2.0
Zr	135	184	161	142	149	167	173	174	220	218	233	161	129	162
Y	11	12	12	13	13	14	12	25	27	24	24	23	24	21
Th	10.0	10.0	13.0	14.0	5.3	8.7	9.0	13.0	8.3	7.7	6.5	5.0	4.5	3.0
Cr	17	17	14	21	269	9	5	21	280	185	160	49	110	107
Co	6	8	9	6	7	6	7	6	7	9	14	17	21	25
Sc	5	4	5	5	9	-	-	9	15	13	12	17	22	17
V	49	47	65	58	56	54	50	41	102	109	71	58	133	138
Cu	28	6	36	11	81	150	13	10300	32	4	9	247	30	18
Zn	41	31	35	42	65	52	44	141	49	113	60	101	77	81
Ni	4	6	5	5	11	10	5	8	3	6	12	14	48	50
La	24	26	26	26	30	29	30	17	27	26	26	9	9	9
Ce	45	48	48	48	55	44	45	38	55	56	57	32	23	26
Nd	22	20	21	22	23	16	17	18	28	28	26	21	15	21
Sm	3.37	3.25	3.32	3.73	3.64	4.00	3.80	3.62	5.16	5.23	5.32	4.45	3.94	4.62
Eu	0.85	1.02	0.94	0.89	0.87	1.00	0.90	0.63	0.97	0.97	1.05	1.16	1.25	1.40
Gd	2.63	2.64	2.56	2.83	3.18	-	-	3.98	5.81	5.24	5.03	4.61	4.72	4.60
Dy	2.35	2.79	2.73	2.88	2.75	-	-	4.25	5.57	5.25	5.21	4.20	4.67	5.10
Ho	0.48	0.55	0.57	0.63	0.54	-	-	0.90	1.24	1.00	0.95	0.75	0.92	0.96
Er	1.36	1.45	1.69	1.78	1.44	-	-	2.45	3.03	2.41	2.70	1.84	2.20	2.23
Yb	1.41	1.41	1.70	1.80	1.43	1.30	1.30	2.46	3.27	2.37	2.66	1.80	2.24	2.17
Lu	0.22	0.22	0.25	0.27	0.21	0.22	0.22	0.41	0.50	0.35	0.40	0.27	0.34	0.33
TempZr	747	768	762	761	778	754	765	796	783	812	811	768	737	745

	Diorite porphyry							Polymictic Breccia					
Sample	CPM-1.22	CPM-1.3	CPM-1.5	P-3-10	1301-250*	11506-30*	11497-278,5*	1301-158*	1301-200*	1301-202*	1301-240*	11506-200*	11506-330*
SiO2	60.93	57.93	56.30	60.21	58.80	55.53	55.32	72.92	63.20	61.30	61.58	68.84	73.43
TiO2	1.19	1.27	1.59	0.79	0.79	1.42	1.29	0.32	0.77	0.84	0.73	0.28	0.29
Al2O3	17.23	17.43	18.38	17.50	16.50	17.20	17.50	12.62	16.10	16.52	16.63	12.77	14.50
Fe2O3	1.89	2.59	2.87	3.55	1.55	3.46	2.88	1.27	1.50	1.48	1.40	2.77	0.10
FeO	2.56	3.56	3.20	1.68	3.88	4.80	5.04	1.20	2.80	3.48	4.00	2.80	1.96
MnO	0.03	0.07	0.11	0.10	0.20	0.08	0.11	0.06	0.11	0.16	0.26	0.03	0.04
MgO	2.19	3.28	4.14	3.47	5.04	4.80	4.24	1.13	2.62	3.70	3.32	1.05	0.89
CaO	0.76	0.90	1.25	0.92	2.33	1.73	2.50	1.87	2.29	1.82	1.38	0.60	0.60
Na2O	8.57	8.04	7.11	8.39	6.56	3.96	6.55	6.30	7.00	7.25	6.25	3.05	4.17
K2O	0.31	0.41	0.96	0.07	1.17	2.15	0.47	0.05	0.10	0.08	0.89	3.26	2.25
P2O5	N/D	N/D	0.21	0.21	0.17	0.24	0.21	0.09	0.22	0.25	0.19	-	0.08
LOI %	2.57	3.22	3.66	2.94	2.96	4.46	3.56	1.86	3.06	2.97	2.99	2.33	1.52
Total	98.23	98.70	99.78	99.83	99.95	99.83	99.67	99.69	99.77	99.85	99.62	97.78	99.83
Ba	45	55	93	<5	87	213	50	23	21	29	77	513	331
Sr	110	107	130	97	142	110	78	43	163	131	200	56	121
Nb	5.6	5.0	5.0	4.0	3.6	4.0	3.9	4.2	5.0	4.1	3.8	4.1	4.2
Hf	5.2	2.2	4.0	2.3	3.6	5.1	5.1	16.0	5.5	5.1	3.8	15.0	16.0
Zr	199	149	175	132	123	168	191	155	196	163	143	140	155
Y	27	18	26	16	14	21	22	21	20	17	14	19	16
Th	4.8	3.0	5.2	<2	5.9	5.3	5.9	5.9	7.7	7.1	5.9	6.5	5.9
Cr	71	90	73	31	140	169	137	296	256	102	68	312	357
Co	16	18	21	11	17	23	23	7	10	17	18	3	2
Sc	17	17	21	11	15	22	20	6	13	14	12	4	4
V	109	123	133	82	142	165	152	53	95	100	108	21	24
Cu	14000	8500	192	67	6	500	16	580	109	46	39	21000	23
Zn	72	84	81	68	110	73	100	36	61	69	98	122	28
Ni	39	39	20	13	33	38	47	16	11	18	18	3	5
La	7	9	14	13	16	15	15	5	18	14	12	12	17
Ce	24	22	35	29	35	35	38	17	39	31	30	32	42
Nd	17	14	23	15	17	21	24	12	17	16	16	21	21
Sm	3.93	3.33	4.49	3.32	3.34	4.46	5.40	3.20	3.64	3.57	3.20	4.98	3.65
Eu	1.19	0.95	1.24	0.95	1.11	1.29	1.46	0.61	0.99	0.96	0.92	0.86	0.67
Gd	4.56	3.81	4.73	3.17	3.41	4.94	5.32	3.71	4.04	3.69	3.09	4.48	3.31
Dy	5.06	3.89	4.85	3.34	3.10	4.77	5.33	3.70	3.93	3.43	3.07	4.40	3.57
Ho	1.00	0.70	0.91	0.67	0.62	0.86	0.98	0.76	0.83	0.69	0.56	0.81	0.74
Er	2.45	1.70	2.31	1.59	1.46	2.27	2.46	1.84	2.10	1.65	1.47	2.01	1.94
Yb	2.40	1.70	2.25	1.57	1.36	2.27	2.37	1.83	2.09	1.59	1.45	1.95	1.92
Lu	0.37	0.25	0.37	0.22	0.21	0.35	0.36	0.27	0.31	0.23	0.21	0.29	0.31
TempZr	770	742	757	736	714	771	750	756	762	750	755	784	804

	Polymictic Breccia		Mafic dykes							
Sample	MB6**	P-4-1	CPM-1.10	CPM-1.25	CPM-1.26	CPM-1.27	P-2-5	P-2-7	P-2-8	P-2-9
SiO2	67.94	71.98	52.52	48.09	51.20	53.28	51.63	53.90	52.35	52.59
TiO2	0.18	0.19	0.94	0.85	0.71	0.53	0.98	1.01	1.19	1.19
Al2O3	12.61	12.16	18.22	16.82	18.21	18.44	18.33	17.68	19.18	18.74
Fe2O3	6.65	1.11	3.63	4.05	2.82	4.15	4.46	3.68	4.98	3.89
FeO	-	4.04	3.92	4.20	4.60	2.40	2.76	4.20	3.72	4.72
MnO	0.08	0.09	0.16	0.19	0.10	0.10	0.11	0.15	0.21	0.22
MgO	2.64	2.11	4.92	7.27	3.94	3.81	5.09	3.55	2.78	3.29
CaO	0.27	0.04	4.98	6.64	4.18	8.04	5.57	6.43	7.80	6.14
Na2O	2.70	5.48	3.88	4.23	5.44	3.98	3.57	3.71	3.61	3.78
K2O	2.84	0.08	2.65	1.88	2.25	1.99	3.75	2.26	1.75	2.55
P2O5	0.06	-	0.15	0.14	0.16	0.17	0.11	0.35	0.43	0.44
LOI %	2.71	2.41	3.72	5.30	5.95	2.64	3.40	2.71	1.76	2.26
Total	98.69	99.69	99.69	99.66	99.56	99.53	99.76	99.63	99.76	99.81
Ba	455	8	442	680	380	320	322	421	401	492
Sr	57	54	433	290	550	471	463	445	503	436
Nb	5.0	8.0	2.5	3.8	3.1	2.5	4.0	4.0	4.0	6.0
Hf	3.2	3.4	2.7	0.2	2.0	1.9	1.8	4.6	4.9	5.2
Zr	117	101	87	61	88	100	77	149	151	154
Y	16	17	16	14	16	10	17	23	28	27
Th	8.7	11.0	3.0	2.5	< 2	3.0	<2	6.5	7.0	6.7
Cr	<1	9	43	269	25	76	45	16	9	9
Co	22	5	26	21	18	12	24	20	20	19
Sc	-	6	22	19	15	15	25	23	23	21
V	18	27	204	180	146	178	196	217	218	204
Cu	5640	2100	47	81	2	76	11	155	220	225
Zn	101	90	88	165	62	60	90	90	210	110
Ni	22	7	21	89	8	21	15	8	4	10
La	2	5	12	8	9	14	8	18	23	22
Ce	4	13	27	18	23	29	20	48	56	58
Nd	<5	8	17	15	17	16	13	28	32	32
Sm	2.00	2.21	3.56	2.89	3.42	3.04	3.07	5.33	7.09	6.98
Eu	0.30	0.29	1.19	0.99	1.07	1.04	1.19	1.38	1.72	1.70
Gd	-	2.78	3.63	2.84	3.06	2.56	3.54	5.27	6.49	6.00
Dy	-	3.39	3.12	3.38	3.25	2.35	3.43	4.87	5.71	5.81
Ho	-	0.71	0.66	0.71	0.62	0.47	0.65	0.86	1.10	1.12
Er	-	1.94	1.64	1.80	1.65	1.26	1.75	2.41	2.90	2.95
Yb	1.70	1.98	1.66	1.78	1.55	1.20	1.69	2.38	2.95	2.94
Lu	0.28	0.30	0.25	0.25	0.23	0.18	0.26	0.38	0.42	0.43
TempZr	780	757	668	585	644	652	647	699	702	710

Most samples came from open pit walls, except GP I samples that came from a few km to the west and southwest of the pit. Samples from drill cores are marked in the table with *. Mayor elements in wt %, trace elements in ppm, <: below limit of detection, -: not analyzed, TempZr: zircon saturation temperature in ºC, **: samples reported by Wittenbrink (2006).

TABLE 2. Sr-Nd isotope data from Mantos Blancos ore deposit.

Sample	Rock unit	Rb ppm	2σ	Sr ppm	2σ	$^{87}Sr/^{86}Sr$	2σ	$^{87}Rb/^{86}Sr$	2σ	$(^{87}Sr/^{86}Sr)_o$
MB1*	Rhyolitic dome	3,155	0,032	37,68	0,30	0,7065	0,00001	0,242	0,004	0,7059
MB6	Polymictic breccia	119,4	1,660	55,21	0,57	0,7184	0,00002	6,264	0,081	0,7059
MB3	GP I	81,19	0,810	391,55	3,13	0,7051	0,00001	0,600	0,008	0,7039
MB4	GP I	79,98	0,800	382,43	3,06	0,7048	0,00001	0,605	0,008	0,7036
MB-sp-7	Diorite porphyry	52		88		0,71452		4,94		0,704549
MB-sp-46	Diorite porphyry	71		100		0,71374		4,04		0,705586
MB-sp-60	Diorite porphyry	120		101		0,71061		2,42		0,705725

Sample	Rock unit	Sm ppm	2σ	Nd ppm	2σ	$^{143}Nd/^{144}Nd$	2σ	$^{147}Sm/^{144}Nd$	2σ	$(^{143}Nd/^{144}Nd)_o$	εNd
MB1*	Rhyolitic dome	4,236	0,004	16,511	0,02	0,51249	0,000006	0,1551	0,0008	0,51234	-2,0
MB6	Polymictic breccia	1,211	0,001	3,352	0,004	0,51267	0,000008	0,2184	0,0011	0,51247	0,1
MB3	GP I	4,29	0,004	24,32	0,031	0,51272	0,000008	0,1067	0,0005	0,51263	3,2
MB4	GP I	4,351	0,004	23,199	0,03	0,51274	0,000007	0,1134	0,0006	0,51264	3,5
MB-sp-7	Diorite porphyry	2		6,56		0,512646		0,1620		0,512498	0,77
MB-sp-46	Diorite porphyry	5,64		24,82		0,512694		0,1208		0,512583	2,45
MB-sp-60	Diorite porphyry	5,49		23,73		0,512569		0,1230		0,512456	-0,03

All samples were obtained from the open pit walls, except samples from GP I unit, located few km to the west and southwest of the pit. The samples MB-sp-7, MB-sp-46 and MB-sp-60 correspond to diorite porphyry unit from the pit (F. Munizaga written communication). All samples were recalculated to 142 Ma, except * recalculated to 155 Ma.

TABLE 3. Melt inclusions analyses from Mantos Blancos ore deposit.

	Polymictic breccia					GP II				
Sample	506a-3	506a-5	506a-2d	Average	Std. Dev.	497-5b	497-3b	497-2b	Average	Std. Dev.
SiO2	72.69	73.00	74.26	73.32	0.83	76.67	72.76	75.25	74.89	1.98
TiO2	0.07	0.01	0.09	0.06	0.04	0.09	0.20	0.17	0.15	0.06
Al2O3	14.26	16.79	13.33	14.80	1.79	12.04	12.07	11.48	11.86	0.33
FeO	1.43	0.17	0.73	0.77	0.63	0.74	2.41	1.85	1.67	0.85
MnO	0.09	0.01	0.04	0.05	0.04	0.01	0.03	0.06	0.04	0.02
MgO	0.51	0.00	0.10	0.21	0.27	0.06	0.87	0.33	0.42	0.41
CaO	2.45	0.47	0.97	1.29	1.03	0.41	1.01	0.45	0.62	0.33
Na2O	3.89	2.11	3.40	3.13	0.92	3.50	2.12	2.89	2.84	0.69
K2O	3.03	3.94	2.52	3.16	0.72	3.86	0.08	1.84	1.93	1.90
Total	98.53	96.55	95.49	96.86	1.54	97.49	91.71	94.77	94.66	2.89
Cu	150	55	67	91	52	60	Nd	1665	863	1135
	Rhyolitic Dome									
Sample	MB5-1x3a	MB5-3x1a	MB5-3x2a	MB5-3x8a	MB5-3x10a	MB5-2x15a	MB5-1x1a	MB5-3x3a	Average	Std. Dev.
SiO2	69.17	73.95	74.94	71.39	77.58	71.77	72.73	72.40	72.99	2.53
TiO2	0.14	0.02	0.13	0.16	0.12	0.04	0.09	0.27	0.12	0.08
Al2O3	14.07	14.12	14.95	16.29	11.81	16.68	21.88	9.48	14.91	3.67
FeO	2.59	0.45	1.13	1.12	1.01	0.88	0.39	2.79	1.29	0.91
MnO	0.03	0.02	0.02	0.02	0.01	0.01	0.02	0.07	0.02	0.02
MgO	0.35	0.02	0.08	0.05	0.03	0.19	0.16	0.46	0.17	0.16
CaO	0.48	0.48	0.61	0.55	0.39	0.46	0.02	0.16	0.39	0.20
Na2O	2.53	3.97	3.09	3.97	3.07	6.22	1.18	3.29	3.41	1.44
K2O	5.35	3.65	4.19	4.39	2.72	4.39	1.00	1.55	3.41	1.52
P2O5	0.03	0.06	Nd	0.03	0.03	0.02	0.05	0.05	0.04	0.02
Total	94.68	96.73	99.24	98.01	96.71	100.70	97.80	90.69	96.82	3.06
Cu	10530	1787	323	373	1170	5783	Nd	13367	4762	5308

Melt inclusions from polymictic breccia came from sample 11506-200 and GP II melt inclusions from sample 11497-320. Melt inclusions from rhyolitic dome were obtained from sample MB5, reported by Wittembrink (2006).Nd: not detected.

IV. TECTÓNICA DEL YACIMIENTO MANTOS BLANCOS

IV.1 Antecedentes tectónicos del Distrito Minero de Mantos Blancos

En el capítulo I de esta Tesis se describe el marco geodinámico y estructural de la Región de Antofagasta durante el Jurásico-Cretácico inferior. En este contexto, es claro que la evolución tectónica de la Cordillera de la Costa en la región ha sido ampliamente dominada por el comportamiento del Sistema de fallas de Atacama (SFA).

En el distrito de Mantos Blancos, la Falla Salar del Carmen constituye la estructura principal o maestra del SFA. Esta falla posee una traza de orientación NNE (Figura 7) y a partir de esta estructura de ramifican fallas secundarias NE de carácter sinestral (Cortés et al., 2000), como las fallas Prat-Alibaud y Latorre, que limitan el entorno cercano al yacimiento y la falla Rencoret hacia el norte. Estructuras asociadas de menor grado, afectan a las rocas en el yacimiento (Cortés et al., 2000; Lattus, 2001).

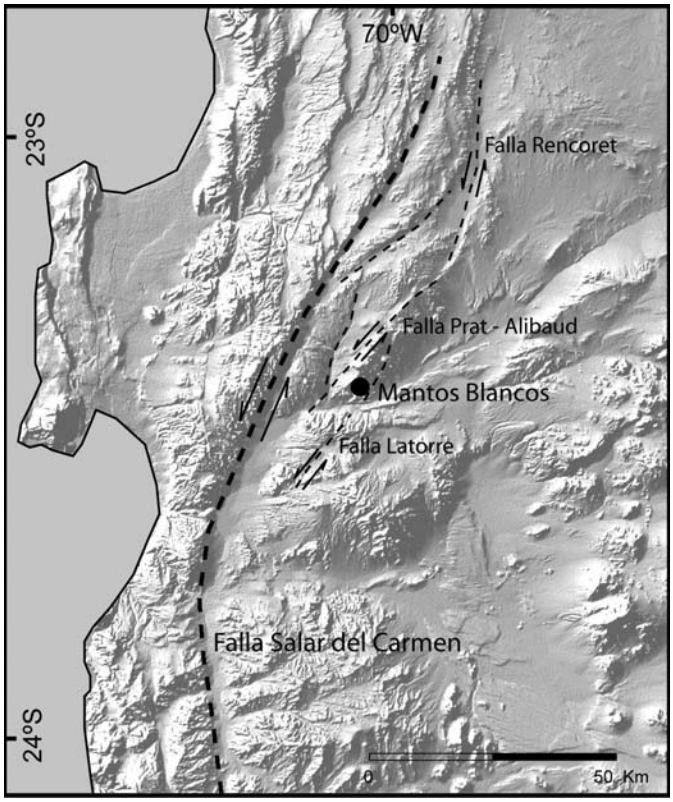

Figura 7. Modelo digital de terreno (SRTM 90m) de la región de Antofagasta, donde se muestran las principales estructuras del SFA y su relación con el yacimiento Mantos Blancos.

Para comprender el contexto estructural e identificar los eventos de deformación frágil desarrollados en el yacimiento, Cortés et al. (2000) han estudiado la cinemática de las estructuras presentes en el Distrito Minero de Mantos Blancos (DMMB) y sugieren la existencia de al menos dos eventos tectónicos sobreimpuestos:

i) tectónica de tipo transcurrente sinestral inducida por ejes de acortamiento subhorizontales de orientación dominante submeridiana. Esta deformación habría afectado notablemente la geometría del cuerpo mineralizado del yacimiento, fragmentándolo y desplazándolo sinestralmente probablemente en el Cretácico Inferior.

ii) deformación caracterizada por dos dominios estructurales de expresión regional, uno caracterizado por transcurrencia dextral inducida por ejes de

acortamiento subhorizontales de orientación NE-SW, y otro por un fallamiento normal generado por ejes de extensión subhorizontal dispuestos en sentido NW-SE. La edad de esta deformación es incierta, sin embargo, sugieren que probablemente ocurrió en el Neógeno.

En base a los trabajos de Pardo-Casas y Molnar (1987) y Jaillard et al. (1990), Cortés et al. (2000) relacionan los eventos de deformación frágil registrados en el DMMB, con la evolución tectónica entre las placas de Nazca y Sudamericana, desde el Jurásico superior al Neógeno (Figura 8). Estos mismos autores señalan que la dirección de acortamiento NS estimada para el primer evento de deformación, no es coherente con la dirección de convergencia entre las placas durante el Cretácico inferior.

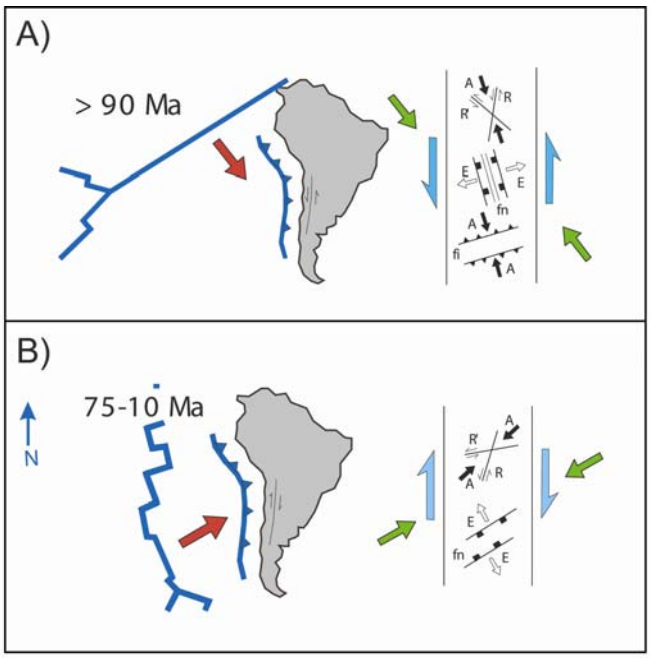

Figura 8. Esquema que relaciona eventos de deformación frágil desarrollados en el DMMB con la evolución tectónica entre las placas de Nazca y Sudamericana, desde el Jurásico superior al Neógeno (Modificado de Cortés et al., 2000). E: eje de extensión, A: acortamiento, fi: falla inversa, fn: falla normal, R: plano de falla sintético, R': plano de falla antitético.

Por otra parte un estudio paleomagnético preliminar realizado en el yacimiento (Tassara et al., 2000), señalan la existencia sistemática de rotaciones horarias de 40°-50° con alguna variabilidad local a la escala de la mina. Estas rotaciones, que son comparables con las registradas en el sector de Baquedano al este de la mina (Arriagada et al., 2003), son las más altas registradas en el margen andino chileno. Las rotaciones horarias medidas en el norte de Chile han sido asignadas al Paleógeno y explicadas por un acortamiento EW diferencial entre el norte y sur del lineamiento Antofagasta- Calama (Figura 9) probablemente ocurrido durante la fase de deformación Incaica (Arriagada et al., 2003; Palacios et al., 2007). A pesar de estas rotaciones horarias sistemáticas registradas en la Cordillera de Domeyko y el valle central hacia la costa de Antofagasta disminuyen notablemente y son prácticamente nulas de Antofagasta hacia el norte.

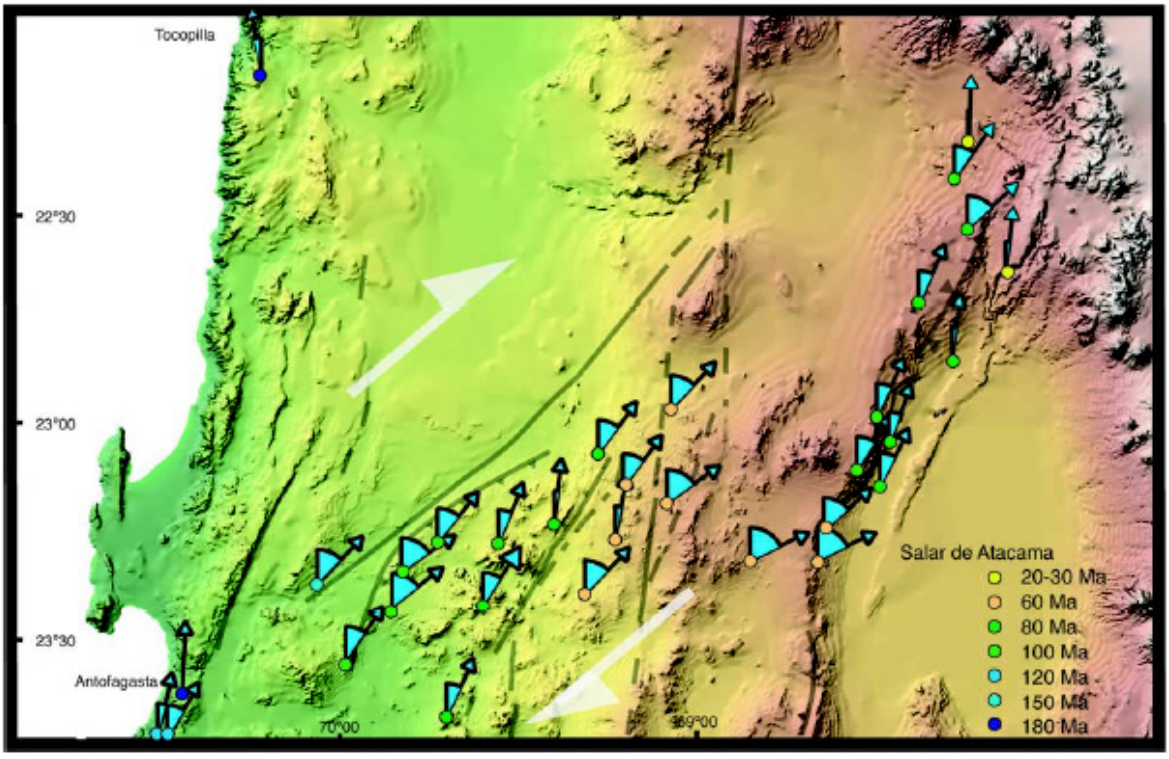

Figura 9. Rotaciones tectónicas en la región de Antofagasta, norte de Chile (tomado de Arriagada et al., 2003).

IV.2 Fundamentación del trabajo realizado

El paleomagnetismo ha sido ampliamente usado como herramienta para comprender la evolución tectónica-estructural en contextos tectónicos diferentes (e.g. Roperch and Carlier, 1992; Beck, 1998; Petronis et al., 2002; Dupont-Nivet, et al., 2003), sin embargo, no son muy numerosos los estudios paleomagnéticos realizados en rocas afectadas por alteración hidrotermal, dado que no es muy claro el efecto que tendría la alteración en las propiedades magnéticas de las rocas. Estudios recientes y en curso han abordado esta línea de investigación (e.g. Alva-Valdivia et al. 2003; Astudillo et al. 2003, 2005; Symons and Arne, 2005; Tapia et al. 2006; Astudillo, 2007), concluyendo que en general cada depósito (y las propiedades magnéticas de sus minerales) responde distintamente dependiendo del tipo y condiciones de la alteración hidrotermal.

Los antecedentes disponibles sugieren que cualquier análisis o modelo que intente explicar la deformación en el yacimiento, o bien, establecer una paleo-dirección de los esfuerzos que controlaron el emplazamiento de la mineralización, es fundamental conocer con certeza la temporalizad y magnitud de estos eventos de deformación. Esto permitiría comprender de mejor manera el contexto original en el cual se formó el yacimiento.

La no concordancia entre la dirección de acortamiento NS estimada por Cortés et al. (2000) para el primer evento de deformación, y la dirección de convergencia entre las placas durante el Cretácico inferior, ha sido explicada por estos autores como una consecuencia local en respuesta a la geometría curva del SFA a la latitud de Antofagasta. Sin embargo, probablemente esta geometría curva del SFA fue adquirida durante la deformación Incaica en el Eoceno-Oligoceno (Arriagada et al., 2003), después de ocurrido el primer evento de deformación. En este contexto, las rotaciones horarias registradas en Mantos Blancos (Tassara et al., 2000) podrían explicar la no concordancia entre la dirección de acortamiento NS estimada por Cortés et al. (2000) para el primer evento de deformación, con la dirección de convergencia entre las placas durante el Cretácico inferior.

En este capitulo se presenta la evolucion tectónica y la historia de deformación ocurrida en el distrito de Mantos Blancos, se realiza una reconstrucción en planta de la geometría original del yacimiento, para comprender la disposición original de los esfuerzos que favorecieron el emplazamiento de la mineralización.

IV.3 Referencias

Alva-Valdivia, L. M., Rivas, M. L., Goguitchaichvili, A., Urrutia-Fucugauchi, J., González, J. A., Morales, J., Gómez, S., Henríquez, F., Nyström, J. O., And Naslund, R. H., 2003. Rock-Magnetic and Oxide Microscopic Studies of the El Laco Iron Ore Deposits, Chilean Andes, and Implications for Magnetic Anomaly Modeling. International Geology Review, v. 45, p. 533–547.

Arriagada C., Roperch P., Mpodozis C., Dupont-Nivet G., Cobbold P. R., Chavin A., Cortés J., 2003. Paleogene clockwise tectonic rotations in the forearc of central Andes, Antofagasta region, northern Chile. J Geophys Res 108 (B1), doi:10.1029/2001JB001598

Astudillo, N., Roperch, P., Townley, B., Belmar, M., and Faundez, M.. 2003. Effects of hydrothermal alteration on the magnetic properties of rocks: case studies for two porphyry copper deposits of Chile. X Chilean Geological Congress, Concepción. Extended abstract.

Astudillo, N., Roperch, P., Townley, B., and Arriagada, C., 2005. A paleomagnetic study within the Chuquicamata porphyry copper deposits, Central Andes, Chile. 6th International Symposium on Andean Geodynamics. ISAG 2005, Barcelona. p. 78-81

Astudillo, N., 2007. Propiedades magnéticas de rocas mineralizadas y su relación con los eventos de alteración hidrotermal en megayacimientos tipo pórfido cuprífero chilenos. Aplicación a la interpretación de sus resultados paleomagnéticos. Unpublished thesis, in prep.

Beck Jr., M.E., 1998. On the mechanism of crustal block rotations in the central Andes. Tectonophysics 299, 75–92.

Cortés, J., González, G., Orrego, M. 2000. Marco estructural del Distrito Minero de Mantos Blancos, Cordillera de la Costa del Norte de Chile. Actas IX Congreso geológico Chileno, Puerto Varas. Vol2, p. 107-100.

Dupont-Nivet, G., R. F. Butler, A. Yin, and Chen, X. 2003. Paleomagnetism indicates no Neogene vertical axis rotations of the northeastern Tibetan Plateau, J. Geophys. Res., 108(B8), 2386, doi:10.1029/2003JB002399.

Jaillard, E., Soler, P., Carlier G., Mourier, T. 1990. Geodynamic evolution of the northern and central Andes during early to middle Mesozoic times: a Tethyan model. Journal of the Geological Society 147: 1009-1022, London.

Lattus J.M., 2001. Geología estructural y paleogeometría del yacimiento Mantos Blancos, II Región de Antofagasta, Chile. Memoria de Titulo, Departamento de Geología, Universidad de Chile, Santiago, 64 p.

Palacios, C., Ramírez, L.E., Townley, B., Solari, M., Guerra, N., 2007. The role of the Antofagasta – Calama lineament on ore deposit deformation in the Andes of northern Chile. Mineralium Deposita, V 42, N3, 301 – 308.

Pardo Casas, F. y Molnar, P. 1987. Relative motion of the Nazca (farallon) and South American plates since Late Cretaceous. Tectonics 6: 233-248.

Petronis, M. S., J. W. Geissman, D. K. Holm, B. Wernicke, and Schauble E. 2002. Assessing vertical axis rotations in large-magnitude extensional settings: A transect across the Death Valley extended terrane, California, J. Geophys. Res., 107(B1), 2010, doi:10.1029/2001JB000239.

Roperch, P. and Carlier, G., 1992. Paleomagnetism of Mesozoic rocks from the central Andes of southern Peru: Importance of rotations in the development of the Bolivian orocline. J. Geophys. Res. 97, 17233–17249.

Symons, D. T. and Arne, D. C., 2005. Paleomagnetic constraints on Zn–Pb ore genesis of the Pillara Mine, Lennard Shelf, Western Australia. Mineralium Deposita, v. 39, p. 944–959.

Tapia, J., Arriagada, C., Townley, B., Belmar, M., Córdova., L., and Astudillo, N., 2006. Alteración hidrotermal y sus efectos sobre propiedades magnéticas en rocas del yacimiento Los Pelambres. Actas XI Congreso Geológico Chileno, Antofagasta. Vol.2, p. 359-362.

Tassara, A.; Roperch, P.; Pavez, A. 2000. Paleomagnetismo de los Yacimientos Mantos Blancos y Manto Verde: Implicancias Tectónicas y Cronológicas. Actas IX Congreso Geológico Chileno. V2. p. 166 – 170.

IV.4 Articulo 3: “Paleomagnetic study in the Mantos Blancos copper deposit: 2D plain view restoration of a dislocated orebody in the Coastal Range of Northern Chile”

Luis E. Ramírez [1*], Pierrick Roperch[2,3], Natalia Astudillo[1,3], Carlos Palacios[1], César Arriagada[1], Miguel A. Parada [1] and Andrés Tassara[4].

[1] Departamento de Geología, Universidad de Chile. Plaza Ercilla 803, Santiago, Chile.

[2] Geosciences Rennes, Université de Rennes1, CNRS, France.

[3] LMTG, UPS, CNRS, IRD, 14 Avenue Edouard, 31400. Toulouse, France

[4]Departamento de Geofísica, Universidad de Chile. Blanco Encalada 2002, Santiago, Chile

[*]Corresponding autor (lramirez@cec.uchile.cl).

Phone: 56 2 9784536

Fax: 56 2 6963050.

Abstract

A paleomagnetic study was conducted in the Mantos Blancos copper deposit and surrounding areas. This study coupled with previous structural data allows define the deformation events and its temporal relationships with the mineralization. Three fault system trending NE, NW and NS, are recognized. The NE system includes subvertical sinistral faults. The NW system consists of subvertical normal faults dipping to the SW and NE, although dextral-slip movements are identified. The NS faults dip between 40 and 70º to the east, and correspond to normal faults with minor dextral-slip components. Paleomagnetic results in 37 sites obtained in late Jurassic granodiorites, rhyolitic dome, rhyolitic tuffs and early Cretaceous basaltic dyke swarm, indicate 30º to 50º of clockwise rotations except for one locality close to the NE Atacama fault system. The magnitude of these rotations is similar to rotations of early Tertiary age reported in other regions of the forearc suggesting that rotations in the Mantos Blancos district also occurred during the Paleogene. The youngest deformation event affecting the deposit is represented by the NS normal fault system and reactivated older faults generated under an extensional regime. These structures displaced the Miocene supergene mineralization. We restored the displacements of faults and tectonic rotations back in time in 2D plane view. The original geometry of the orebody is an elongated body of nearly EW orientation, suggesting that this direction favored the mineralization emplacement.

Keywords: Paleomagnetism, Copper deposit, Coastal Range, Chile

Introduction

The Coastal Range of northern Chile (22°-24°S) hosts numerous copper deposits that range from small surface manifestations to big mineralized bodies like the Mantos Blancos district. These deposits form two NS-trending metallogenic belts separated by the Atacama Fault System (Figure 1). The western belt comprises late Jurassic breccia–pipe feeding stratabound–volcanic hosted and disseminated to veins–type mineralization (Maksaev and Zentilli, 2002; Ramírez et al., 2006; Oliveros, 2005; Maksaev et al., 2007). The eastern slopes of the Coastal Range host the early Cretaceous metallogenic belt, which consists of medium size porphyry copper mineralization (Camus, 2003; Maksaev et al., 2006). Mineral exploration in the zone is obstructed by the intensive and long-lived post-mineralization tectonic deformation extending through ~150 Ma (Pichowiak et al, 1990; Scheuber and Andriessen, 1990; Scheuber and Gonzalez, 1999), which has prevented the recognition of a structural control model for the mineralization. The late Jurassic-early Cretaceous Mantos Blancos deposit is the major orebody in this region, with pre-mining resources of 500 million tons with 1% Cu. Ramírez et al. (2006) studied the geological and structural setting of the copper mineralization at Mantos Blancos, detailing the feeder system of the hydrothermal activity and its evolution. In this paper we report a paleomagnetic study of the Mantos Blancos district (Figure 2). We have used the vertical-axis rotations provided by the paleomagnetic data together with independent structural data to define the successive deformations events of the district. By using these data finally we have restored the original shape of the Mantos Blancos orebody that allows us to identify a possible structural control on the mineralization.

Geologic and tectonic setting

The subduction–related, Jurassic to early Cretaceous magmatic belt along the Coastal Range of northern Chile, is formed by a thick pile (>7000 m) of basalts and andesites (La Negra Formation; Garcia, 1967) that are intruded by granitic to

dioritic plutonic rocks. The volcanic sequence is mainly of calc-alkaline composition and presents thin intercalations of calcareous sediments. Based on radiometric age data and paleontological arguments, this volcanic event occurred in northern Chile essentially through the whole Jurassic (Rogers and Hawkesworth, 1989; Pichowiak, 1994; Gelcich et al., 2004; Kramer et al., 2005; Oliveros, 2005). The intrusive rocks, also of calc–alkaline composition, include granites, tonalites, granodiorites, and diorites of early Jurassic to early Cretaceous age (200 to 130 Ma; Scheuber and González, 1999). The Jurassic volcanic pile was deposited without significant relief building, in an extensional setting (Dallmayer et al., 1996; Maksaev and Zentilli, 2002). The Jurassic-early Cretaceous tectonic evolution in the Coastal Range has been interpreted in terms of coupling and decoupling between the down-going and overriding plates (Scheuber and González, 1999). These authors suggest a first tectonic stage between 195 and 155 Ma when the construction of the intra-arc magmatic belt was dominated by NS-trending sinistral strike-slip motions along the Atacama Fault System (AFS). The AFS, is a complex association of NS trending mylonitic and cataclastic zones and brittle faults exposed along the Coast Range of northern Chile, between 22°S and 29°S (Hervé, 1987; Scheuber and Adriessen, 1990; Grocott et al., 1994; Scheuber and González, 1999). Subduction rollback and subsequent decoupling of the upper plate from the slab between 160 to 150 Ma, triggered an EW-trending extensional regime, and at the end of the Jurassic and beginning of the Cretaceous, plate coupling along the subducted plate seems to have been reactived as it is suggested by the return of sinistral strike-slip deformation along the AFS (Scheuber and González, 1999). Late Cretaceous deformation occurred essentially in the Central Depression. Although Paleogene deformation appears to be localized mostly in the Precordillera or Domeyko Cordillera (Reutter et al., 1996; Mpodozis et al., 1993), regional paleomagnetic data, obtained in the forearc domain in the southern segment of the Central Andes (Figure 1) indicate clockwise tectonic rotations of up to 65° (Arriagada et al. 2003; 2006). Although Taylor et al. (2005, 2007) argue that rotations predate late Eocene transpression along the Precordillera, Arriagada et al., (2003, 2006) find an apparent relationship between

tectonic rotations and structural trends and suggest that rotations occurred mainly during the Eocene - early Oligocene Incaic orogenic event. Late Miocene-early Pliocene trench-parallel shortening in the northern Coastal Range (Allmedinger et al., 2005) produced EW-striking south-dipping reverse faults. However, the dominant neotectonic signature in the forearc is arc-normal extension (Loveless et al., 2005), mainly related to NS-trending east-dipping normal faults (González et al., 2003, 2006).

The Mantos Blancos mining district

The eastern and western boundaries of the Mantos Blancos ore deposit are marked by NNE to NS trending faults, which separate the ore deposit from early to middle Jurassic tonalite to granodiorite plutonic rocks (Cortés et al., 2007; Figure 2). To the north, the middle to late Jurassic volcanic tuffs that host mineralized intrusive bodies, are intruded by a middle Jurassic granodiorite. To the south, the ore deposit is limited by an ENE-trending fault, separating it from the Jurassic andesitic to basaltic sequence of the La Negra Formation (Cortés et al. 2007). Late Cretaceous dioritic and granodioritic porphyries crop out 5 km to the S and SW of the main ore deposit and other small bodies of late Jurassic equigranular granodiorite also crop out 10 km southwest of the deposit (Oliveros et al., 2007).

The lithological anatomy of the Mantos Blancos ore deposit consists of a late Jurassic – early Cretaceous igneous complex (155-141 Ma) hosted into felsic tuffs and mafic to intermediate lava flows of the La Negra formation (Oliveros, 2005; Ramírez et al., 2006), oriented NW-SE and inclined 30° to the SW (Cortés et al., 2007). The igneous complex is formed by an early rhyolitic dome intruded by a stock-sill system of dioritic and granodioritic porphyries, and late mafic dyke swarms (Figure 3).

The geology of the Mantos Blancos ore deposit is described in detail by Ramírez et al. (2006, 2007), who recognized two superimposed hydrothermal events: (1) phyllic alteration probably related to rhyolitic dome emplacement and felsic

magmatic-hydrothermal brecciation at ~155 Ma, and (2) potassic, propylitic and sodic alterations at ~141-142 Ma, coeval with the emplacement of dioritic and granodioritic porphyries, and basaltic dykes (Ramírez et al., 2006). Main ore formation is genetically related to the second hydrothermal event, represented by hydrothermal breccias, disseminations and stockwork style mineralization, associated with potassic, propylitic and sodic alterations. The potassic alteration is characterized by K-feldspar, quartz, tourmaline, biotite–chlorite, magnetite, chalcopyrite, digenite, and minor pyrite. Propylitic alteration occurs extensively in the whole deposit overprinting and obliterating the potassic alteration assemblage. It occurs as disseminations and veinlets of quartz, chlorite, epidote, calcite, albite, sericite, hematite and minor chalcopyrite, galena, and pyrite (Ramírez et al., 2006). A swarm of N 25–30° E striking and subvertical pebble-dykes with propylitic alteration was observed. Both potassic and propylitic alterations were overprinted by sodic alteration, containing albite (replacing feldspar), hematite, pyrite, chalcopyrite, and Ag-rich digenite, with minor amounts of quartz. This mineral assemblage is very extensive, centered on the magmatic and hydrothermal breccias, and occurs as disseminations, cavity fillings, and sharp veinlets (Ramírez et al., 2006).

Structures at deposit scale

The local structural framework, at the deposit scale, is characterized by three systems of faults, which trend NE, NW and NS (Figure 3). The NE-trending faults are mainly subvertical structures and consist in zones of intense fracture cleavage where slickensides, grooves, and secondary riedel shears can be observed. These kinematic indicators demonstrate sinistral movements along the main shear zones that are consistent with the observed 100 to 200 m sinistral displacement suffered by pebble-dykes. These structures experienced normal vertical block faulting, as evidenced by vertical slickensides and grooves, developed in supergene copper minerals. The principal NE trending fault in the deposit (Tercera fault, see Figure 3) evidence a total displacement of 390 m and 200 m of sinistral and vertical

movements, respectively (Lattus, 2001). However, the NE-trending Quinta fault also registered dextral cinematic indicators. The NW-trending faults are vertical to sub vertical structures dipping to the SW and NE. Slickensides and grooves on the surface of these faults, as well as displacement of rock units along them, evidenced normal and dextral strike-slip movements. The NS-trending faults mainly dip between 40° and 70° to the east, corresponding to normal faults with minor dextral strike-slip components, as indicated by slickensides and grooves. Displacements of volcanic tuffs over the rhyolitic dome indicate 100 to 150 m of downward movements in the centre of the ore body. Late and post-mineralization basaltic dykes are sub vertical and trend NNE, and subordinately NS to NNW. Most of the contacts with the host rock are shear zones. These dykes are 1 to 12 m wide and represent about 15% of the total rock volume in the ore deposit (Ramírez et al., 2006).

Paleomagnetic study

Paleomagnetic sampling and methods

A total of 37 sites (Figures 2,3) were sampled using a portable drill core, and the cores were oriented using a magnetic and solar compass whenever possible. In the open pit, 27 sites were sampled in the rhyolitic dome, rhyolitic tuffs, granodiorites and late-mineralization basaltic dykes (Table 1, Figure 3). Out of the pit 10 sites were obtained in lavas from La Negra formation, Jurassic intrusive rocks and Cretaceous basaltic dykes (Figure 2). Measurements were made in the Paleomagnetic Laboratory at the University of Chile. Samples were either demagnetized with alternating fields or stepwise thermally demagnetized in ten to fifteen steps from 150ºC to 680ºC in an ASC furnace with magnetic field < 20nT in the sample region. At each step, room temperature susceptibility was measured to monitor chemical changes during heating. Remanent magnetizations were measured with a JR5A Agico spinner magnetometer. Magnetic susceptibility was measured with a Bartington susceptibilitiy meter. Isothermal Remanent

Magnetization (IRM) was given with a pulse electromagnet and Magnetic Suceptibility (K) versus temperature curves were done with the Agico KLY3-CS3 instrument, to obtain Cuire temperatures of magnetic minerals. Characteristic remanent magnetizations (ChRM) were analyzed by principal component analysis (Kirschvink, 1980) to determine sample ChRM directions. Site-mean directions were calculated by applying Fisher statistics (Fisher, 1953). The expected direction and tectonic rotations at each paleomagnetic site were calculated using the appropriate age reference paleomagnetic pole for South America (Besse and Courtillot, 2002). Petrographic observations, scanning electron microscopy (SEM) and qualitative compositional analyses (JEOL 6360 LV) were carried out in order to identify the magnetic minerals, textures and its relation with hydrothermal alteration. In order to simplify the description and interpretation of the paleomagnetic data, we grouped these data into three different units: i) the dyke complex, ii) the mineralized rocks (rhyolitic dome, rhyolitic tuffs and granodiorites in the pit) and iii) the Mantos Blancos distrital rocks (sites located out of the open pit).

Magnetic mineralogy and determination of characteristic directions

The dyke complex

From 11 sites of the dyke complex, we obtained 61 samples (Table 1, Figure 3). Most samples from the dyke complex have high magnetic susceptibility, suggesting magnetite as the main stable magnetic mineral in the dykes, which contrasts with the natural magnetic properties of the mineralized rocks (Figure 4). Magnetic susceptibility experiments show the destruction of a magnetic phase near 300-350°C interpreted as evidence for maghemitization (Figure 5a). Optical and SEM observations show numerous large grains of exsolved and oxidized titanomagnetites (Figure 6a,b). Isothermal remanent magnetization (IRM) acquisition indicates saturation is almost attained at 300mT. The relatively high Hcr values above 60mT (Figure 5b) may be a consequence of maghemitization or related to hematitess-ilmenitess, associated with titanomagnetite exsolution (Figure 6a,b). Characteristic directions were determined after thermal or AF

demagnetization, obtaining similar results (Figure 5c). Most samples have normal polarity magnetizations. However, some dykes (MCD-09) show both normal and reverse polarity magnetizations. A mean direction (Table 2) was calculated for the dyke complex by combining normal and reverse polarity ChRMs as well as great circles using the McFadden and McElhinny (1988) procedure (Figure 5d).

The mineralized rocks

From 16 sites of the mineralized rocks, we obtained 101 samples (Table 1, Figure 3). The magnetic properties of the felsic units within the Mantos Blancos mine are characterized by low magnetic susceptibility (Figure 4). IRM acquisitions show the presence of low and high coercivity minerals (Figure 7a). Most sites show in thin sections small hematitized magnetites and disseminated hydrothermal hematite in the groundmass. Hematite associated with Cu sulfides in veinlets was also observed. The characteristic directions in these sites records both normal and reverse polarity, and are antipodal (Figure 7b, 7c). However, at two sites (MR-04,12) within the rhyolitic tuffs unit only hematite can be identified (Figure 6c,d) and the ChRM is characterized by high unblocking temperatures (Figure 7b, 7c). Site MR- 12 has a normal polarity while site MR-04 has a reverse polarity magnetization and both have high inclination. The site-mean directions are given in Table 2.

The Mantos Blancos distrital rocks

From 9 sites of the distrital rocks group, we obtained 59 samples (Table 1, Figure 2). North of the Mantos Blancos mine, four sites (MDR-06, MDR-07, MDR-08, MDR-10) were drilled in a tonalitic to granodioritic early Jurassic intrusive (182±4 Ma K-Ar in biotite, 180.7±1.8 Ma 40Ar/39Ar in amphibole; Cortés et al., 2007) close to the contact with Paleozoic schists. This contact zone is characterized by the presence of a visible subvertical NE-SW foliation at the border zone, that diminishes towards the centre of the intrusive. The magnetization in the intrusive has a normal polarity, however, it has steep inclination and declination deflected toward the NW (see below for details). Just south of the mine we sampled a granodioritic porphyry which also records a normal polarity with a declination

strongly deflected toward the east (site MDR-03). A similar direction is recorded by an upper Jurassic granodiorite (site MDR-04; 148.2±0.5 Ma 40Ar/39Ar in hornblende; Oliveros, 2007) located 10 km to the SW of the mine. The contact between this granodiorite and volcanic rocks is characterized by the presence of a NW-SE mylonite zone steep inclined to the east, developed mainly in the volcanic rocks. Scheuber and Gonzalez (1999), interpreted this as a ductile normal fault, and reported a K-Ar cooling age of 152±4 Ma. In La Negra volcanic rocks, the site MDR-05 records a reverse polarity magnetization (Figure 8a,b). After tilt correction (regional attitude of 30° toward the SW), the inclination is nearly horizontal (Table 2). Magnetic susceptibility is high due to a large number of partially oxidized magnetite grains (Figure 6e,f) and magnetite is the main carrier of the remanent magnetization with unblocking temperature of the characteristic magnetization in the range 500-575°C (Figure 8). However, this site records a well-developed magnetic fabric unlikely to be a primary feature. We can however discard the hypotesis of a remagnetization associated with the nearby intrusion recording normal polarity at site MDR-04. The nature of the magnetization is thus unknown but likely syn or post-tectonic. The site-mean directions are given in Table 2.

AMS fabric

Several studies have shown that anisotropy of magnetic susceptibility (AMS) is a strong tool to determine magma flow in dykes (e.g Tauxe et al., 1998) and to describe the structure related to pluton emplacement (e.g. Bouchez, 1997; Parada et al., 2005). AMS was measured in dykes, mineralized rocks and distrital igneous rocks (Table 3).

The dyke complex

In dykes, imbricated magnetic fabric is the main criteria to determine magmatic flow and the flow direction is best determined near the chilled margins of the dykes (Tauxe et al., 1998). Although an open pit may provide appropriate outcrops, the intense fracturation, particularly near the dyke contacts impeded a detailed

sampling. Only one dyke (MDC-11, NS oriented) exhibits the magnetic fabric well organized with a NS subvertical foliation and subhorizontal lineation (Figure 9a). This dyke has the highest magnetic susceptibility and scarce evidence of maghemitization. In the other dykes, AMS is lower in intensity and the maximum and minimum sucesptibility axis (Kmax, Kmin) are often mixed. These dykes are affected by maghemitization and present relatively high Hcr values, suggesting that a significant amount of magnetites (and maghemites) are near the single threshold domain. Taking into account that single magnetite domain have inverted AMS tensors (minimum susceptibility along the long axis of the magnetite particle), mixed tensors within dykes might be the consequence of maghemitization and reduction in grain size. It is therefore not possible to use the shape of the AMS ellipsoid to determine magmatic flow within these dykes. However, the NE-SW orientation of MCD-09 and MCD-10 dykes is roughly defined by the AMS (Figure 9a).

The mineralized rocks

In these rocks, magnetic susceptibility is in general low and AMS is not strongly developed, however several sites record an organized AMS. Most sites show subvertical foliations and subhorizontal or gently dipping lineations oriented NE-SW (Figure 9b).

The Mantos Blancos distrital rocks

To the north of deposit, the four sites drilled in a tonalitic to granodioritic Jurassic intrusion are located near the contact with Paleozoic schist. The magnetic fabric (Table 3) in the intrusion is characterized by a subvertical NNE trending magnetic foliation with southward dipping lineations (Figure 9c). The observed AMS in the intrusive rocks is not developed in a basaltic dyke that intrude it (MDR-09, anisotropy degree of 1.005), suggesting that the dyke emplacement postdated the acquisition of the magnetic fabric. It allow interpret a AMS fabric aquiered during thr pluton emplacement. The characteristic directions determined at sites MDR-08 and site MDR-10 in the Jurassic intrusion are also different from the one recorded by the dyke and we suspect that the intrusion was slightly tilted toward the south-

southwest before the dyke emplacement as it is the case with the La Negra volcanics in the district. If this interpretation is correct, after applying a tilt correction of 30° to the SW, the magnetic foliation is still subvertical, but the magnetic lineation is more subhorizontal and the primary magnetization is in better agreement with the one recorded by the dyke (Table 2). To the south of deposit at sites MDR-04 and MDR-05, AMS is well developed and the orientations of the magnetic foliation agree with a NW-SE trending mylonite zone. Scheuber and Gonzalez (1999), interpreted this as a ductile normal fault, and reported a K-Ar cooling age of 152±4 Ma. The magnetic lineation in the intrusive and La Negra volcanic rocks are steep (Figure 9c), suggesting only vertical displacement along this fault. The magnetic fabric in the La Negra volcanics could be acquired synchronously with emplacement of the pluton, nevertheless, the observation of magnetizations of opposite polarities contradict this interpretation. Probably the magnetization in volcanic rocks was acquired during the mylonite formation and after the tilt of the volcanic sequence.

Discussion

Pre-mineral deformation and age of La Negra tilting

The occurrence of southwest tilted lavas of La Negra formation demonstrated that part of the rocks of the area experienceed tilting. To the south of Mantos Blancos mine, volcanic rocks from La Negra Formation are inclined 30º-40º to the SW, and near the deposit are inclined 30° to the SW (Cortés et al. 2007). Such a tilt may explain the steep inclination recorded at two sites within the mine where the magnetization is carried by hematite possibly of primary origin (MR-04+12) and is coherent with the disposition of rhyolitic dome host rocks. A similar tilt might explain the steep inclinations and NW declinations recorded by the early Jurassic tonalite located to the north of the mine (MDR-08+10). In the deposit, the characteristic magnetization of dykes of early Cretaceous age and mineralized rocks do not evidence this tilting. The paleomagnetic data indicate a first stage of

tectonic activity characterized by ~30° SW tilting within the Mantos Blancos district that probably occurred in the late Jurassic, early after to the volcanic activity and previous to the main mineralization event and to the early Cretaceous dyke emplacement. This upper Jurassic deformation event possibly occurred under the extensional regime, reported by Scheuber and Gonzalez, (1999).

Magnetization related to the hydrothermal activity

In the open pit, the mineralized rocks record both normal and reverse polarity magnetization. Propylitic and sodic hydrothermal alteration assemblages are observed in the samples from the pit but the intensity of alteration is variable and we have not been able to clearly establish a relationship between the magnetic polarity and the hydrothermal alteration assemblage. The two sites in the rhyolitic tuffs, where the magnetization corresponds to magnetic carriers with high unblocking temperatures, seem to have hematite of primary origin (MR- 04+12).

In analyzed dykes from the deposit, the different polarities are associated with different rock textures and probably correspond to a time of emplacement encompassing more than a polarity chron because the rate of geomagnetic reversals is high during the Mesozoic prior to the long normal Cretaceous superchron. The dykes showing reverse polarity magnetizations have incipient biotitization, in which the micas are altered to chlorite. In the case of the dykes with normal polarity, magnetites show oxidation textures, possibly related to chloritization of the mafic minerals in the matrix. Therefore, in both cases, the characteristic directions could be considered as representative of emplacement time and/or hydrothermal activity. There is also evidence for maghemitization with both normal and reverse magnetization within a sample as in dyke MDC-09 (Figure 5). The normal polarity magnetization is recorded in the same temperature interval 200-400°C where we observe a drop in magnetic susceptibility at room temperature after heating and we interpret the change in susceptibility as the destruction of maghemite. The reverse polarity is recorded by magnetite with unblocking temperature above 500°C. The clear antipodal relationship displayed by

both magnetizations (Figure 10) suggests that no significant tilting or vertical rotations occurs in the time interval between the acquisition of the primary magnetization recorded in magnetite and the maghemitization event.

The concordance between dyke orientation and AMS foliation suggest that dykes were emplaced in tensional structures without shear stress.

Paleomagnetic rotations

The site-mean directions for each locality (Figure 10) and the tectonic rotations and inclination errors are given in Table 2. Using the available radiometric ages from Munizaga et al., (1991) and Oliveros (2005), Ramirez et al. (2006) indicate that magmatism and the associated hydrothermal events occurred in the time interval 155-140Ma with an older phyllic alteration probably related to felsic magmatic-brecciation at ~155Ma and younger (~142-141Ma) potassic propylitic and sodic alterations coeval with dioritic and granodioritic stocks. This time interval corresponds to a time of a significant worldwide plate evolution with a peculiar hairpin in the South American apparent polar wander path (Besse and Courtillot, 2002) and a particular low paleolatitude during Berriasian time for the South American plate. For this reason we calculate the rotations and inclination errors by comparing the observed paleomagnetic directions with the expected directions at 155Ma and 140Ma. For the mineralized rock, using an age of 155Ma minimizes the calculated rotations and inclination errors. The same is observed for the late mineralization dykes if we choose an age of 150Ma instead of 140Ma. Our preferred age is thus the age that minimizes the tectonic rotations and differences in inclination between the expected and the observed inclinations. Although the impossibility to determine precisely the paleohorizontal in these rocks makes this approach slightly speculative, the paleomagnetic data favour a late Jurassic age rather than an early Cretaceous age for the mineralization.

In the district, most sites evidence clockwise rotations, except in one locality (MDR-08+10) that show counterclockwise rotation but the steep inclination also indicates

rotation about non-vertical axis with a possible 30° tilt to the SW (Table 2). In the open pit, we also observe steeper inclinations than expected at sites MR-04+12 where the characteristic magnetization is carried only by hematite. After correction of a pre-mineralization tectonic tilt of 30° to the SW, the tilt corrected magnetization indicates a 47.1±6.4° clockwise rotation. The dyke complex evidence 30.4°±6.5° clockwise rotation. This magnitude is equivalent within error to that registered at sites MR-07+11 (39±5.7°) and MR-08+14 (33.7±7.9°) in the pit. South of the pit, a 45.5±7.7º clockwise rotation is observed at sites MDR-04+05. The clockwise rotation event must be younger than the mineralization event and dyke swarm emplacement.

Cortés et al. (2000) studied the structural framework of the Mantos Blancos mining district and suggest an early Cretaceous deformation event induced by NS shortening direction, which resulted in a sinistral shear dislocation of orebody. Cortés et al. (2000) noted that this NS direction is different to the NW-SE plate convergence direction estimated by Pardo-Casas and Molnar, (1987) and Jaillard et al., (1990), between Nazca and Sudamerica plates during the early Cretaceous. Probably this disagreement is caused by the clockwise tectonic rotations.

Post-mineral deformation and 2D plain view restoration of deformation

The present structural-paleomagnetic study confirms the large clockwise rotations previously reported in the region (e.g. Arriagada et al., 2003). The paleomagnetic results obtained in the Mantos Blancos ore body suggest that probably the whole deposit would have rotated 30-40º as a nearly rigid block. The major faults in the deposit are the currently oriented NE structures, which evidence sinistral displacements of mineralized rocks and dextral movement along the Quinta fault. We speculate that this sinistral fragile deformation occur contemporaneously with the early Cretaceous deformation episode along the AFS with mylonites showing sinistral shear that developed at ~ 125 Ma (Scheuber and Gonzalez, 1999, Cembrano et al., 2005).

The Mantos Blancos mine is located close to the north of the Antofagasta - Calama Lineament (ACL). In order to explain the large clockwise rotations found across the forearc, especially in the Baquedano area, Arriagada et al., (2003) proposed that the ACL corresponds to an important dextral strike - slip NE - trending fault system (2003). Palacios et al., (2006) found that apparent displacements in metallogenic belts of different ages across the ACL support the hypotesis of the ACL as a major dextral fault system striking NE-SW. Probably the ACL resulted from a differential EW shortening to the north and south, and accommodated via clockwise rotations the deformation to the south during de Eocene-Oligocene (Arriagada et al., 2003).

Despite the large-scale evidence for a major dextral fault system and the location of the Mantos Blancos deposit nearby the apparent trace of the ACL, the lack of a significant brittle deformation showing significant dextral displacement is puzzling. Within the Mantos Blancos deposit, the paleomagnetic results, especially those within the dyke system, are best explained by a rigid rotation of the whole deposit. While the paleomagnetic results obtained south of the Mantos Blancos deposit and near Baquedano (Arriagada et al., 2003) do not depart from the general clockwise rotation observed within the mine, the results from the sites located about 10km to the NNW of the mine and those south of Antofagasta (Figure 1, Arriagada et al., 2003) depart significantly. This may suggest that the clockwise rotations are accommodated mainly along the major faults of the AFS (Figure 1, 2) and not within the minor faults of the Mantos Blancos deposit. Considering the magnitude of the clockwise rotations in the deposit the currently NE sinistral faults were originally NS oriented.

The youngest deformation event affecting the deposit is represented by the NS normal faults and the reactivation of older faults under an extensional regime. These structures controlled and displaced the secondary mineralization, as evidenced by vertical slickensides and grooves developed in supergene copper minerals. Oxidation and supergene mineralization in the Coastal Range have been dated between 21 and 14 Ma (Camus, 2003), coinciding with those reported for the rest of the northern Chilean forearc (Arancibia et al. 2006). During the Miocene, the

dominant neotectonic regime in the forearc is arc-normal extension (Loveless et al., 2005), mainly related to NS-trending east-dipping normal faults (González et al., 2003, 2006).

Considering the Miocene to recent extension, Eocene-Oligocene clockwise tectonic rotations and early Cretaceous NE faults displacements, we propose a 2D plane view restored shape for the main orebody. From field and borehole information, we estimate the dip of major faults and its displacements. We restored manually the displacements of faults and tectonic rotations back in time, in 2D plain view at one fixed level (~700 m.a.s.l.). The result of the restoration shows an elongated body of nearly EW orientation at early Cretaceous times, previous to the sinistral displacements of major faults that dislocate the orebody and the clockwise rotations (Figure 11d).

Conclusions

In the Mantos Blancos district, at least four deformation events can be recognized: i) Late Jurassic tilting to the southwest previous to the hydrothermal alteration event related to copper mineralization, ii) sinistral displacement of part of the orebody (Figure 11) along an currently oriented NE deformation zone during the early Cretaceous, iii) clockwise rotations during Eocene-Oligocene and iv) a late deformation stage associated with EW extension, coeval and post-supergene mineralization. According with the plane view restoration, the Mantos Blancos orebody had an EW elongated shape prior to deformation. There is no significant relative rotation between the Mantos Blancos mine and localities immediately to the south of the postulated Antofagasta-Calama lineament. The main traces of the Atacama Fault System are more likely candidates to accommodate the decrease in the magnitude of clockwise rotations toward the Coastal Cordillera.

Acknowledgements

This study was funded by FONDEF (CONICYT, Chile), grant DO1-1012, assigned to the authors and to the Mantos Blancos division of Anglo American Chile. Permission for publication was established between the University of Chile, the Chilean Government and the Company grant-related contract. Thanks to the geologists of the Mantos Blancos mine for his valuable assistance. The first author carried out his PhD studies with a financial grant from a MECESUP scholarship.

References

Allmendinger, R. W., González, G., Yu, J., Hoke, G., Isacks, B., 2005. Trench – parallel shortening in the Northern Chilean Forearc: Tectonic and climatic implications. GSA Bulletin. 117: 89 – 104.

Arancibia, G., Matthews, S.J., Pérez de Arce, C., 2006. K–Ar and 40Ar/39Ar geochronology of supergene processes in the Atacama Desert, Northern Chile: tectonic and climatic relations. Journal of the Geological Society, V 163, N 1, 107-118.

Arriagada C., Roperch P., Mpodozis C., Dupont-Nivet G., Cobbold P. R., Chavin A., Cortés J., 2003. Paleogene clockwise tectonic rotations in the forearc of central Andes, Antofagasta region, northern Chile. J Geophys Res 108 (B1), doi:10.1029/2001JB001598.

Arriagada C, Roperch P, Mpodozis C, Fernandez, R., 2006. Paleomagnetism and tectonics of the southern Atacama Desert (25–28ºS), northern Chile. TECTONICS, VOL. 25, DOI:10.1029/2005TC001923.

Besse, J., and Courtillot, V., 2002. Apparent and true polar wander and the geometry of the geomagnetic field over the last 200 Myr: J. Geophys. Res., v.107 (B11), 2300, DOI:10.1029/2000JB000050.

Bouchez, J-L., 1997. Granite is never isotropic: an introduction to AMS studies of granitic rocks. In: Bouchez, J-L. (Ed.), Granite: From Segregation of Melt to Emplacement Fabrics. Kluwer Acad. Publ, Dordrecht, 35-38.

Camus, F., (2003) Geología de los sistemas porfíricos en los Andes de Chile. SERNAGEOMIN, Chile, p 267

Cembrano, J., González, G.; Arancibia, G.; Ahumada, I.; Olivares, V.; Herrera, V. 2005. Fault zone development and strain partitioning in an extensional strike-slip duplex: a case study from the Atacama Fault System, northern Chile. Tectonophysics 400: 105-125.

Cortés, J. 1998. Geología, estructuras y geoquímica preliminar del Distrito Minero de Mantos Blancos, Cordillera de la Costa, Segunda Región de Antofagasta, Chile. Memoria de Titulo (Inedito) Universidad Católica del Norte, Departamento de Ciencias Geológicas, 183 p.

Cortés, J., Marquardt, C., González, G., Wilke, H., Marinovic, N. 2007. Carta Mejillones y Península de Mejillones, Región de Antofagasta. Servicio Nacional de Geología y Minería, Carta Geológica de Chile, Serie Geología Básica, 1 map 1:100.000. Santiago.

Dallmeyer, R. D., Brown, M., Grocott, J., Taylor, G. K., Treolar, P.J., 1996. Mesozoic magmatic and tectonic events within the Andean plate boundary zone, 26°- 27°30´ S, North Chile: Constraints from 40Ar/39Ar mineral ages. The Journal of Geology, 104: 19 – 40.

Fisher, R.A., 1953. Dispersion on a sphere. Proceedings of the Royal Society of London, Series A, Vol. 217, p. 295-305.

García, F., 1967. Geología del Norte Grande de Chile. In Simposium sobre Geosinclinal Andino, No. 3. Sociedad Geológica de Chile, 138 p.

Gelcich, S., Davis, D. W., Spooner, E. T. C., 2004. Onset of early Jurassic magmatism in northern Chile: Precise U – Pb zircon ages for the La Negra Formation and the Flamenco Pluton in the Coastal Cordillera of Chañaral. IAVCEI General Assembly, Pucón – Chile. Electronic version.

González, G., Cembrano, J., Carrizo, D., Macci, A., Schneider, H., 2003. The link between forearc tectonics and Pliocene – Quaternary deformation of the Coastal Cordillera, northern Chile. Journal of South American Earth Sciences, 16: 321 – 342.

González G., Dunai T., Carrizo D., Allmendinger R., 2006. Young displacements on the Atacama Fault System, northern Chile from field observations and cosmogenic 21Ne concentrations. Tectonics, Vol. 25, No. 3, TC3006.

Grocott, J., Brown, M., Dallmeyer, R.D., Taylor, G.K. & Treloar, P.J. 1994. Mechanism of continental growth in extensional arcs: An example from de Andean plate-boundary zone. Geology, 22, 391-394.

Hervé, M., 1987. Movimiento sinistral en el Cretácico Inferior de la Zona de Falla Atacama al norte de Paposo (24ºS), Chile. Revista Geológica de Chile, Nº 31, pp. 37-42.

Jaillard, E., Soler, P., Carlier G., Mourier, T. 1990. Geodynamic evolution of the northern and central Andes during early to middle Mesozoic times: a Tethyan model. Journal of the Geological Society 147: 1009-1022, London.

Kramer, W., Siebel, W., Romer, R. L., Haase, G., Zimmer, M., Ehrlichmann, R., 2005. Geochemical and isotopic characteristics and evolution of the Jurassic volcanic arc between Arica (18°30´S) and Tocopilla (22°S), North Chilean Coastal Range. Chemie der Erde, Geochemistry, 65: 47 – 78.

Kirschvink, J.L., 1980, The least-squares line and plane and the analysis of paleomagnetic data: Geophys. J. R. Astron. Soc., v. 62, p. 699–718.

Lattus J.M., 2001. Geología estructural y paleogeometría del yacimiento Mantos Blancos, II Región de Antofagasta, Chile. Unpublished B.Sc. Thesis, Departamento de Geología, Universidad de Chile, Santiago, 64 p.

Loveless, J. P., Hoke, G. D., Allmendinger, R. W., González, G., Isacks, B. L., Carrizo, D. A., 2005. Pervasive cracking of the northern Chilean Coastal Cordillera: New evidence for forearc extension. Geology, 33: 973 – 976.

Maksaev, V., Zentilli, M., (2002) Chilean stratabound Cu-(Ag) deposits: An overview. In: Potter TM (ed) Hydrothermal iron oxide copper-gold and related deposits: A global perspective 2. PCG pp 185-205.

Maksaev, V., Munizaga, F., Fanning, M., Palacios, C., Tapia, J., 2006. SHRIMP U – Pb dating of the Antucoya Porphyry Copper Deposit: Evidence of an Early Cretaceous metallogenic epoch in the Coastal Cordillera of Northern Chile. Mineralium Deposita. DOI 10.1007/s00126-006-0091-5.

Maksaev, V., Townley, B., Palacios, C. and Camus, F., 2007. Metallic ore deposits. In: Moreno T. and Gibbons, W. (eds) The Geology of Chile. The Geological Society, London, p. 179-199.

McFadden, P.L., McElhinny, M.W., 1988, The combined analysis of remagnetization circles and direct observations in paleomagnetism: Earth Planet. Sci. Lett., v. 87, p. 161–172.

Oliveros, V., 2005. Les formations magmatiques jurassiques et mineralisation du nord Chili, origine, mise en place, alteration, metamorphisme: etude geochronologique et geochemie. Ph.D Thesis. Universite de Nice-Sophia Antipolis, France, 296 p.

Palacios, C., Ramírez, L.E., Townley, B., Solari, M., Guerra, N., 2006. The role of the Antofagasta – Calama lineament on ore deposit deformation in the Andes of northern Chile. Mineralium Deposita, In press. Parada, M.A., Roperch, P., Guiresse, C., Ramírez, E., 2005. Magnetic fabrics and compositional evidence for the construction of the Caleu pluton by multiple injections, Coastal Range of central Chile. Tectonophysics 399, 399-420.

Pardo Casas, F. y Molnar, P. 1987. Relative motion of the Nazca (farallon) and South American plates since Late Cretaceous. Tectonics 6: 233-248.

Pichowiak, S., Buchelt, M., Damm, K.W., 1990. Magmatic activity and tectonic setting of early stages of Andean cycle in northern Chile. Geol. Soc. Am. Sp. Paper, 241: 127 – 144.

Pichowiak, S., 1994. Early Jurassic to early Cretaceous magmatism in the Coastal Cordillera and the Central Depression of North Chile. In: Reutter, K.-J., Scheuber, E., Wigger, P. (eds).

Tectonics of the Southern Central Andes. Structure and evolution of an active continental margin. Springer Verlag, 203 – 217.

Ramírez, L.E., Palacios, C., Townley, B., Parada, M.A., Sial, A.N., Fernández-Turiel, J.L., Gimeno, D., García-Valles, M., Lehmann, B. 2006. The Mantos Blancos copper deposit: an upper Jurassic breccia-style hydrotermal system in the Coastal Range of Northern Chile. Mineralium Deposita V41, 246-258. DOI 10.1007/s00126-006-0055-9.

Ramírez, L.E., Parada, M.A., Palacios, C., Wittenbrink, J. 2007. Magmatic evolution of the Mantos Blancos copper deposit, Coastal Range of northern Chile: insight from Sr–Nd isotope, geochemical data and silicate melt inclusions. Resource Geology, in press.

Rogers, G., Hawkesworth, C. J. 1989. A geochemical traverse across the North Chilean Andes: evidence for crust generation from the mantle wedge. Earth and Planetary Science Letters, 91: 271 – 285.

Scheuber, E., Andriessen, P.A.M., 1990. The kinematic and geodynamic significance of the Atacama fault zone, northern Chile. Journal of Structural Geology, V. 12, No 2, pp. 243-257.

Tauxe, L., Gee, J.S., Staudigel, H., 1998. Flow directions in dikes from anisotropy of magnetic susceptibility data: the bootstrap way. Journal of Geophysical Research 103, 17775–17790.

Taylor, G. K., Dashwood, B., Grocott, J., 2005, Central Andean rotation pattern: Evidence from paleomagnetic rotations of an anomalous domain in the forearc of northern Chile, Geology, 33 (10), 777-780.

Taylor, G.K., Grocott, J., Daswood, B, Gipson, M., Arévalo, C., 2007, Implications for crustal rotation and tectonic evolution in the Central Andes forearc: New paleomagnetic results from the Copiapó region of northern Chile, 26º to 28ºS, J. Geophys. Res. 112, B01102, doi:10.1029/2005JB003950,

Scheuber, E., González, G., 1999. Tectonics of the Jurassic-early Cretaceous magmatic arc of the North Chilean Coastal Cordillera (22° - 26°S): A story of crustal deformation along a convergent plate boundary. Tectonics 18: 895-910.

Figure captions

Figure 1. Shaded relief image (SRTM 90 m digital elevation model) of Antofagasta area showing the location of Mantos Blancos copper deposit and main structural features of the region (ACL: Antofagasta-Calama lineament). Tectonic rotations of Jurassic-Cretaceous rocks (Arriagada et al., 2003), late Jurassic (triangle) and early Cretaceous (square) copper deposits are also shown.

Figure 2. Geological map of the Mantos Blancos district and location of paleomagnetic sites. Tectonic rotations with errors (deviations of arrows from a N-S direction) calculated in this work are shown. Some sites were grouped to made the calculations, however, in the figure only one arrow is shown, see text for details. Geological map modified after Cortés (1998).

Figure 3. Geological map and paleomagnetic sampling location within the open pit. The paleomagnetic sites for mineralized rocks and dykes are shown by circles and squares respectively. Tectonic rotations with errors (deviations of arrows from a N-S direction) calculated in this work are shown. Some sites were grouped to made the calculations, however, in the figure only one arrow is shown, see text for details.

Figure 4. Log-log plot of magnetic susceptibility versus intensity of natural remanent magnetization in samples from the dyke swarm and mineralized rocks.

Figure 5. a) Magnetic susceptibility variation versus temperature for samples from dykes. Large susceptibility decrease near 300°C and non reversible heating (thick line) and cooling curves (thin line) indicate evidence for strong maghemitization in several dykes except in dyke MDC-11 (sample MDC-1107C) with magnetite being the main magnetic mineral, b) Examples of IRM acquisition in dykes. Reverse field measurements indicate high Hcr values above 50mT. c) Orthogonal demagnetization diagram in dykes. Most samples have a normal polarity magnetization with unblocking temperatures above 300°C, however some samples have normal and reverse polarity magnetizations. Normal and reverse polarity ChRMs are antipodal. d) Equal area stereonet of characteristic directions for

dykes, open circles and filled circles represent normal and reverse polarity, respectively.

Figure 6. A) Transmitted light microscope image of dyke sample MDC-10-04, B) SEM image of oxidized titanomagnetite from dyke sample MDC-10-04, C) Transmitted light microscope image of tuff MR-12-07C, D) SEM observation of hematite (same sample as C), E) Transmitted light microscope image of lava from La Negra formation MDR-4-03C and F) Partially oxidized magnetite grains from La Negra formation lava (sample MDR-4-04C) observed under reflected light microscope.

Figure 7. a) Examples of IRM acquisition for samples from the mineralized rocks. b) Orthogonal demagnetization diagrams for samples from the mineralized rocks. The ChRMs with unblocking temperatures between 500-590°C are carried by magnetite 24 except at two sites (MR-04, MR-12) where the ChRM is carried by hematite, c) Equal area stereonet of characteristic directions for four sites in the mineralized rocks and two sites with ChRM carried by hematite in rhyolitic tuffs. Open circles and filled circles represent normal and reverse polarity, respectively.

Figure 8. a) Examples of thermal and AF demagnetization in sites of Mantos Blancos district, located to the north and south of the mine b) Equal-area stereonet of characteristic directions and planes for the three sites south of the mine. Open circles and filled circles represent normal and reverse polarity, respectively.

Figure 9. AMS ellipsoids directions for a) dyke complex, b) mineralized rocks and c) distrital rocks out of the pit.

Figure 10. Equal-area stereonet of mean-site directions. Open circles and filled circles represent normal and reverse polarity, respectively. The expected paleomagnetic directions are shown as stars, according to the estimated age of acquisition of ChRM.

Figure 11. Restoration in 2D plain view of the Mantos Blancos copper deposit. a) Current configuration and block model of the deposit, where the shape of main orebody (oregrade > 1% Cu at ~700 m.a.s.l.) is shown in dark grey, b) orebody

geometry at time before Miocene, c) orebody geometry before Eocene-Oligocene Incaic clockwise rotations (40º) and d) original orebody geometry and orientation, at early Cretaceous, previous to the sinistral movements of major faults in the deposit.

Table captions

Table 1. Natural remanent magnetization and susceptibility of paleomagnetic sites.

Table 2. Summary of the paleomagnetic results and tectonic rotations. Age: estimated age of magnetization. Dec Inc a95: observed paleomagnetic direction. Lat VGP Long: reference magnetic pole. Dexp Incl: expected direction by reference pole in the site. Rot ±DR: tectonic rotation and error. Err_I ±EI: difference between observed inclination and expected inclination and error. For simplicity the calculations were made considering that all sites are located at 23.42ºS - 70.05ºW.

Table 3. AMS data of paleomagnetic sites.

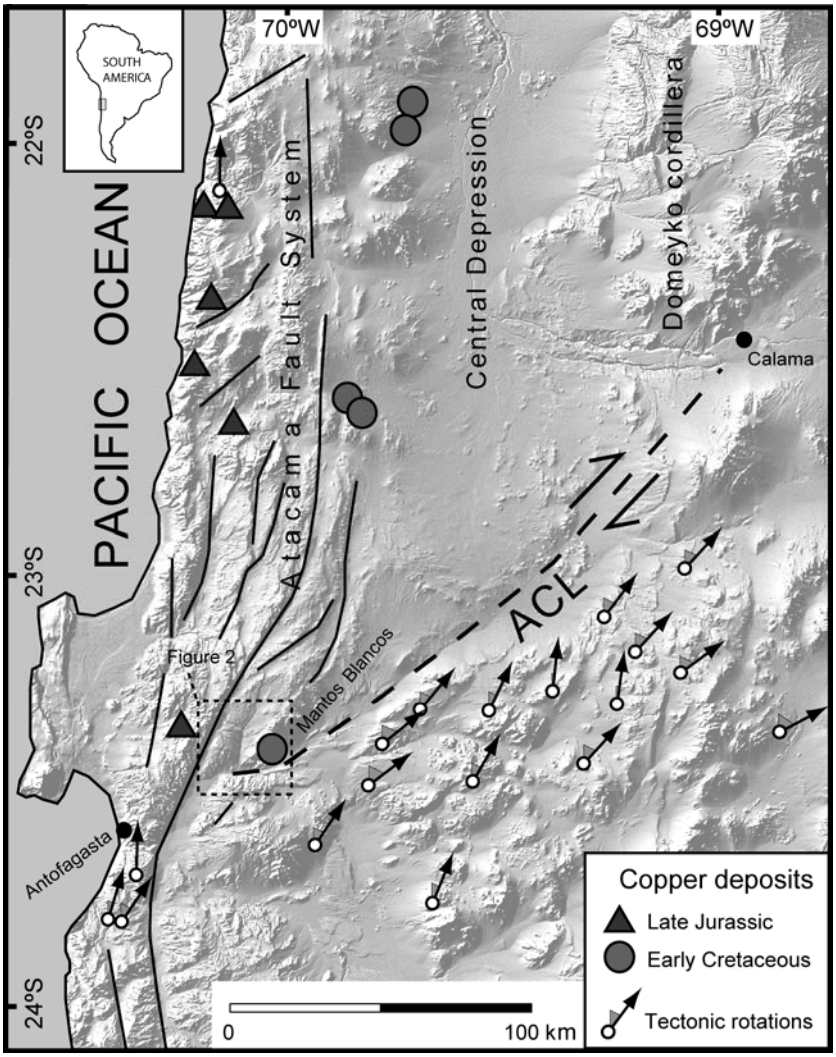
70ºW
69ºW
22ºS
23ºS
24ºS
SOUTH AMERICA
PACIFIC OCEAN
Atacama Fault System
Central Depression
Domeyko cordillera
Calama
ACL
Figure 2
Mantos Blancos
Antofagasta
Copper deposits
Late Jurassic
Early Cretaceous
Tectonic rotations
0
100 km

FIGURE 1

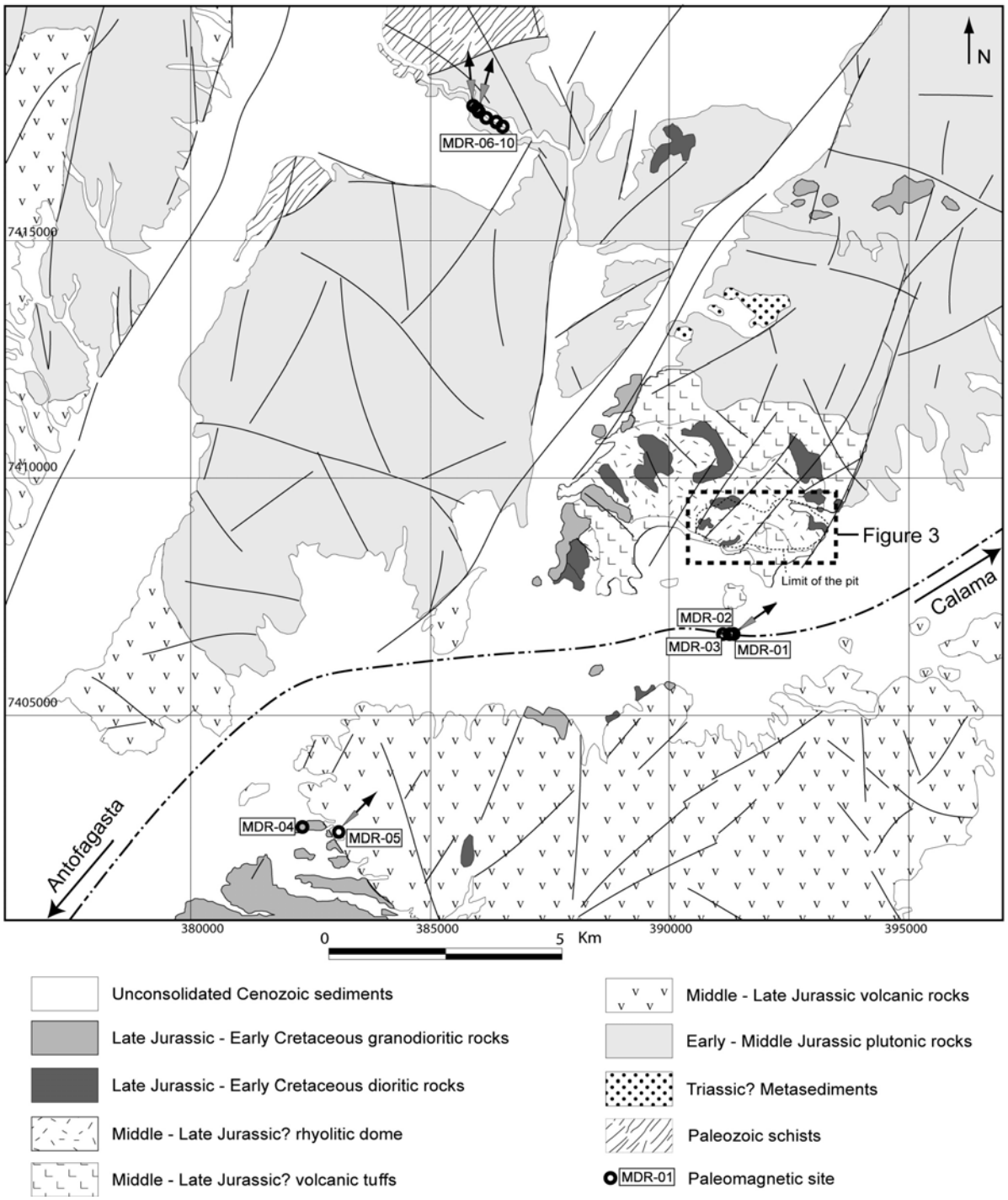
N
MDR-06-10
7415000
7410000
7405000
Figure 3
Limit of the pit
Calama
MDR-02
MDR-03
MDR-01
MDR-04
MDR-05
Antofagasta
380000
385000
390000
395000
0
5
Km
Unconsolidated Cenozoic sediments
Late Jurassic - Early Cretaceous granodioritic rocks
Late Jurassic - Early Cretaceous dioritic rocks
Middle - Late Jurassic? rhyolitic dome
Middle - Late Jurassic? volcanic tuffs
Middle - Late Jurassic volcanic rocks
Early - Middle Jurassic plutonic rocks
Triassic? Metasediments
Paleozoic schists
MDR-01 Paleomagnetic site

FIGURE 2

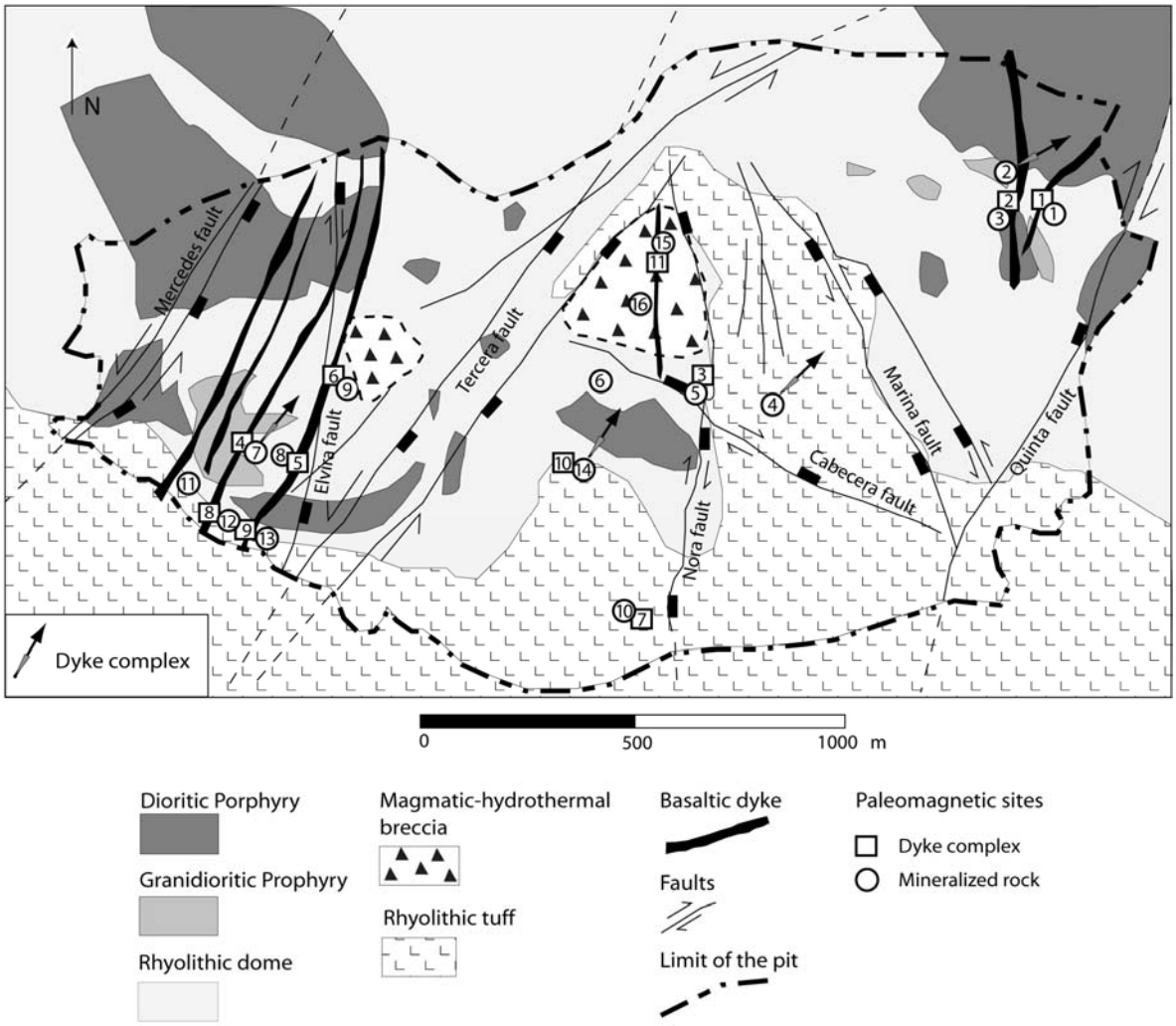
N
Mercedes fault
Elvira fault
Tercera fault
Nora fault
Cabecera fault
Marina fault
Quinta fault
Dyke complex
0
500
1000 m
Dioritic Porphyry
Granidioritic Prophyry
Rhyolithic dome
Magmatic-hydrothermal breccia
Rhyolithic tuff
Basaltic dyke
Faults
Limit of the pit
Paleomagnetic sites
Dyke complex
Mineralized rock

FIGURE 3

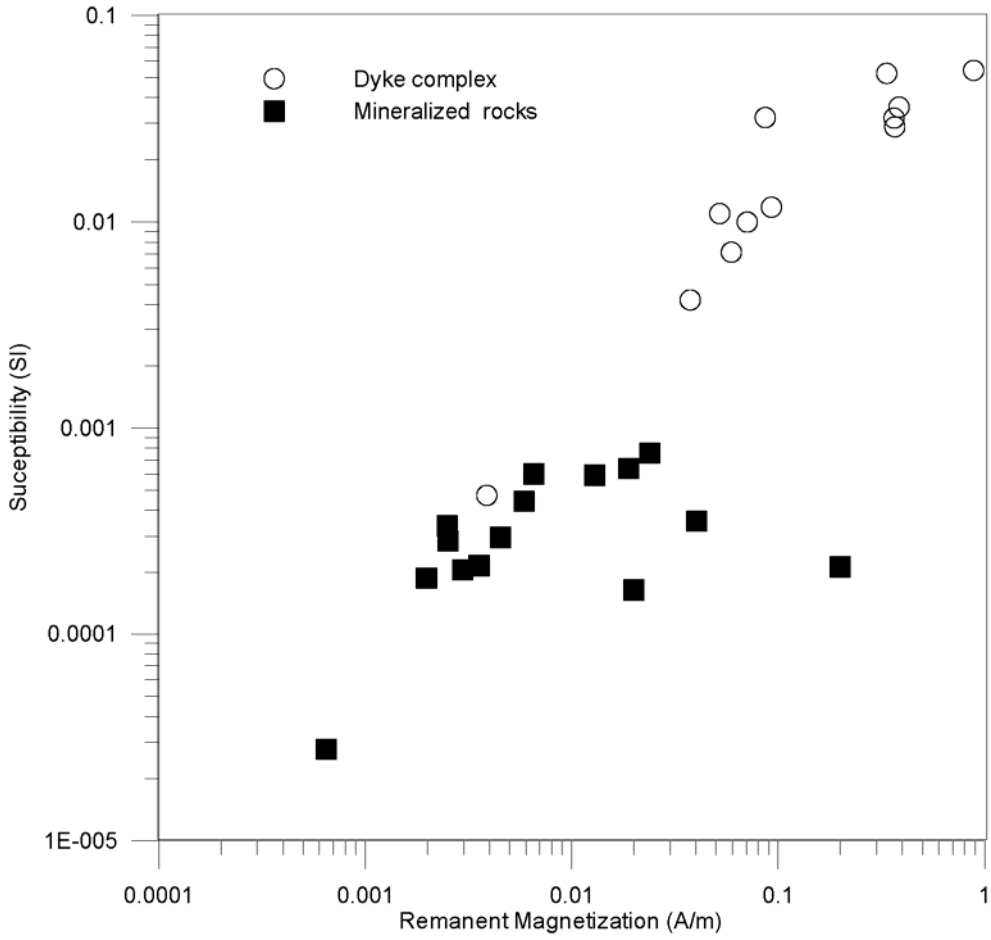
Dyke complex
Mineralized rocks
Suceptibility (SI)
0.1
0.01
0.001
0.0001
1E-005
0.0001
0.001
0.01
0.1
1
Remanent Magnetization (A/m)

FIGURE 4

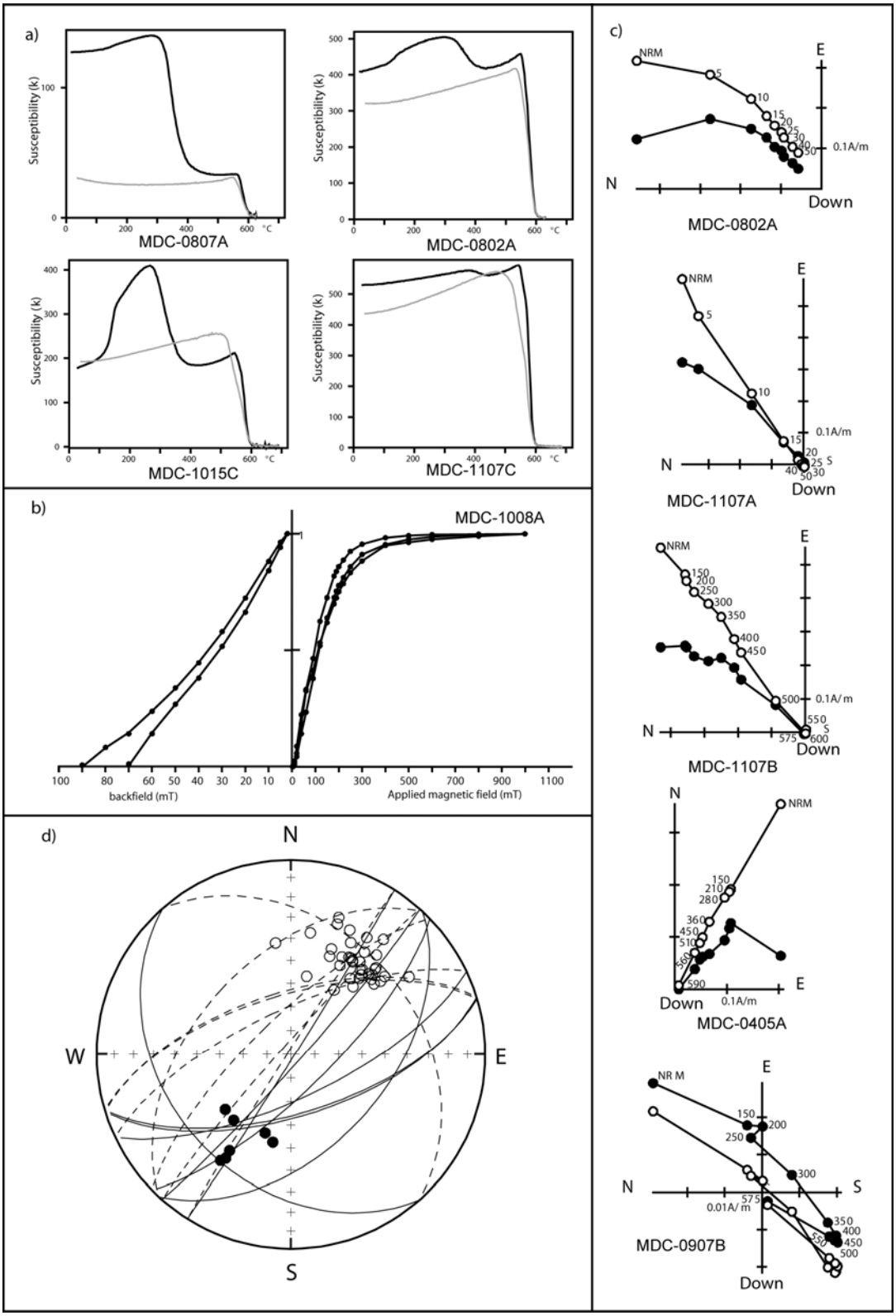
a)
Susceptibility (k)
MDC-0807A
MDC-0802A
MDC-1015C
MDC-1107C
°C
b)
MDC-1008A
backfield (mT)
Applied magnetic field (mT)
c)
NRM
E
N
Down
0.1A/m
MDC-0802A
MDC-1107A
MDC-1107B
MDC-0405A
MDC-0907B
NR M
0.01A/ m
d)
N
W
E
S

FIGURE 5

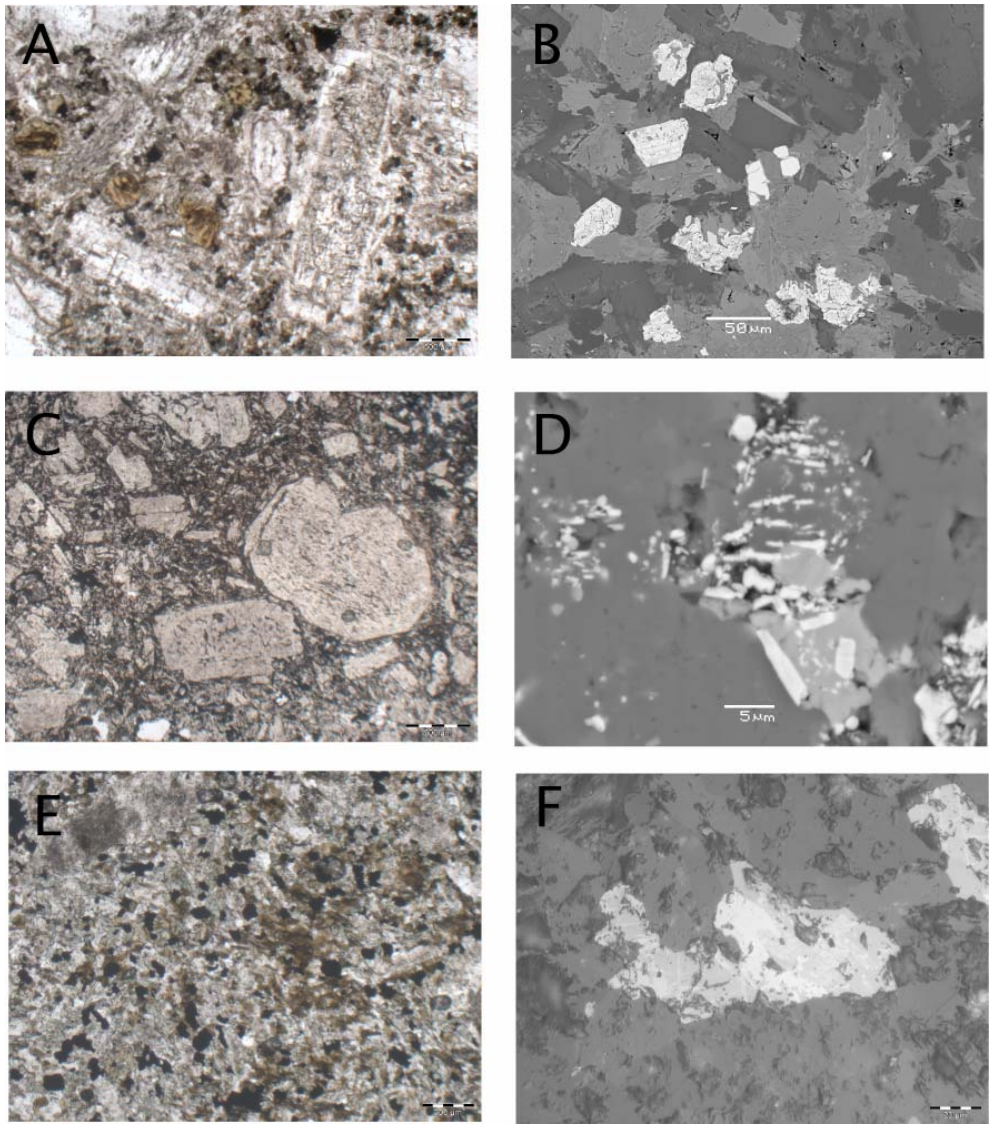

FIGURE 6

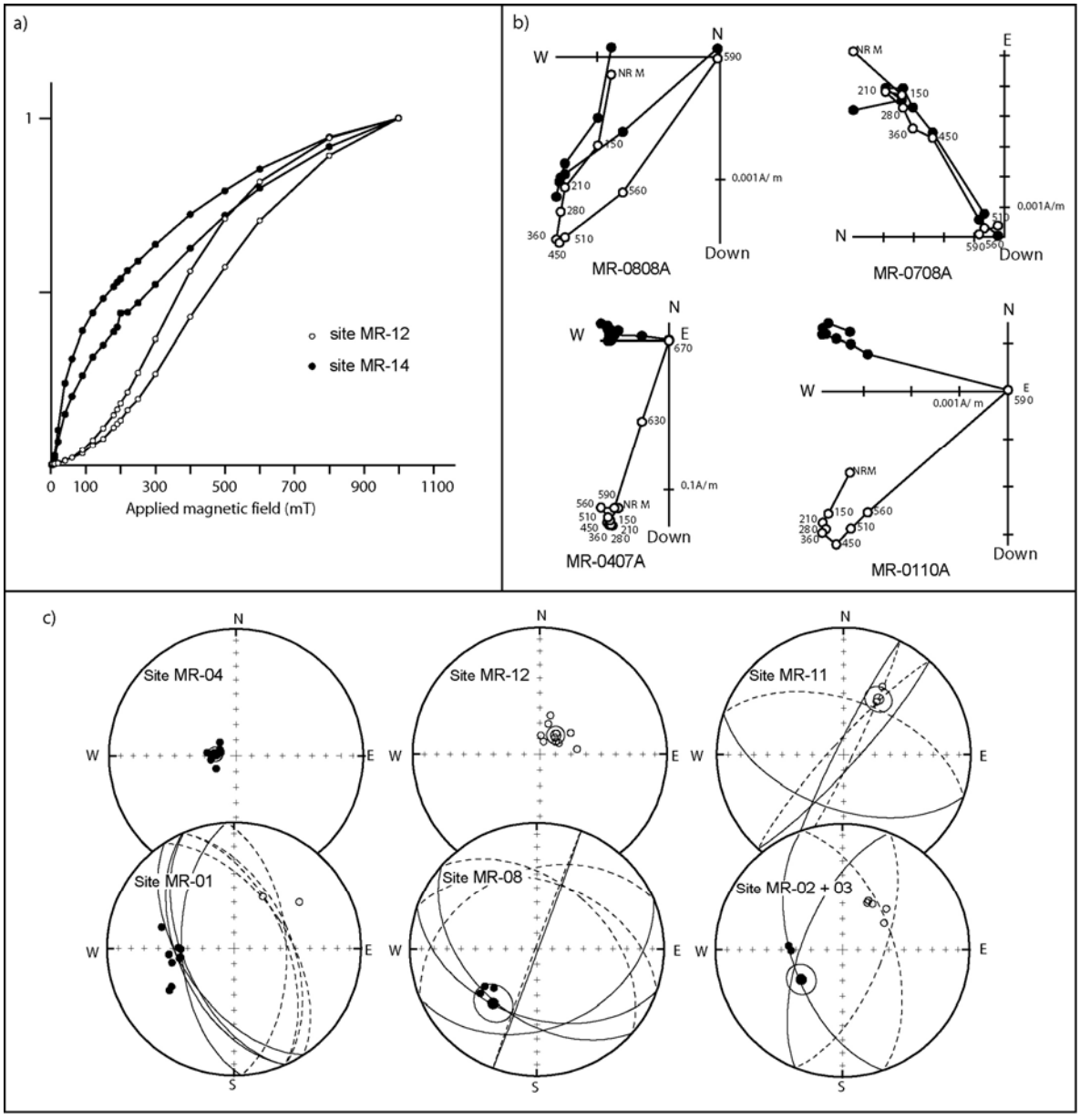
a)
1
site MR-12
site MR-14
0 100 300 500 700 900 1100
Applied magnetic field (mT)
b)
N
W
NR M
590
150
210
280
360
450
510
560
0.001A/ m
Down
MR-0808A
E
NR M
210
150
280
360
450
0.001A/m
N
590
560
Down
MR-0708A
N
W
E
670
630
590
560
NR M
510
150
450
210
360
280
0.1A/m
Down
MR-0407A
N
W
E
590
0.001A/ m
NRM
210
150
560
280
510
360
450
Down
MR-0110A
c)
N
Site MR-04
W
E
Site MR-01
S
Site MR-12
Site MR-08
Site MR-11
Site MR-02 + 03

FIGURE 7

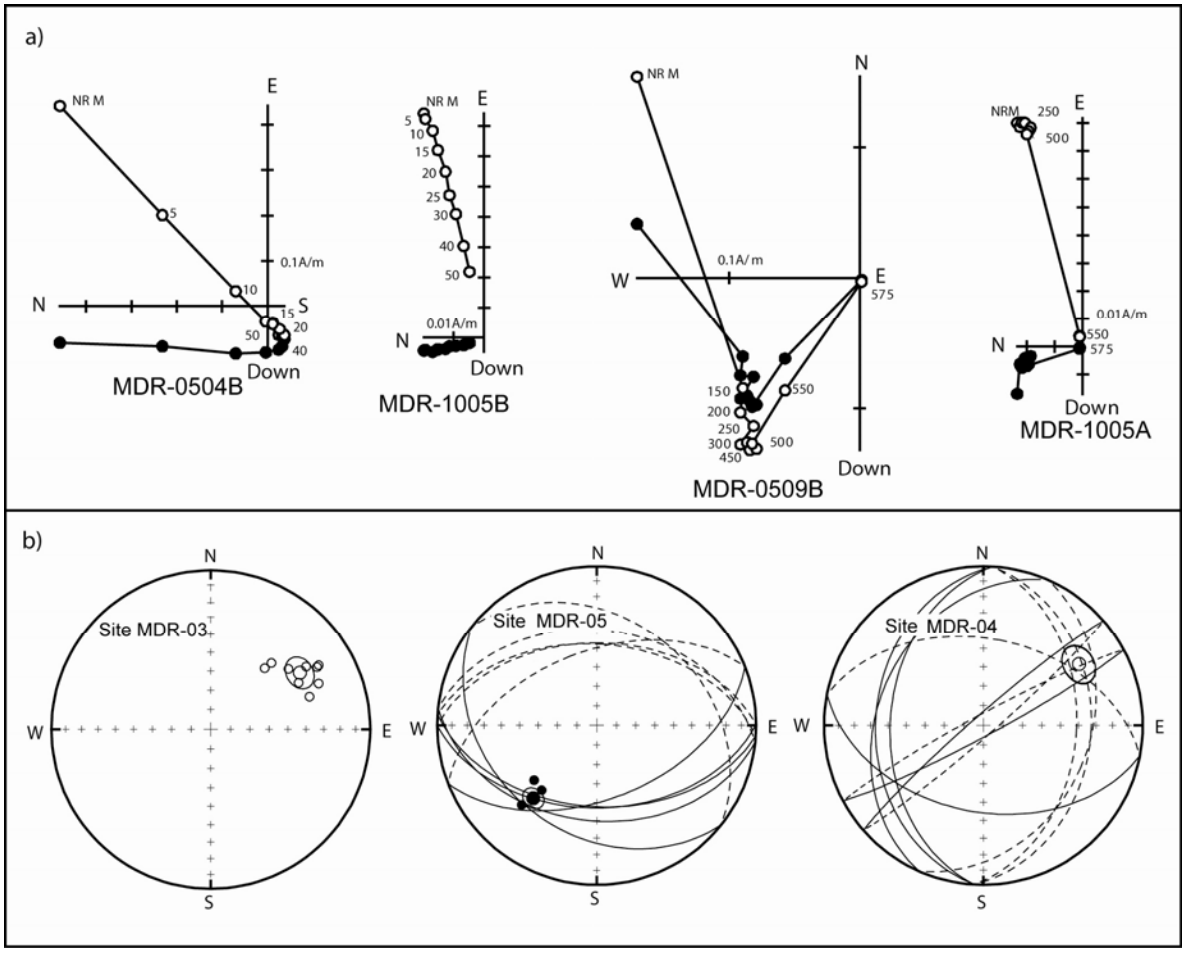
a)
NR M
E
N
S
0.1A/m
Down
MDR-0504B
MDR-1005B
MDR-0509B
MDR-1005A
NRM
250
500
550
575
0.01A/m
W
b)
Site MDR-03
Site MDR-05
Site MDR-04

FIGURE 8

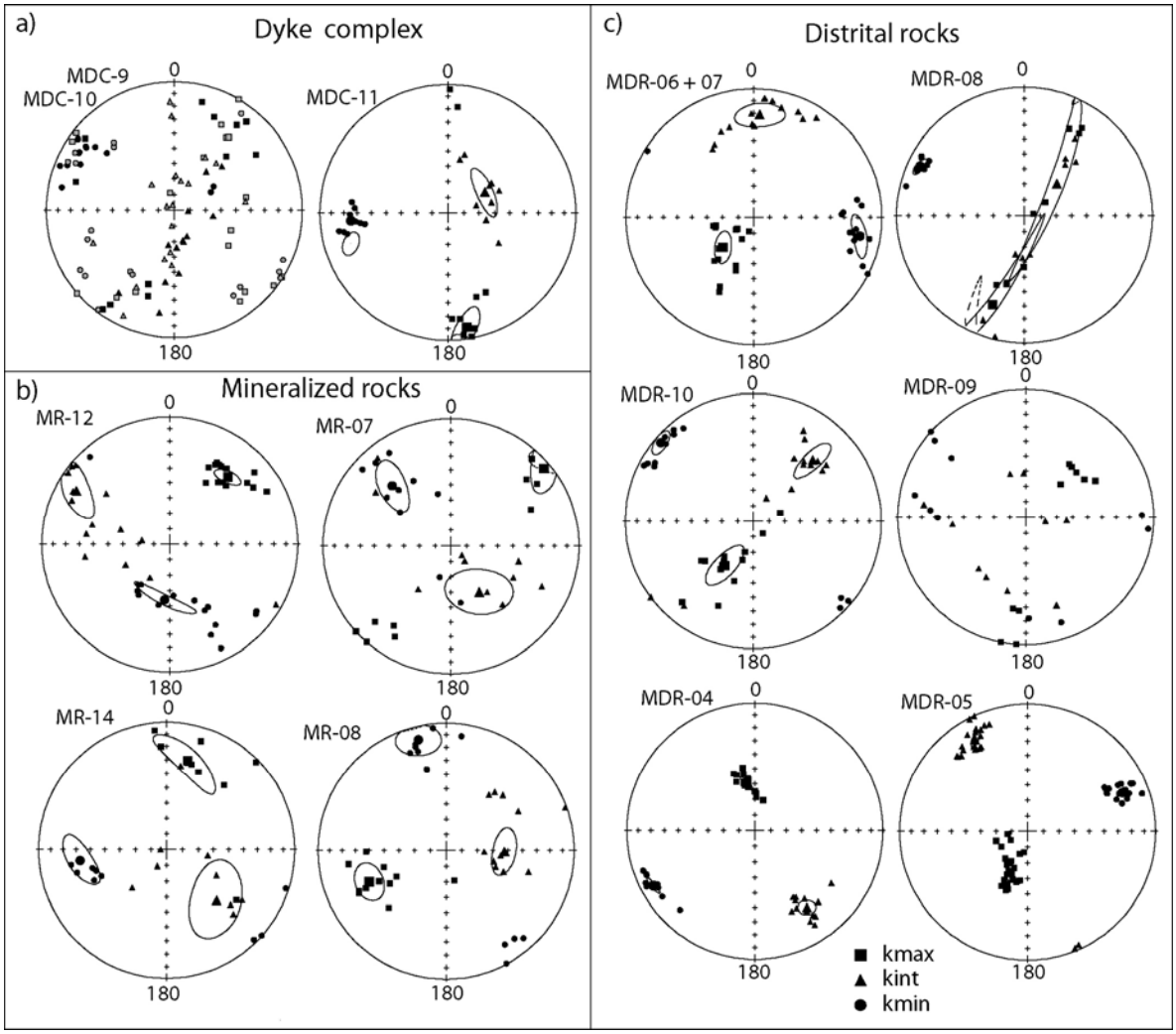
a)
Dyke complex
MDC-9
MDC-10
MDC-11
b)
Mineralized rocks
MR-12
MR-07
MR-14
MR-08
c)
Distrital rocks
MDR-06 + 07
MDR-08
MDR-10
MDR-09
MDR-04
MDR-05
0
180
kmax
kint
kmin

FIGURE 9

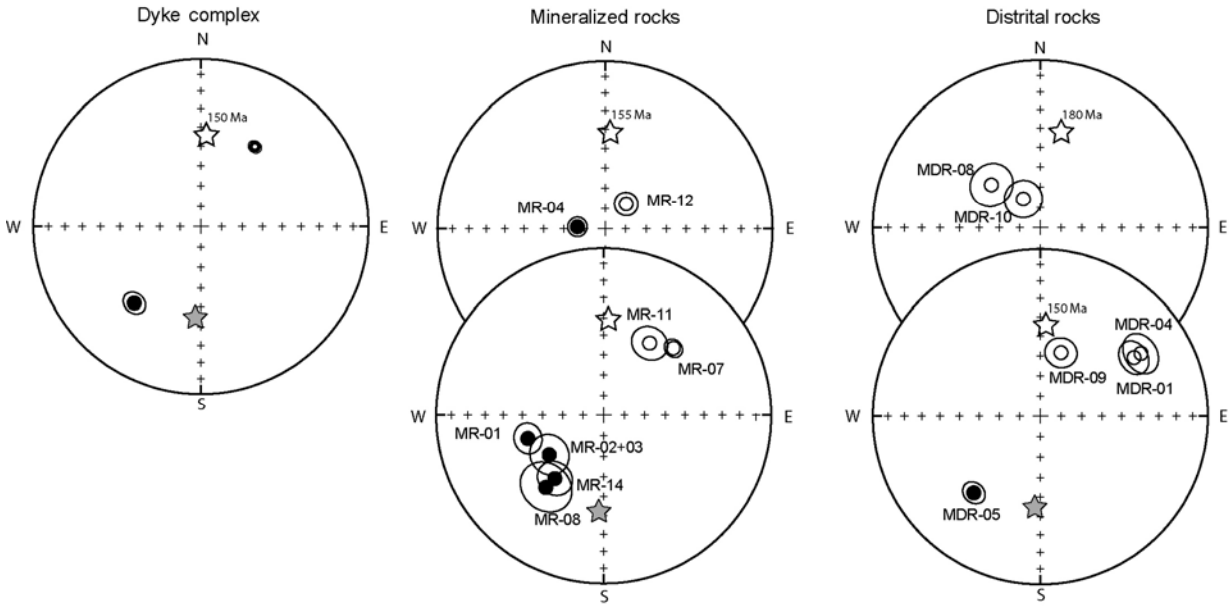
Dyke complex
N
150 Ma
W
E
S
Mineralized rocks
N
155 Ma
MR-04
MR-12
W
E
MR-11
MR-07
MR-01
MR-02+03
MR-14
MR-08
S
Distrital rocks
N
180 Ma
MDR-08
MDR-10
W
E
150 Ma
MDR-04
MDR-09
MDR-01
MDR-05
S

FIGURE 10

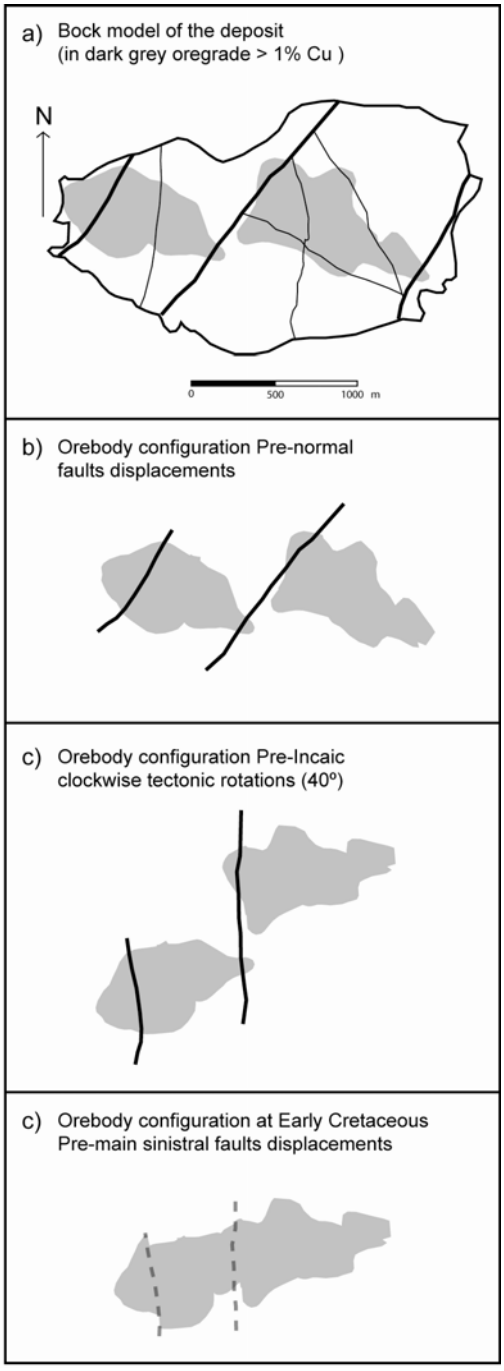
a) Bock model of the deposit
(in dark grey oregrade > 1% Cu)
N
0
500
1000 m
b) Orebody configuration Pre-normal
faults displacements
c) Orebody configuration Pre-Incaic
clockwise tectonic rotations (40º)
c) Orebody configuration at Early Cretaceous
Pre-main sinistral faults displacements

FIGURE 11

TABLE 1

Site	Samples	Lithology	NRM (A/m)	K (SI)
Dyke Complex				
MDC-01	4	Basaltic dyke	3.850E-01	3.600E-02
MDC-02	3	Basaltic dyke	3.880E-03	4.730E-04
MDC-03	4	Basaltic dyke	7.080E-02	1.000E-02
MDC-04	2	Basaltic dyke	3.350E-01	5.230E-02
MDC-05	10	Basaltic dyke	3.640E-01	3.180E-02
MDC-06	6	Basaltic dyke	8.660E-02	3.200E-02
MDC-07	2	Basaltic dyke	5.930E-02	7.160E-03
MDC-08	7	Basaltic dyke	3.670E-01	2.890E-02
MDC-09	7	Basaltic dyke	5.210E-02	1.100E-02
MDC-10	10	Basaltic dyke	9.280E-02	1.180E-02
MDC-11	6	Basaltic dyke	8.850E-01	5.410E-02
Mineralized rocks				
MR-01	12	Granodiorite	3.560E-03	2.160E-04
MR-02	5	Granodiorite	2.500E-03	3.370E-04
MR-03	4	Rhyolitic dome	6.470E-04	2.780E-05
MR-04	8	Rhyolitic tuff	1.990E-01	2.130E-04
MR-05	8	Rhyolitic dome	4.520E-03	2.960E-04
MR-06	4	Rhyolitic tuff	1.290E-02	5.920E-04
MR-07	10	Rhyolitic dome	2.510E-03	2.850E-04
MR-08	11	Rhyolitic dome	1.980E-03	1.880E-04
MR-09	6	Rhyolitic dome	2.960E-03	2.060E-04
MR-10	7	Rhyolitic tuff	2.000E-02	1.650E-04
MR-11	5	Rhyolitic dome	2.390E-02	7.580E-04
MR-12	9	Rhyolitic tuff	4.030E-02	3.550E-04
MR-13	1	Rhyolitic tuff	-	-
MR-14	6	Rhyolitic tuff	1.890E-02	6.390E-04
MR-15	2	Rhyolitic dome	6.540E-03	6.000E-04
MR-16	3	Rhyolitic dome	5.900E-03	4.430E-04
Distrital rocks				
MDR-01	6	Basaltic dyke	3.750E-02	4.210E-03
MDR-02	5	Andesite	3.370E-02	4.920E-04
MDR-03	8	Granodiorite	2.200E-01	2.410E-04
MDR-04	9	Granodiorite	8.370E-01	2.330E-02
MDR-05	11	Andesite	4.560E-01	7.440E-02
MDR-06	4	Tonalite	2.120E-02	5.360E-03
MDR-07	4	Tonalite	7.120E-03	4.330E-03
MDR-08	6	Tonalite	7.400E-03	1.880E-03
MDR-09	5	Basaltic dyke	1.440E-02	1.250E-03
MDR-10	7	Tonalite	1.910E-02	1.080E-02

TABLE 2

Site	L/P	N	Dec	Inc	α 95	k	Age	Lat VGP	Long	P 95	Dexp	Incl	Rot	±DR	Err_I	±EI
MR-01	11/4	15	252.9	50.9	7.1	30										
MR-02 + 03	7/2	9	234.0	57.0	9.6	30										
Mean		24	245.8	53.6	5.8	26.9	140	77.5	238.2	8.1	349.8	-28.8	76.0	10.3	24.8	11.7
							155	**87.3**	**39.6**	**3.8**	**2.8**	**-42.1**	**63.0**	**8.5**	**11.5**	**6.1**
MR-07	8/1	9	45.7	-41.5	4.4	144										
MR-11	2/3	5	32.2	-47.3	8.4	129										
Mean	10/4	14	41.8	-43.2	4.2	92	**155**	**87.3**	**39.6**	**3.8**	**2.8**	**-42.1**	**39.0**	**5.7**	**1.1**	**5.2**
MR-04	7/0	7	273.8	76.6	4.7	168										
MR-12	10/0	10	40.2	-74.1	5.7	72										
Mean		17	59.7	-76.6	4.7	59	155	87.3	39.6	3.8	2.8	-42.1	56.9	16.9	34.5	5.5
*		17	49.9	-46.9	4.7	59	**155**	**87.3**	**39.6**	**3.8**	**2.8**	**-42.1**	**47.1**	**6.4**	**4.8**	**5.5**
MR-08	3/4	7	218.8	44.1	12.2	28										
MR-14	2/5	7	215.6	49.6	7.1	95										
Mean	5/9	14	216.5	46.4	6.2	45	140	77.5	238.2	8.1	349.8	-28.8	46.7	9.9	17.6	11.8
							155	**87.3**	**39.6**	**3.8**	**2.8**	**-42.1**	**33.7**	**7.9**	**4.3**	**6.4**
MDC	43/8	51	33.9	-41.8	3.1	41	140	77.5	238.2	8.1	349.8	-28.8	44.1	7.5	13.0	11.0
							150	**85.8**	**61.6**	**6.3**	**3.5**	**-44.5**	**30.4**	**6.5**	**-2.7**	**6.8**
MDR-01	9/0	9	57.6	-34.2	7.6	46	140	77.5	238.2	8.1	349.8	-28.8	67.8	10.0	5.4	12.3
							150	**85.8**	**61.6**	**6.3**	**3.5**	**-44.5**	**54.1**	**9.3**	**-10.3**	**8.8**
MDR-04	0/6	6	57.7	-29.7	9.0	95										
MDR-05	4/5	9	221.0	39.3	5.3	107										
Mean		15	229.0	35.1	5.4	55.1	**150**	**85.8**	**61.6**	**6.3**	**3.5**	**-44.5**	**45.5**	**7.7**	**-9.4**	**7.7**
MDR-08	4/0	4	311.4	-58.0	10.4	78										
MDR-10	7/0	7	329.5	-73.7	9.1	44										
Mean		11	320.0	-68.2	7.8	35	180	78.4	26.6	7.6	12.7	-42.0	-52.7	18.4	26.2	10.2
*		11	7.8	-51.9	7.8	35	**180**	**78.4**	**26.6**	**7.6**	**12.7**	**-42.0**	**-4.9**	**12.2**	**9.9**	**10.2**
MDR-09	8/0	8	18.5	-57.2	7.5	56	140	77.5	238.2	8.1	349.8	-28.8	28.7	13.0	28.4	12.3
							150	**85.8**	**61.6**	**6.3**	**3.5**	**-44.5**	**15.0**	**12.5**	**12.7**	**8.7**

* Tilt correction of 30° to the SW.

TABLE 3

		K max					K int					K min												
Site	**N**	**k1**	**D1**	**I1**	**p1**	**p2**	**k2**	**D2**	**I2**	**p1**	**p2**	**k3**	**D3**	**I3**	**p1**	**p2**	**lin**	**fol**	**ani**	**k**	**t**	**shape**	**r**	**P'**
MR-04	7	1.010	352.3	29.7	31.3	11.1	1.002	106.5	35.7	33.7	26.9	0.989	233.6	40.0	30.1	10.9	1.008	1.013	1.022	0.623	0.23	oblate	1.021	1.022
MR-07	10	1.014	50.0	5.9	17.7	7.4	1.001	148.6	54.9	21.7	14.4	0.985	316.0	34.4	19.6	7.8	1.012	1.016	1.029	0.769	0.13	oblate	1.029	1.029
MR-08	11	1.020	247.9	35.3	10.9	10.0	1.000	91.2	52.4	14.6	7.6	0.980	346.1	11.4	13.2	10.7	1.020	1.020	1.041	1.030	-0.01	prolate	1.040	1.041
MR-12	15	1.020	40.5	30.9	8.2	4.2	0.998	300.0	17.0	21.2	7.5	0.982	185.3	53.7	21.1	3.4	1.023	1.017	1.040	1.356	-0.15	prolate	1.039	1.040
MR-14	9	1.019	13.3	29.0	25.3	7.7	1.002	135.4	43.8	24.9	16.5	0.979	262.8	32.3	17.2	7.9	1.018	1.023	1.041	0.776	0.13	oblate	1.041	1.041
MDC-09	9	1.009	162.7	25.7	53.5	13.4	1.001	287.8	50.1	56.5	18.5	0.991	57.8	28.2	42.6	6.1	1.008	1.010	1.018	0.769	0.13	oblate	1.018	1.018
MDC-10	13	1.008	208.1	8.3	22.9	6.8	1.002	87.2	74.2	22.8	8.3	0.990	300.1	13.4	9.8	4.4	1.006	1.011	1.017	0.515	0.32	oblate	1.017	1.018
MDC-11	9	1.021	170.7	10.0	15.8	5.6	1.011	60.6	62.9	16.3	5.4	0.968	265.3	24.9	7.5	5.0	1.009	1.045	1.054	0.205	0.66	oblate	1.054	1.058
MDR-04	14	1.034	350.0	59.3	5.6	1.5	1.008	145.9	28.4	6.0	4.5	0.958	241.7	10.6	5.0	1.6	1.026	1.052	1.079	0.494	0.33	oblate	1.078	1.080
MDR-05	23	1.065	203.1	61.4	5.7	2.1	1.000	330.4	18.3	5.2	2.0	0.935	67.7	21.2	3.7	1.4	1.065	1.070	1.139	0.921	0.04	oblate	1.135	1.139
MDR-06+07	14	1.052	225.5	62.3	10.6	5.2	1.001	3.3	21.2	13.5	8.9	0.947	100.1	16.9	12.5	4.8	1.051	1.056	1.110	0.914	0.04	oblate	1.107	1.110
MDR-08	9	1.028	199.7	26.6	69.5	3.4	1.026	45.3	60.9	69.5	4.7	0.946	295.2	10.8	5.4	2.8	1.003	1.084	1.087	0.031	0.94	oblate	1.087	1.100
MDR-09	10	1.002	22.0	0.0	76.7	12.4	1.001	112.0	73.9	76.6	10.7	0.997	292.0	16.1	22.3	10.7	1.001	1.004	1.005	0.234	0.62	oblate	1.005	1.006
MDR-10	13	1.032	212.5	55.8	17.2	6.3	1.011	44.1	33.7	17.3	4.8	0.957	310.5	5.4	6.7	4.9	1.021	1.056	1.078	0.367	0.46	oblate	1.077	1.081

V. DISCUSIÓN

V.1 Edad del domo riolítico

Las rocas riolíticas que hospedan parte de la mineralización en el yacimiento Mantos Blancos, presentan una intensa alteración, lo cual, ha dificultado establecer la edad de estas rocas por métodos radiométricos. Estas rocas fueron definidas informalmente como la Secuencia Volcánica Mantos Blancos (SVMB; Chávez, 1985), constituida por "flujos y brechas volcánicas de composición andesítica, dacítica y riolítica", cuya potencia mínima fue estimada por Cortés (1998) en 2800 m. En base a similitudes litológicas, Chávez (1985) correlacionó la SVMB con rocas queratofídicas (rocas volcánicas calcoalcalinas, intermedias a félsicas, con metasomatismo sódico), descritas por Harrington (1961) en el norte de Chile, asignadas al Triásico Inferior. Dataciones K/Ar en biotitas de granodioritas que intruyen a esta secuencia (Chávez, 1985) entregaron edades de 147 $\pm$ 1 y 147 $\pm$ 4 Ma, permitiéndole a este autor, asignarle a la SVMB una edad mínima Jurásico medio. Por otra parte, en base a estudios isotópicos Rb/Sr, Tassinari et al. (1993), sugieren una edad de la SVMB de ~175 Ma, asumiendo razones iniciales de $^{87}Sr/^{86}Sr$ mas bajas que las registradas por estas rocas (~0.706), equivalentes a las de la Formación La Negra (~0.703).

Recientemente se han reportado 4 edades U-Pb en circón de rocas del yacimiento (Cornejo et al., 2006). Las edades reportadas corresponden a: i) intrusiones subvolcánicas (180.8 ± 0.2 y 181.4 ± 0.3), ii) domo (181.8 ± 0.6) y iii) ignimbrita (181.7 ± 0.2). Estos resultados sugieren que las rocas de caja de la mineralización tienen una edad cercana a 180 Ma. Por otra parte, datos de U-Pb en circones (Proyecto FONDEF 1012), de las mismas rocas, muestran una compleja historia magmática, ya que los cristales de circones se presentan en su mayoría zonados, registrando edades que abarcan prácticamente todo el

Jurásico. Por lo tanto, es difícil establecer con claridad el significado de las edades sugeridas entorno a ~180 Ma.

A continuación se detallan los resultados de los análisis U-Pb en circones, obtenidos en el marco del proyecto FONDEF 1012, "Fundamentos metalogénicos, mineralógicos y geoquímicos para una exploración innovativa de depósitos de cobre: aplicaciones en la Cordillera de la Costa del Norte de Chile".

Metodología

Tres muestras de domo riolítico y una muestra de toba riolítica en el yacimiento, además de una muestra del plutón Alibaud (aproximadamente 4 km al norte de la mina) fueron investigadas para obtener su edad U-Pb en circones.

Los análisis U-Pb en circones de estas muestras fueron realizados por Gastón Guiliani en CRPG/CNRS (Nancy, Francia) con una microsonda iónica Cameca IMS 1270. Los circones fueron montados en una resina epóxica junto con un circón estándar (91500 de Ontario, Canada), con una edad de 1062 ± 0.4 Ma (Wiedenbeck et al., 1995). Los circones fueron pulidos y cubiertos con una película de oro. Para caracterizar su estructura interna, se tomaron imágenes de los circones con electrones retrodispersados (BSE) en un equipo SEM (Hitachi 2500). El procedimiento analítico usado se detalla en el trabajo de Deloule et al. (2002). Cada análisis consistió en 16 ciclos sucesivos, y cada ciclo comenzó con la medición de $^{196}Zr_2O$ (masa de referencia), seguido de ^{204}Pb, ^{206}Pb, ^{207}Pb, ^{208}Pb, ^{238}U, ^{248}ThO and ^{238}UO. El tamaño de los puntos analíticos fue variable entre 30x40 μm. Correcciones para el plomo común fueron realizadas usando el contenido medido de ^{204}Pb y el modelo de evolución de plomo de Stacey and Kramers (1975). En algunos casos, los puntos analíticos incluyen pequeños volúmenes de resina epóxica, sin

embargo, las mediciones no muestran rezones inusuales de $^{206}Pb/^{204}Pb$, por lo que fueron incluidos como parte de los datos analizados.

Los datos isotópicos con su incertezas analíticas, y edades calculadas se muestran en la Tabla 1. Los circones tienen contenidos de Pb muy bajos (entre 2 y 30 ppm) con un baja proporción de plomo común (0 a 9%). La mayoría de los datos ^{206}U-^{238}Pb y ^{207}U-^{235}Pb no son concordantes entre si dentro del error analítico, por lo tanto solo las edades individuales de ^{206}U-^{238}Pb se han usado para la interpretación.

Resultados

Dieciséis mediciones de edad fueron realizadas en nueve circones provenientes de tres muestras del domo riolítico, en las cuales se distinguen dos tipos de circones: cristales zonados y no zonados (Tabla 1). Las edades obtenidas de los circones del domo riolítico evidencian una compleja historia magmática: el diagrama de densidad de probabilidad relativa de la edad ^{206}Pb-^{238}U muestra una distribución multi-modal, con varios *peaks* a los 197-203, 171-178 y 155-157 Ma, respectivamente (Figura 10). Los dos peaks más antiguos corresponden principalmente a edades obtenidas de puntos analíticos realizados en el centro de circones zonados, y probablemente representan circones magmáticos heredados. El *peak* mas joven (155–157 Ma) es interpretado tentativamente como la edad de emplazamiento del domo riolítico, aunque estas edades provienen de distintas zonas de cristales: (1) un punto analítico que alcanza distintas zonas de crecimiento de la parte interior de un cristal posee 155.9 ± 6.7 Ma, y (2) un cristal no zonado, 157.1 ± 4.5 Ma.

Cinco edades en igual número de circones no zonados, fueron obtenidas en una muestra de toba riolítica cerca del yacimiento. Los resultados indican un rango de edad que abarca todo el Jurásico al Cretácico inferior. El significado de la edad más joven, de ~140 Ma es difícil de precisar, sin embargo, en esta muestra se observan los mismos *peaks* de edades que en las muestras del domo, sugiriendo que la edad entre 155-160 Ma, podría corresponder a la edad de emplazamiento de estas rocas.

Cuatro circones provenientes del plutón Alibaud, fueron datados mediante nueve determinaciones de edades, en los cuales solo un cristal evidencia zonación. Las edades ^{206}U-^{238}Pb evidencian dos peaks principales (Figura 10), con valores promedio muy diferentes: la edad más antigua de 190.1 ± 2.4 Ma probablemente refleja circones heredados del Jurásico inferior y el peak de 173.1 ± 1.9 Ma, probablemente registra la edad de cristalización del magma.

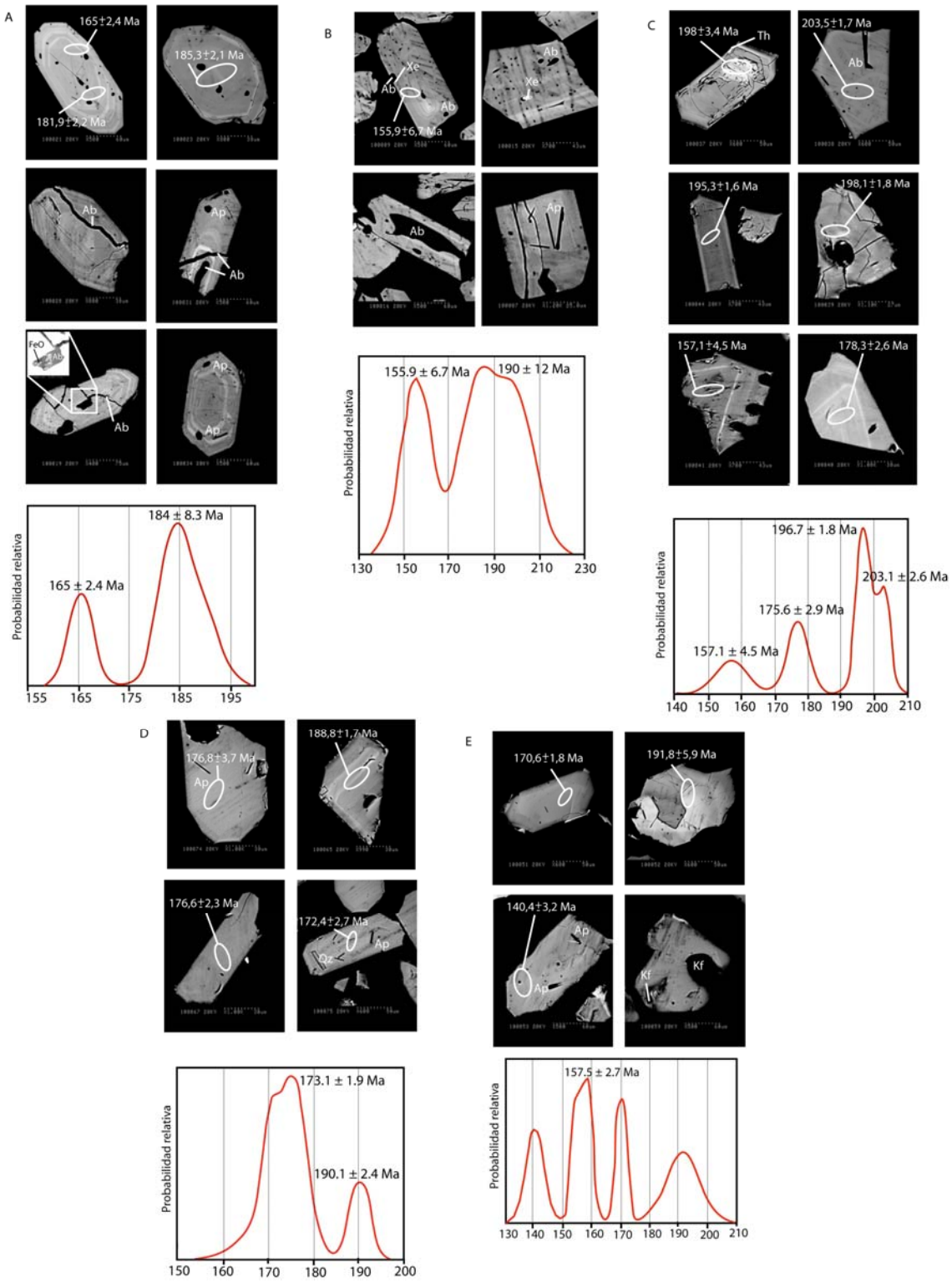

Figura 10. Imágenes de circones analizados (BSE) y diagramas de densidad de probabilidad relativa de edades 206U-238Pb. A),B),C) muestras de domo riolítico, D) plutón Alibaud y E) toba riolítica. Ab: albita, Ap: apatito, Xe: Xenotime Th:Thorianita? Qz: cuarzo, Kf: feldespato potásico.

Tabla 1. Datos geocronológicos U - Pb de circones provenientes del Distrito Minero de Mantos Blancos (Proyecto FONDEF 1012).

	Contenido (ppm)			Medido			Razones corregidas						Edad (Ma)			
	Pb	U	Th	$^{206}Pb/^{204}Pb$	$^{207}Pb/^{206}Pb$	σ	$^{206}Pb/^{238}U$	σ	$^{207}Pb/^{235}U$	σ	$^{206}Pb/^{238}U$	σ	$^{207}Pb/^{235}U$	σ
							Domo riolítico							
*	11	456	121	3763	0.04796	0.01384	0.08859	0.01023	0.07970	0.00606	181.9	2.2	176.0	3.0
*	10	430	143	3299	0.05218	0.01719	0.10321	0.01657	0.06592	0.01000	165.4	2.4	174.1	3.6
*	2	88	71	987	0.04838	0.09010	0.24008	0.02734	0.08008	0.01353	189.5	3.2	184.3	15.3
*	7	281	127	3248	0.04663	0.01993	0.12966	0.01993	0.08256	0.00383	185.3	2.1	174.5	3.7
*	5	235	183	7805	0.04730	0.01282	0.17495	0.01301	0.06133	0.00487	155.9	6.7	150.4	6.3
*	10	383	356	1340	0.05131	0.01917	0.26305	0.01189	0.07038	0.00427	199.9	8.5	204.3	8.7
*	10	406	414	4146	0.04913	0.01155	6.30967	0.02833	0.06650	0.00392	182.6	7.8	180.5	7.4
	8	295	89	17797	0.03884	0.01544	0.07759	0.16454	0.05165	0.00324	196.7	1.5	155.9	2.5
	21	753	247	31400	0.05030	0.00471	0.08447	0.00976	0.05321	0.00410	203.5	1.7	204.0	1.8
*	30	1136	661	336	0.04177	0.07459	0.07618	0.08021	0.05029	0.01607	198.0	3.4	167.8	11.8
	5	201	65	3210	0.04343	0.01318	0.16599	0.07931	0.05263	0.00558	198.1	1.8	174.0	2.6
*	10	409	107	17884	0.04786	0.01711	0.10760	0.01241	0.05781	0.01320	178.3	2.6	172.4	3.6
*	4	180	433	3238	0.07395	0.02384	0.54331	0.01627	0.03422	0.02834	157.1	4.5	227.8	7.7
*	25	960	433	47797	0.04887	0.00471	0.14607	0.00994	0.06119	0.00438	195.3	1.6	191.2	1.7
*	6	234	145	10063	0.04595	0.02306	0.10090	0.01889	0.04346	0.01485	175.6	2.8	163.7	4.3
*	14	529	147	67926	0.03175	0.01190	0.06508	0.01028	0.06001	0.00852	202.2	2.2	132.6	2.0
							Granodiorita Alibaud							
	5	224	152	9453	0.05134	0.01639	0.20691	0.01262	0.04915	0.00596	170.2	1.6	176.1	3.0
	4	165	87	8617	0.05725	0.00994	0.15931	0.01665	0.05292	0.01135	176.6	2.3	201.3	3.0
*	7	286	165	21142	0.05266	0.00704	0.11209	0.02557	0.06022	0.00564	188.7	1.7	198.4	2.1
	6	265	167	7811	0.05435	0.01030	0.20420	0.00980	0.05256	0.01438	172.4	2.7	187.8	3.3
	7	276	150	15677	0.05604	0.01031	0.21402	0.01307	0.06284	0.00504	191.5	1.7	212.6	2.6
	5	219	164	17505	0.05098	0.01445	0.16480	0.01707	0.04764	0.01561	173.2	2.9	177.8	3.7
	5	218	130	5326	0.05427	0.02212	0.16636	0.02003	0.05509	0.01995	176.8	3.7	191.9	5.3
	25	1115	759	10931	0.06469	0.04218	6.88964	0.17028	0.05623	0.02758	168.7	4.7	215.6	9.8
	4	181	69	4115	0.05629	0.02300	0.16550	0.02576	0.05723	0.01052	176.0	2.2	197.6	4.7
							Toba riolítca							
	2	106	63	63	0.04840	0.03118	0.11368	0.04310	0.03330	0.02175	140.4	3.2	139.2	5.0
	17	650	349	349	0.05078	0.00804	0.29023	0.01773	0.07961	0.03029	191.7	5.9	194.7	5.7
	6	241	177	177	0.04991	0.01903	0.25761	0.02008	0.05226	0.00811	170.6	1.8	172.0	3.5
	2	99	46	46	0.04930	0.04125	0.18255	0.02500	0.04867	0.01166	155.2	2.1	155.6	6.2
	6	292	257	257	0.05353	0.00659	0.30488	0.00979	0.04826	0.00894	159.3	1.8	172.1	2.1

* Circones zonados

En rocas del domo riolítico, dentro del yacimiento, Oliveros (2005) obtuvo edades $^{40}Ar/^{39}Ar$ en sericita (*in situ* en plagioclasa) en torno a ~ 155 Ma. Estas edades han sido interpretadas como registros de un primer evento de mineralización en el yacimiento (Oliveros, 2005; Ramírez et al., 2006), el cual estaría centrado en brechas ígneas hidrotermales monomícticas de composición riolítica. Estas brechas monomícticas sólo poseen fragmentos del domo riolítico, y una matriz composicionalmente similar, sugiriendo que el emplazamiento del domo y la formación de estas brechas probablemente ocurrieron cercanos en el tiempo.

Las observaciones de campo y los antecedentes expuestos en los distintos capítulos de esta tesis sugieren que parte importante de la SVMB correspondería a un cuerpo intrusivo hipabisal de composición riolítica, emplazado con una geometría en forma de domo o lacolito. Este habría intruido (~155-160 Ma) una secuencia de tobas, brechas volcánicas e intercalaciones sedimentarias subordinadas, ubicadas probablemente en la base de la Formación La Negra. La parte baja de esta secuencia dominada por tobas y brechas volcánicas, está intruida al norte del yacimiento por el plutón Alibaud (~173 Ma), lo que permite asignarle una edad mínima Jurásico medio.

V.2 Profundidad de Mineralización

En Mantos Blancos, las inclusiones fluidas analizadas se encontraron en tres tipos de vetillas (alteración potásica, sódica y propilítica) y en cuarzos incluidos en amígdalas de sills dioríticos, representando las principales etapas del segundo evento de mineralización hidrotermal en el yacimiento. Todas las muestras fueron obtenidas en la parte central del yacimiento y de acuerdo a la clasificación de Nash (1976), las inclusiones fluidas reconocidas son: I (líquido–dominante sin cristales de halita), II (vapor–dominante sin cristales de halita), y IIIb (vapor–dominante con cristales de halita). La ubicación de las muestras, tablas y figuras con los resultados principales del estudio de inclusiones fluidas se muestran en el Capítulo III de esta tesis (ver Ramírez et al., 2006).

En base a los datos experimentales disponibles de inclusiones fluidas, es posible realizar una estimación única de temperatura y condiciones de presión, a partir de las asociaciones de ebullición (Roedder y Bodnar, 1980). Los datos de las otras inclusiones (sin evidencia de ebullición) solo proveen información de presiónes y temperaturas mínimas. La Figura 11 presenta el diagrama de fases del sistema NaCl-H_2O, mostrando las asociaciones de ebullición relacionadas a la alteración potásica y sódica.

Las inclusiones de tipo II (muestras Q-1 y Q –1-1), poseen los valores más altos de temperatura de homogenización (Th) en el campo de vapor. Para la contraparte de fluidos salinos (salmueras), la curva de ebullición indica presiones de entrampamiento entre 360 y 380 bar. Si se asume condiciones hidrostáticas dominantes y 1 g/cm^3 de carga hidrostática, esta ebullición temprana debe haber ocurrido a ~3.5 km de profundidad.

Los datos exhibidos en la Figura 11, permiten suponer que los fluidos representados por las inclusiones de tipo II (Q-1 y Q-1-1), evolucionaron descendiendo su temperatura y presión de 500ºC y 500 bar, intersectando la curva critica, resultando en una continuación de la ebullición potásica.

Como evidencian los datos geológicos de campo, la actividad magmática continuó con la intrusión de sills dioríticos, los cuales presentan actualmente

alteración potásica entre 360 y 720 msnm. Estos cuerpos tabulares horizontales cortan a la brecha central a diferentes niveles, lo que probablemente selló el sistema. Este sello pudo haber producido sobrepresurización hidrotermal causando ebullición durante la alteración sódica.

La ebullición relacionada a la alteración sódica, ocurrió a elevaciones actuales entre 696 y 720 msnm, temperaturas de 349º a 423ºC, y salinidades entre 42-49 a 12.6-13.9 % peso NaCl equiv., en el limite de la curva fraga-dúctil. La presión inferida de la curva de ebullición varia entre 100 y 210 bar, indicando una paleo-profundidad de entrampamiento del orden de los ~2 km, bajo condiciones hidrostáticas (Figura 11).

Los datos de inclusiones fluidas pueden interpretarse como eventos de ebullición y asociados a decomprensión episódica debido a sobrepresurización de fluidos, hidrofracturamiento y bruscos cambios de condiciones litostáticas a hidrostáticas dominantes, lo cual ocurrió a una paleo-profundidad aproximada de entre 3.5 y 2.0 km.

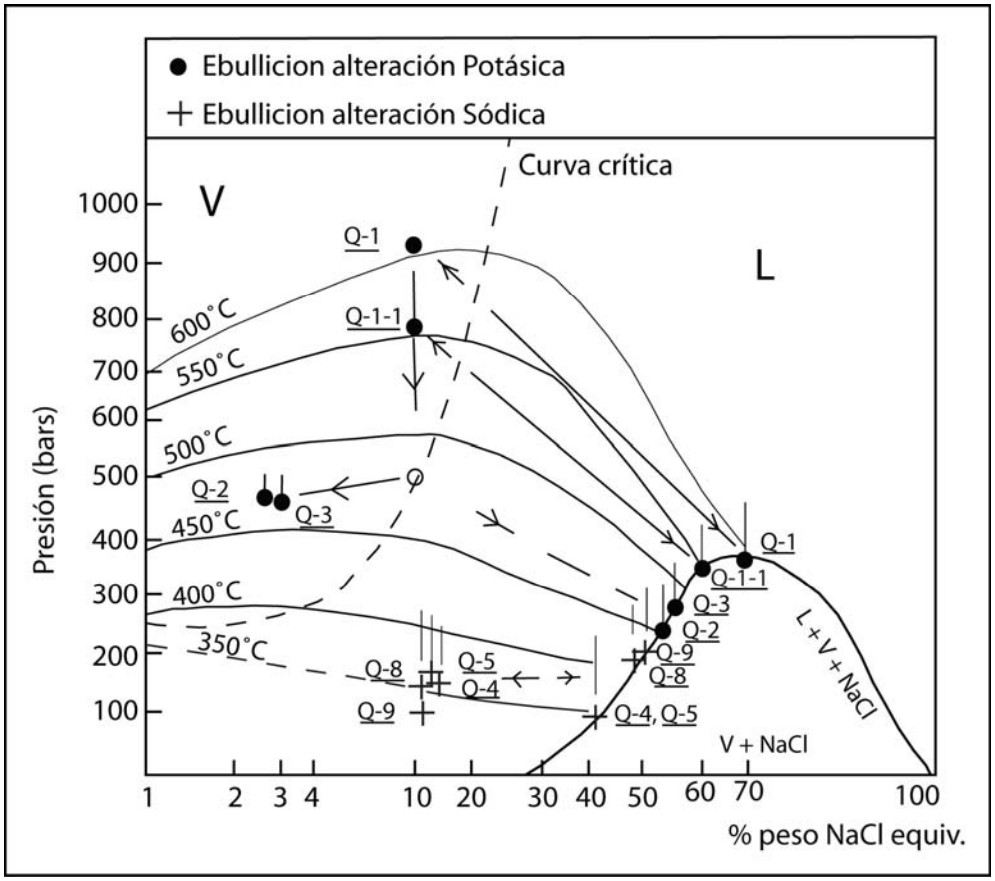

Figura 11. Diagrama de fase NaCl-H_2O, donde se muestran las asociaciones de ebullición de inclusiones fluidas obtenidas de cuarzos de alteración potásica y sódica.

La paleo-profundidad determinada por los datos de inclusiones fluidas para la mineralización en Mantos Blancos, es comparable a los pocos datos disponibles de los depósitos Jurásicos estratoligados de Cu - (Ag). Estos datos sugieren que, asumiendo condiciones de presión hidrostáticas dominantes, fluidos salinos a temperaturas moderadas depositaron metales en un rango de profundidad de 1 a 3 km (Maksaev y Zentilli, 2002). Esta estimación es consistente con datos de trazas de fisión en apatito, que sugieren una baja denudación (<2 km asumiendo una paleo gradiente geotermal de 30ºC/km) de las intrusiones Jurásico-Cretácico inferior a lo largo de la Cordillera de la Costa en la sección norte de la región de Antofagasta (Maksaev, 1990, 2000; Andriessen et al., 1994).

V.3 Referencias

Bodnar RJ, Vityk MO (1994) Interpretation of microthermometric data for H2O-NaCl fluid inclusions. In: Devivo B, Frezzotty ML (eds.) Fluid Inclusion in Minerals: Methods and Applications. Blackburg. VA, pp. 117 – 130.

Cornejo, P., Latorre, J.J., Matthews, S., Marquardt, C., Toloza, R., Basso, M., Rodríguez, J., Ulloa, C. 2006. U/Pb and $^{40}Ar/^{39}Ar$ geochronology of volcanic and intrusive events at the Mantos Blancos copper deposit, II Region, Chile. Actas XI Congreso Geológico Chileno, Antofagasta.

Cortés, J. 1998. Geología, estructuras y geoquímica preliminar del Distrito Minero de Mantos Blancos, Cordillera de la Costa, Segunda Región de Antofagasta, Chile. Memoria de Titulo (Inedito) Universidad Católica del Norte, Departamento de Ciencias Geológicas, 183 p.

Chávez, W. 1985. Geological setting and the nature and distribution of disseminated copper mineralization of the Mantos Blancos district, Antofagasta Province, Chile. PhD Thesis, University at California, Berkeley, USA. 142 pp

Chivas AR, Wilkins WT (1977) Fluid inclusion studies in relation to hydrothermal alteration and mineralization at the Koloula porphyry copper prospect, Guadalcanal. Econ Geol 72: 153 – 169.

Deloule, E., Alexandrov. P., Cheilletz, A., Laumonier, B., Barbey, P. (2002). In-situ U–Pb zircon ages for Early Ordovician magmatism in the eastern Pyrenees, France: the Canigou orthogneisses. Int. J Earth Sci 91: 398–405.

Fournier RO (1991) The transition from hydrostatic to greater than hydrostatic fluid pressure in present active continental hydrothermal systems in crystalline rock. Geophys Res Lett 18: 955 – 958.

Fournier RO (1999) Hydrothermal processes related to movement of fluid from plastic into brittle rock in the magmatic – epithermal environment. Econ Geol 94: 1193 – 1212.

Harrington, H.J. 1961. Geology of parts of Antofagasta and Atacama provinces, northern Chile. American Association of Petroleum Geologists, Bulletin, Vol. 45, No. 2, p. 169- 197.

Hezarkhani A, Williams – Jones AE (1998) Controls of alteration and mineralization in the Sungun porphyry copper deposit, Iran: evidence from fluid inclusions and stable isotopes. Econ Geol 93: 651 – 670.

Miller, C.F. and Meschter, S.M. (2001). Zircon saturation temperatures and preservation of inheritance: implications for contrasting mechanisms of felsic magma generation. 11ª Annual V. M. Goldschmidt Conference.

Nash JT (1976) Fluid-inclusion petrology. Data from porphyry copper deposits and applications to exploration. US Geological Survey Professional Paper 907D, 16p.

Oliveros, V. 2005. Les formations magmatiques jurassiques et mineralisation du nord Chili, origine, mise en place, alteration, metamorphisme: etude geochronologique et geochemie. PhD Thesis. Universite de Nice-Sophia Antipolis, France. 285 pp

Proyecto FONDEF D01I 1012 (2002-2004). Fundamentos metalogenicos, minerlogicos y geoquimicos para una explicacion innovativa dedepositos de cobre: aplicaciones en la Cordillera de la Costa del Norte de Chile. Inedito.

Roedder E (1984) Fluid Inclusions. Mineralogical Society of America. Reviews in Mineralogy 12, 643 p.

Roedder E, Bodnar RJ (1980) Geologic pressure determinations from fluid inclusion studies. Annual Review of Earth and Planetary Science 8: 263 – 301.

Stacey, J.S., Kramers, J.D. 1975. Approximation of terrestrial lead isotope evolution by a two-stage model. Earth Planet Sci Lett 26: 207–221

Tassinari C, Munizaga F, Ramírez R. 1993. Edad y geoquímica isotópica Rb-Sr del yacimiento de cobre Mantos Blancos: relación temporal con el magmatismo jurásico. Rev Geol Chile 20: 193 – 205.

Ulrich T, Günther D, Heinrich C (2002) The evolution of a porphyry Cu–Au deposit, based on LA–ICP–MS analysis of fluid inclusions: Bajo de la Alumbrera, Argentina. Econ Geol 97: 1889 – 1920.

Wiedenbeck, M., Allé, P., Corfu, F., Griffin, W.L., Meier, M., Oberli, F., Von Quadt, A., Roddick, J.C., Spiegel, W. (1995). Three natural zircon standards for U–Th–Pb, Lu–Hf, trace elements and REE analyses. Geostand Newslett 19:1–23

VI. CONCLUSIONES

En el Distrito Minero de Mantos Blancos se reconocieron distintos tipos de rocas ígneas, las cuales fueron agrupadas y denominadas informalmente como Complejo Igneo de Mantos Blancos. Este consiste en rocas riolíticas hipabisales emplazadas como domo y brechas ígneas-hidrotermales monomícticas de composición riolítica, intruidas por pórfidos dioríticos y granodioríticos, en forma de stocks y sills. Los pórfidos dioríticos-granodioríticos localmente gradan hacia superficie a brechas ígneas-hidrotermales polimícticas. Todas estas rocas se encuentran mineralizadas en grados variables. Diques máficos (dioríticos principalmente) cortan todas las rocas mencionadas previamente y son esencialmente tardi-mineral y estériles.

El yacimiento Mantos Blancos se habría formado por dos eventos hidrotermales de edad Jurásico superior-Cretácico inferior. El evento más antiguo ocurrió en el Jurásico superior (~155 Ma), coetáneo con brechización magmático-hidrotermal de composición riolítica y alteración fílica asociada. El evento más joven representa la etapa principal de mineralización ocurrida durante el Cretácico inferior (~141-142 Ma) y está genéticamente relacionado al emplazamiento de sills-stocks granodioríticos y dioríticos de textura porfídica, y la formación coetánea de brechas polimícticas magmático-hidrotermales. Probablemente, ambos eventos hidrotermales contribuyeron en la, extensa pero irregular, distribución de mineralización hipógena. Las zonas de alta ley están restringidas a las partes altas de las brechas polimícticas magmático-hidrotermales formadas durante el segundo evento de mineralización.

El principal evento de mineralización está caracterizado por tres tipos de alteración-mineralización: una etapa temprana de alteración potásica, propilítica

y una tardía de alteración sódica. Las etapas de alteración potásica y propilítica ocurrieron contemporáneas a las intrusiones de stocks porfídicos dioríticos y granodioríticos, a la formación de las brechas ígneas-hidrotermales y al emplazamiento tardío de sills y diques. La alteración sódica tardía, desarrollada centralmente en las brechas ígneas-hidrotermales y sus cercanías, está asociada a un intenso fracturamiento y brechización (incluyendo los sills) y la depositación principal de mineralización. La distribución de leyes, alteración, y la zonación de sulfuros de cobre indican que los cuerpos de brechas ígneas-hidrotermales representan los conductos alimentadores del sistema hidrotermal. La actividad hidrotermal fue seguida por la intrusión de un enjambre de diques dioríticos.

Las asociaciones de sulfuros hipógenos muestran una zonación vertical y lateral, centrada en los cuerpos de brechas ígneas-hidrotermales polimícticas. Una zona estéril de pirita en profundidad está sobreyacida por calcopirita-pirita y seguida hacia arriba y lateralmente por calcopirita-digenita o calcopirita-bornita. La asociación digenita-calcosina supérgena caracteriza las partes centrales de alta ley en los cuerpos de brechas.

Evidencias de ebullición asociada a la alteración potásica fue encontrada en muestras hasta una elevación de 684 msnm. A esta elevación, los valores de temperatura de homogenización de inclusiones fluidas exceden los 450º C. Los fluidos hidrotermales dentro de las brechas ígneas-hidrotermales evolucionaron siguiendo un patrón de enfriamiento, como lo indican los datos de inclusiones fluidas en cuarzos de asociaciones minerales propilíticas. El emplazamiento de sills dioríticos y granodioríticos que cortan las brechas ígneas-hidrotermales en distintos niveles, probablemente sellaron el sistema hidrotermal, causando sobre-presurización de fluidos, hidro-fracturamiento en las rocas y produciendo la ebullición asociada a la alteración sódica. Estos resultados pueden ser interpretados como eventos de ebullición y descompresión asociada, ocurrida episódicamente debido a sobrepresurización de fluidos, hidro-fracturamiento, y cambios drásticos de condiciones litostáticas a hidrostáticas, lo cual probablemente ocurrió a una paleo-profundidad aproximada de entre 3.5 y 2.0 km.

Los resultados de isótopos de azufre realizados en sulfuros hipógenos sugieren una fuente magmática dominante para este elemento, e indican una relación cogenética para los sulfuros analizados. Isótopos de C-O en calcitas de la alteración propilítica sugieren un origen magmático para el C, probablemente de origen mantélico, y un fraccionamiento del O que sigue la tendencia de rocas alteradas por fluidos hidrotermales a baja temperatura.

Las rocas del domo riolítico representan una característica litológica distintiva dentro del magmatismo Jurásico en la Cordillera de la Costa del norte de Chile, el cual está dominado por rocas volcánicas andesíticas-basálticas de la formación La Negra. Estas rocas ácidas conforman un cuerpo intrusivo hipabisal de composición riolítica, emplazado con una geometría en forma de domo o lacolito. Este habría intruido (~155-160 Ma) una secuencia de tobas, brechas volcánicas e intercalaciones sedimentarias subordinadas, ubicadas probablemente en la base de la Formación La Negra.

La signatura isotópica de Sr-Nd enriquecida del domo riolítico junto con la baja temperatura de saturación de circón de ~750ºC, son indicios de una fuente cortical dominante para estas rocas félsicas, probablemente formadas por fusión parcial de rocas cuarzo-feldespáticas de origen cortical. El desarrollo coetáneo de magmas máficos derivados del manto y magmas ácidos derivados de la corteza en el depósito Mantos Blancos sugieren una relación de causa-efecto, en la cual la fuente de calor para la generación de los fundidos riolíticos pudo ser la intrusión de magmas máficos en la corteza félsica.

En las rocas de composición intermedia, se identificaron dos patrones de fraccionamiento distintos, basados en los patrones de REE y vectores de fraccionamiento de Rayleigh. La distribución de las HREE en forma cóncava y la ausencia o pequeña anomalía negativa de Eu en los diques máficos, pórfidos dioríticos y pórfidos granodioríticos I (GP I), sugiere un fraccionamiento dominado por hornblenda, consistente con la dirección del vector de fraccionamiento de este mineral. Estos datos sugieren una derivación de GP I desde un magma parental diorítico. Por otra parte, la anomalía negativa de Eu en los pórfidos granodioríticos II (GP II), sugiere un fraccionamiento dominado por plagioclasa. Sin embargo, el fraccionamiento por si solo no puede explicar

la generación de GP II, lo que se puede explicar por mezcla magmática y la generación de las brechas ígneas-hidrotermales polimícticas por *mingling*. GP II exhibe las temperaturas de saturación de circón más altas, consistentes con un *input* termal derivado de la intrusión de los magmas máficos en el sistema magmático félsico.

Las similitudes composicionales entre el domo riolítico y las inclusiones fundidas en cuarzo, independiente de la roca huésped, sugiere un origen común. Más aún, la composición riolítica invariable de las inclusiones fundidas en fenocristales de cuarzo formados tempranamente, la cual es independiente de la composición química de la roca huésped, indica que pueden representar la composición extrema del miembro félsico de la mezcla, mientras que el pórfido diorítico representaría la composición del extremo máfico. La mezcla de magmas probablemente causó el escape temprano de fluidos ricos en cobre desde el magma máfico, contribuyendo a la mineralización en las brechas magmáticas-hidrotermales, las rocas granodioríticas y el domo riolítico.

En el distrito de Manos Blancos, se reconocieron cuatro eventos de deformación:

i) Basculamiento de las rocas del distrito hacia el sur-oeste, previo a la alteración hidrotermal relacionada a la mineralización de cobre, ii) transcurrencia sinestral en una zona de deformación principal actualmente orientada NE durante el Cretácico inferior, iii) rotaciones en sentido horario con eje vertical, durante el Eoceno-Oligoceno y iv) una última etapa de deformación asociada a extensión EW, contemporánea y posterior a la mineralización supergena, de probable edad Miocena.

La restauración en planta realizada, sugiere que el cuerpo mineralizado de Mantos Blancos tenía originalmente una forma elongada en dirección EW antes de la deformación, dirección que favoreció el emplazamiento de la mineralización.